Faculteit Bio-ingenieurswetenschappen

Academiejaar 2015-2016

Reactivity of 3-oxo-β-lactams with respect to primary amines: An experimental and theoretical approach

Jelle De Moor

Promotoren: Prof. Dr. ir. M. D'hooghe and Prof. Dr. ir. V. Van Speybroeck

Tutoren: ir. H. Goossens, ir. D. Hersen and ir. N Piens

Masterproef voorgedragen tot het behalen van de graad van

Master in de bio-ingenieurswetenschappen: Chemie en bioprocestechnologie

Faculteit Bio-ingenieurswetenschappen

Academiejaar 2015-2016

Reactivity of 3-oxo-β-lactams with respect to primary amines: An experimental and theoretical approach

Jelle De Moor

Promotoren: Prof. Dr. ir. M. D'hooghe and Prof. Dr. ir. V. Van Speybroeck

Tutoren: ir. H. Goossens, ir. D. Hersen and ir. N Piens

Masterproef voorgedragen tot het behalen van de graad van

Master in de bio-ingenieurswetenschappen: Chemie en bioprocestechnologie

Gent, June 2016

De promotors, De auteur,

Prof. dr. ir. M. D'hooghe Prof. Dr. ir. V. Van Speybroeck Jelle De Moor

Acknowledgments

Here I am, at the end of five years of, I have to admit, hard work at the Bio-science engineering faculty of the university of Ghent. Ever since the beginning of my first bachelor year, I have been so motivated to complete this education and I enjoy the knowledge and life lessons I have acquired during those five years. I am proud to deliver this Master dissertation as the last work at this faculty and as proof that I am ready to move on to a next chapter.

Before I leave the university ground, I want to show my gratitude to many people that were involved in this Master dissertation.

Professor M. D'hooghe and professor V. Van Speybroeck, my promotors, I would like to thank you for the opportunity that you have given me to start my thesis in your research groups. The supervision and the openness for any questions have helped me a lot to move on when reaching a dead end.

Besides my promotors, I had a team of three supervisors where I could always count on. Hannelore, Dietmar and Nicola, a big thanks to you since I was supervised in a superior way. I could always count on your support, your counsel and remarks in order to elevate the level of this Master dissertation. Nicola, you have guided me through all new and difficult steps in the lab and you were there anytime I needed advice for further investigation. Dietmar, you were there to guide me through the new world of programming and I could count on your solutions to every possible error that sometimes mysteriously occured on my screen. Hannelore, I would like to thank you for you good insights you gave me into molecular modeling when analyzing the molecular structures together. In addition, I would like to thank the guest associate professor Saron Catak for her computational input in this thesis during the short stay in Belgium.

Furthermore, I would like to thank all thesis and doctoral researchers at the lab for the motivation to spend whole days in the lab and to show me how work and pleasure are fused. But also at the CMM in Zwijnaarde, I could count on my fellow researchers Dietmar and Pieter for a great time in the office.

Besides academic support, I want to show my gratitude to all people that surrounded me during not only this thesis but the last five years in Ghent. 'De Bende', and especially Pieter, Anke, Alicia and Eva, for the best years as a student. Also my friends from Aalst I could count on to get my head of this thesis and just enjoy some free time, to find motivation and start again the next day. Since the beginning of this academic year, I met Febe and I want to thank her for the patience she had with me, always working on my thesis and for the unconditional support.

Last, but not least, my parents. They are the reason I am standing here now, at the end of my education. The endless support and believe in me have made me who I am and got me to where I am standing now. The appartment in Gent I could stay in, and how they've always spoiled me with food so I never lost time I could spent on schoolwork. They also made sure I always had a car available

when I had to drive to Zwijnaarde. My gratitude can not be expressed in words.

Finally, I want to show my support for the future 3-oxo-β-lactam investigators. This precious work is the conjuncture of three thesis students, Lieselotte, Lotte and I. Please take care of this work and I am looking forward to hear about your results.

Jelle De Moor, June 5th 2016

Contents

Chapter 1

Background and goals

1.1 Background

The research on β-lactams or azetidin-2-ones has been increased tremendously since the discovery of penicillin by Fleming in 1928.[1] β-lactams show a very high bioactivity and are therefor used in many applications in organic and medicinal chemistry. Their largest application is the therapeutic use against bacterial infections.[2] Shortly after their first use as antibiotics, drug resistant bacteria began to emerge in many hospitals in the 1930s.[3] These events have led to the synthesis of a variety of modified β-lactams to broaden the spectrum for bacterial fight.

The importance of β-lactams in medicinal chemistry cannot only be attributed to the antibacterial properties of this four-membered ring system. In recent years, there has been renewed interest in the synthesis and modification of β-lactams to obtain compounds with diverse pharmacological properties such as cholesterol absorption inhibitory, vasopressin V1a antagonist, antidiabetic, anti-inflammatory, antiparkinsonian, anti-HIV activity, etc. (See Figure 1.1).[4,5]

The skeleton of the β-lactam ring facilitates ring opening reactions. This unique property can be exploited for the regioselective synthesis of compounds and has been collectively termed as the "β-lactam synthon method", first introduced by Ojima.[6,7] The synthesized compounds can be amino acids (both protein and non-protein), medicinally active compounds (like taxoids), cytotoxins, alkaloids, etc.[8] Besides β-lactam ring openings, ring expansions and rearrangements, yielding 3- to 8-membered aza heterocycles, are very common in modern organic and medicinal chemistry.[9–12] Polymerization of β-lactams to nylon-6-polymers, both condensative and anionic, have been investigated as well.

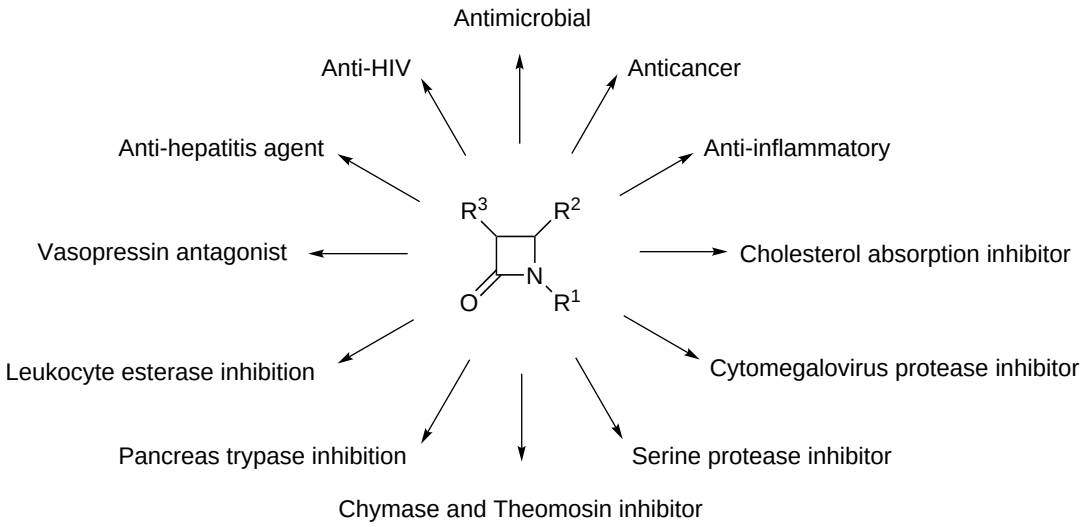

Figure 1.1: Pharmacological applications of β-lactams.[4]

They contain more amide groups and hence resemble silk more closely than the common nylon-6 polyamide.[13]

The "β-lactam synthon method" will be applied in this work for the preparation of 3-oxo-β-lactams **1**. The reactivity of these β-lactams toward the synthesis of 3-imino-β-lactams **5** will be explored to fathom the synthetic potential of azetidin-2-ones.

1.2 Goals

The first part of this work handles the experimental work in which the last experiments on the reactivity of 3-oxo-β-lactams **1** with respect to primary amines are performed. In the second part, the experimental outcome is supported by a computational analysis.

This work is the follow-up study of two previous Master dissertations by L. Crul[14] and L. Demeurisse[15] in which the reactivity of 3-oxo-β-lactams **1** with respect to primary amines was investigated (Scheme 1.1). Their findings proved to be in disagreement with previous experiments in literature. Alcaide *et al.*[16] claimed that treatment of 3-oxo-β-lactams **1** with primary amines did not give rise to the desired 3-imino-β-lactams **5** (Reaction proceeding downwards in Scheme 1.1), but to the C2-C3 ring opening products, α-aminoamides **3**, by carbon monoxide elimination (Reaction proceeding to the left in Scheme 1.1). These α-aminoamides **3** were formed with a variety of side-chains on 3-oxo-β-lactams **1** and different primary amines. However, the experiments of L. Crul and L. Demeurisse on these reactions led to the formation of other products, ethanediamides **4**. This C3-C4 ring opening re-

action gives rise to the formation of ethanediamides **4**, which is unprecedented in literature (Reaction proceeding to the right in Scheme 1.1).

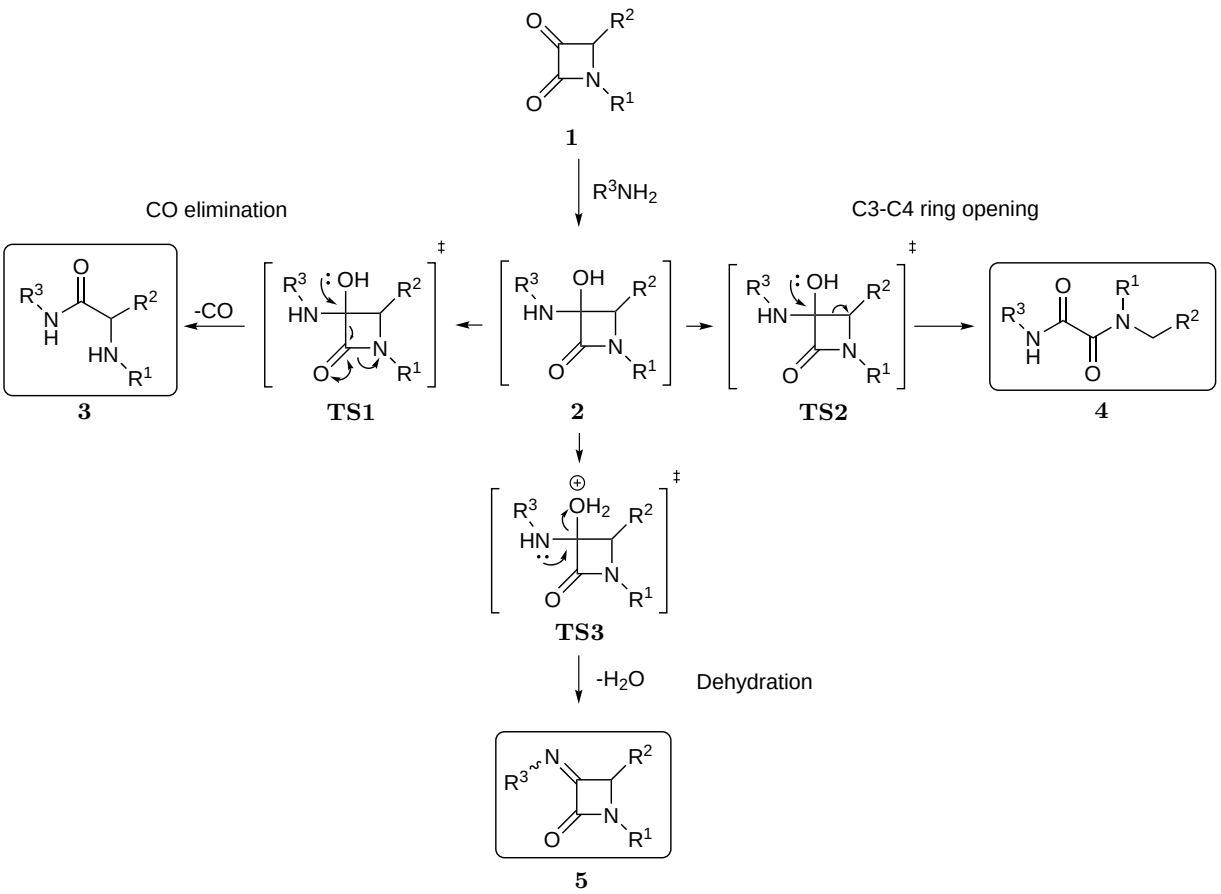

Scheme 1.1: Reactivity of 3-oxo-β-lactams with respect to primary amines.

L. Demeurisse concluded an aryl substituent on the C4-carbon atom to be the major driving force for C3-C4 ring opening of 3-oxo-β-lactams **1** to ethanediamides **4**. Both electron withdrawing (R^2 = 4-fluorophenyl) and electron donating (R^2 = 4-methoxyphenyl) aryl substituents on the β-lactam C4 position gave rise to the formation of ethanediamides **4**. However, this hypothesis can only be proved by carrying out additional experiments. An electron donating alkyl C4 substituent in combination with both electron donating and electron withdrawing N1 substituents should be tested for selective formation of 3-imino-β-lactams **5** or α-aminoamides **3**. Despite α-aminoamides **3** have only been obtained in small amounts, they can be expected to be formed during reaction of 3-oxo-β-lactams **1** with an alkyl C4 substituent and an elektron withdrawing N1 substituent. It is the purpose of the experimental part of this dissertation to investigate both reactions with an electron donating (*e.g.* R^1 = 4-methoxyphenyl) and with an electron withdrawing (*e.g.* R^1 = 4-fluorophenyl) N1-substituent in combination with an alkyl C4 substituent. The results are discussed in Chapter 3.

The theoretical part of this work (Chapter 4) will analyze the three pathways in Scheme 1.1 computationally. Firstly, possible reaction paths will be searched for by means of *ab initio* molecular

modeling and the reaction barriers and relative stabilities of ground states will be compared to locate the most probable pathway. Both reactions with and without the aid of an extra molecule will be considered. Secondly, an implicit solvent model will be used to investigate the influence of the solvent environment. finally, the influence of several β-lactam side-chains on the energetics of each reaction will be evaluated. The resulting trends will be compared to literature in order to validate the models.

Chapter 5 will give a brief overview of the experimental and computational results. General conclusions are taken and the outlook for further investigation is given.

Chapter 2

Literature overview

2.1 A brief history

Although penicillin **6** was first discovered by Alexander Fleming in 1929,[1] other β-lactam containing substances had been studied earlier. In 1907, the synthesis of β-lactams (or azetidin-2-ones) had already been investigated by the German chemist Herman Staudinger.[17] He proved ketenes to be synthetically important intermediates for the production of β-lactams. His research preluded a time of thorough investigation of β-lactam antibiotics such as penicillins **6** and cephalosporins **7**.

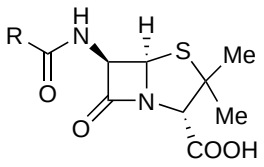

6

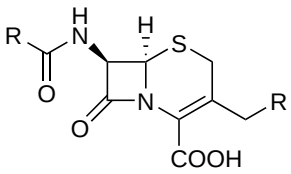

7

By the end of the twentieth century, computational analysis of β-lactams was made possible since computers were performing at such an advanced level to depict complex multi-electron systems. The density function theory (DFT), a quantum mechanical molecular modeling method, was first applied to solid-phase physics at the end of 1970s. Although it was not until the very end of the twentieth century that the used functionals in this theory were considered refined enough to find their application in the study of chemical substances by better modeling the exchange and correlation interactions.

In this chapter, a brief overview will be given of theoretical studies performed on the synthesis, reactivity and conformation of β-lactams (see Figure 2.1). A few examples will be discussed thoroughly

to show how theoretical studies can help to understand the experimental outcome of reactions.

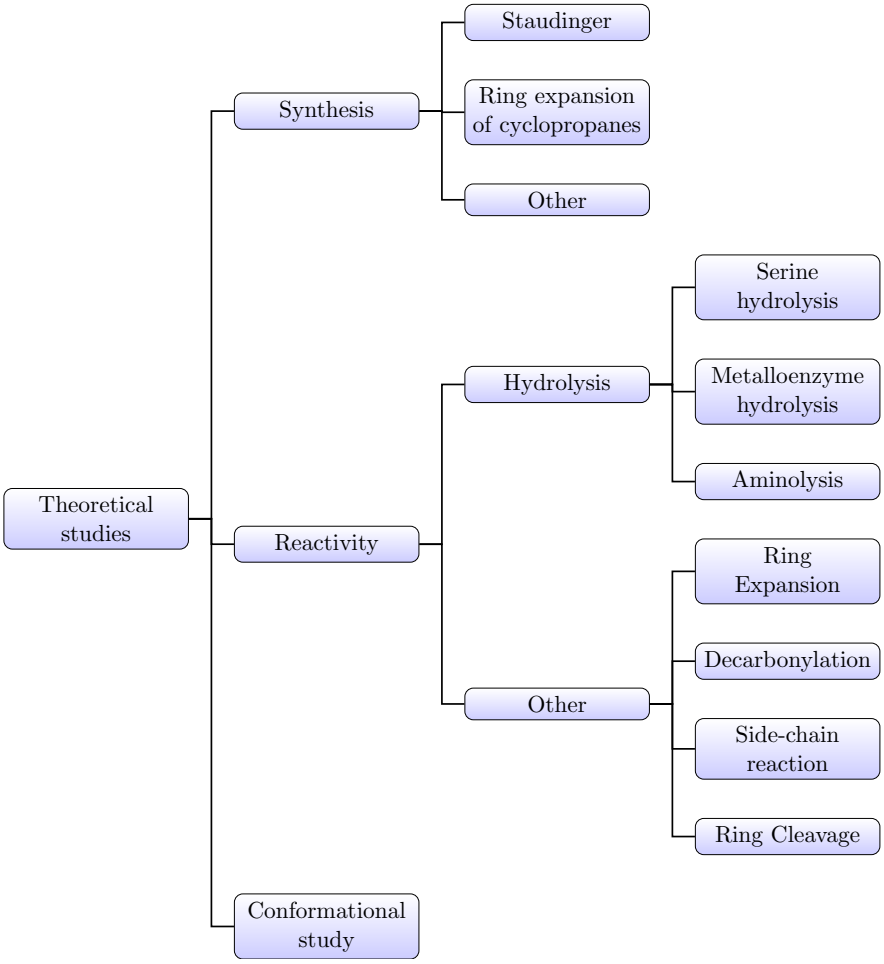

Figure 2.1: Overview of theoretical study fields for β-lactams

2.2 Synthesis of β-lactams

Most computational studies performed on β-lactams concern the Staudinger synthesis, also known as the cycloaddition mechanism. Another common β-lactam synthesis method, ring expansion of cyclopropanes, will be considered afterwards. Finally, an overview of theoretical studies on less common synthesis pathways will be given.

The Staudinger synthesis is one of the most important and direct routes for the formation of β-lactams.[18] The reaction involves a [2+2] cycloaddition between ketenes **9** and imines **10**. The ketenes **9** are generated from the according acid chlorides **8** and a tertiairy amine, functioning as a base. The imine's **10** nitrogen atom performs a nucleophilic attack on the sp-hybridized carbon atom of the ketenes **9** with formation of zwitterionic intermediates **11**. For most substitution patterns, the reaction leads to *cis*-β-lactams **13** by immediate conrotatoric electrocyclic ring formation. In some cases,

depending on the substitutes at the C3 and C4 positions of the ring, *trans*-β-lactams **14** are major[19] or even exclusive[20,21] products. This diastereoselectivity is the result of the competition between direct ring formation and isomerization to intermediate zwitterions **12**, leading to **13** and **14** as final products, respectively.

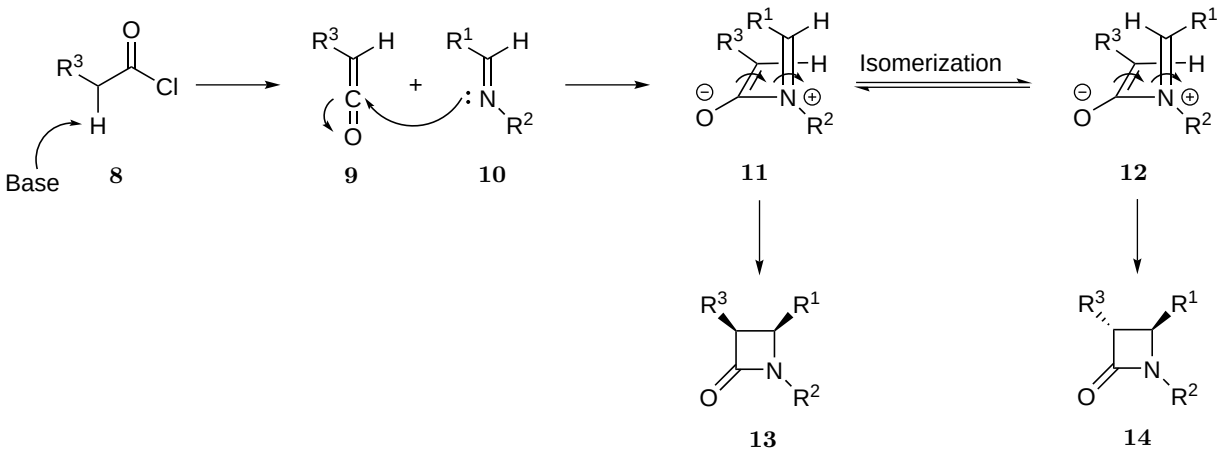

Besides experimental circumstances like temperature, pressure and solvents, the *cis*/*trans* ratio depends on the substituents of the ketenes **9** and imines **10**. Electron donating substituents (*O*-alkyl, *O*-aryl, *O*-alkylaryl) on the ketenes **9** and electron withdrawing substituents on the imines **10** induce a faster direct ring formation, thus favoring the formation of *cis*-β-lactams **13**. Meanwhile, electron withdrawing groups (*S*-alkyl, *S*-aryl, Cl, Br, F) on the ketene **9** and electron donating groups on the imine **10** disfavor the direct ring closure leading to the formation of *trans*-β-lactams **14**. Some substituents (vinyl, PhthNCH=C=O) on the ketenes, called Sheehan-ketenes,[22,23] show a moderate rate of direct ring-closure, giving rise to a complex mixture of *cis*-β-lactams **13** and *trans*-β-lactams **14**.[22–24]

Most theoretical studies aim to explain the stereoselectivity of the Staudinger synthesis by looking at the configuration (E/Z) of the starting imines[25] or at the torquoelectronic effect of the ketenes[22] and imines substituents.[26] Initially, Cooper *et al.*[27] established a concerted reaction mechanism on the RHF/3-21G level of theory. However, Sordo *et al.*[28] and Cossio *et al.*[25] showed in 1992 that the Staudinger synthesis proceeds *via* a stepwise mechanism with conrotatory electrocyclic ring closure. The enantioselectivity is in many cases experimentally determined while theoretical studies show the exact reaction mechanism in which the reaction proceeds from reactant, over a transition state, to the according product.

More recent theoretical studies explain the formation of aza-lactams,[29] spiro-β-lactams,[30] *N*-silyl-azetidin-2-ones[31] and bis-β-lactams.[32] For example, in the work discussed below, Luis *et al.*[33] investigated the selectivity to form, either δ-lactams or β-lactams out of chloro-cyan-ketenes.

Chloro-cyan-ketenes **15** react with unstaturated imines **16**, followed by a cyclization reaction, yielding either β-lactams **18** or δ-lactams **20**. The experiments[34,35] in diethyl ether led to the formation of the δ-lactam **20** if R = H and β-lactam **18** if R = Ph. β-lactam **18** formation occurs *via* the Staudinger synthesis while the δ-lactam **20** is formed *via* an aza-Diels-Alder reaction. Moreover, the experiments showed exclusive stereoselective formation of *trans*-β-lactams and *cis*-δ-lactams. The aim of the theoretical study is to elucidate the kinetics of the two competitive reactions and the stereoselectivity of the β-lactam and δ-lactam formation. ELF (electron localization function) will be used to analyze the cyclization process and compare both pathways. This topological analysis method is a powerful tool to investigate chemical bonding.[36]

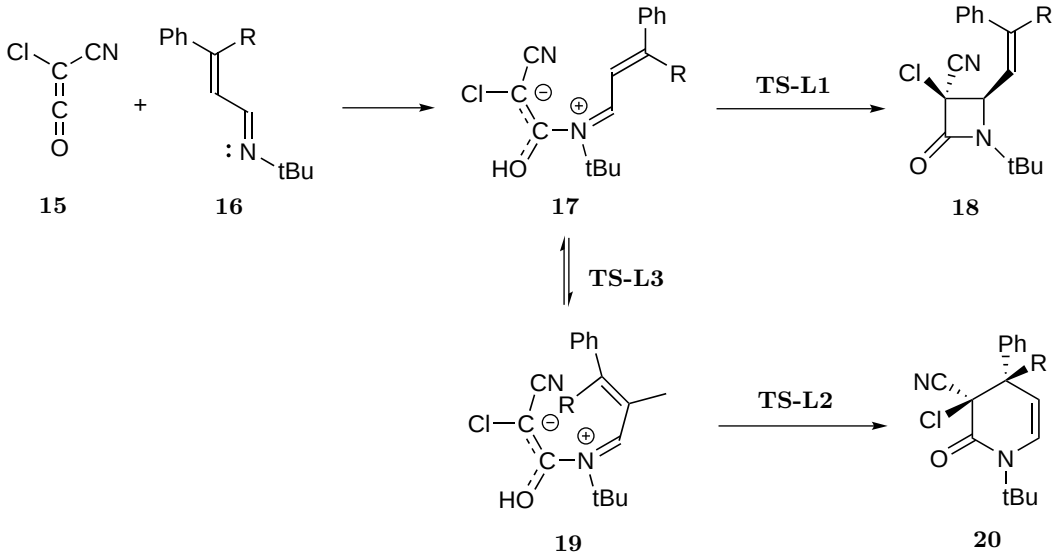

DFT computations were carried out using an exchange-correlation functional (MPWB1K) and the standard 6-311G(d,p) basis set. To take into account the diethyl ether solvent, a polarizable continuum model (PCM) was used (implicit solvation, see Section 4.1.3). First, the nucleophilic attack of the imine **16** on the chloro-cyan-ketenes **15** yielding the zwitterionic intermediate **17** was investigated. This reaction has a small kinetic barrier (value not reported) and is strongly exothermic with reaction enthalpies of 107.2 and 199.7 kJ.mol^{-1} for the imines **16** with R = H and R = Ph, respectively. Experimental results[34] showed that this nucleophilic attack induces a complete *endo* selectivity, i.e. the cyano side-chain of the ketene is oriented toward the sp^2 hybridized imine nitrogen during the attack. Besides the exo/endo conformation of the reactant, the *s-cis* and *s-trans* conformations of the unsaturated imine **16** play an important role. Since the *s-trans* conformations are more stable than the *s-cis* ones, the *s-trans* configuration with an *endo* selectivity was chosen as a model system for theoretical investigation of the initial nucleophilic attack.

From the *s-trans* imine **16**, the *s-trans* zwitterionic intermediate **17** is initially formed. Due to free C2–C3 bond rotation of the *s-trans* **17**, it can equilibrate easily to the *s-cis* zwitterionic intermediate **19**

with low rotational activation enthalpies 44.4 (R = H) and 47.3 kJ.mol^{-1} (R = Ph). The formation of δ-lactams **20** from the *s-cis* zwitterionic intermediate **19** is kintetically more favorable than the formation of β-lactams **18** from the *s-trans* ones **17** by about 40 kJ.mol^{-1}. This is probably due to the formation of the highly strained four-membered ring. Since the rotation via **TS-L3** is faster than the cyclization reactions, the *s-cis* and *s-trans* intermediates are in equilibrium. In other words, the cyclization reactions are rate determining for β- and δ-lactam formation. The overall energy profiles for R = H and R = Ph are shown in Figure 2.2.

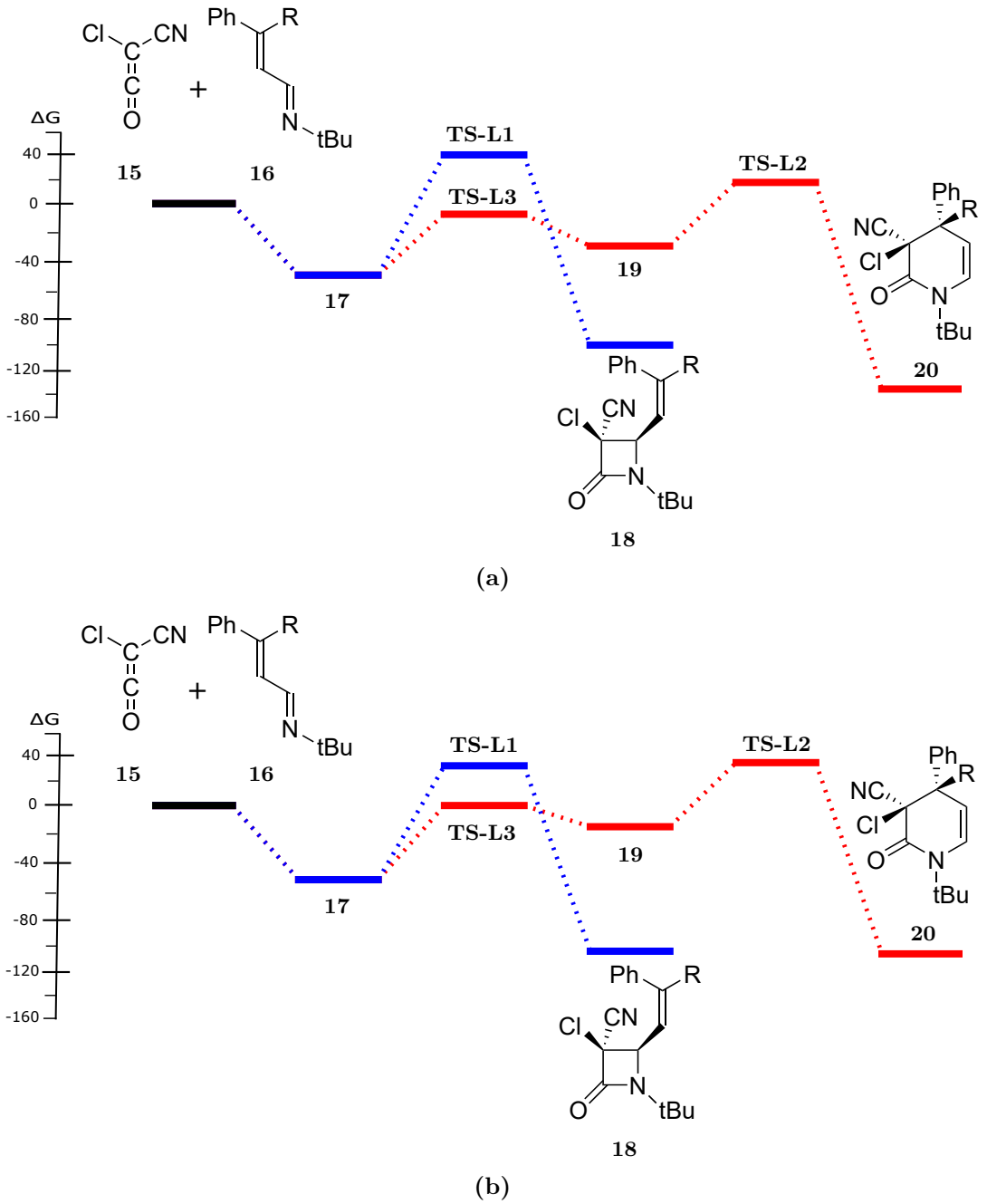

Figure 2.2: Free energy profile for R = H **(a)** and R = Ph **(b)** (MPWB1K/6-311G(d,p), 298 K, 1 atm, IEF-PCM with diethyl ether, energies in kJ.mol^{-1})[33]

For R = H, **TS-L2** is 23 kJ.mol^{-1} more stable in free energy than **TS-L1**. Hence, δ-lactam **20** is formed. However, when R is replaced by a phenyl group, **TS-L1** is 9.2 kJ.mol^{-1} more stabel than **TS-L2** and thus β-lactam **18** is formed. This change of selectivity is attributed to the steric hindrance of the extra phenyl substituent, which increases the free energy of **TS-L2** by 17.2 kJ.mol^{-1} with respect to **TS-L1**.

Besides the selective formation of either β-lactams or δ-lactams, the origin of the cis/trans selectivity in the formation of β-lactams and δ-lactams was investigated. Experimentally, *cis*-δ-lactam and *trans*-β-lactam were formed. During β-lactam formation, the *trans* N–C configuration in **17** is conserved. This leads to a **TS-L1** in which the cyano and the chain are in *trans* relationship. During δ-lactams **20** formation however, the relative position of the phenyl group in **19** has changed by C2–C3 bond rotation. The phenyl group stays in this position, giving rise to the *cis*-δ-lactam **20**.

The ELF topological analysis proved that the N–C single bond electron density can be attributed to the lone pair of the nitrogen atom. The formation of this bond begins at a distance of 1.92 Å while the C–C double bond on the imine **16** remains unpolarized. Hence, the conjugated system of the amine **16** does not participate in the N-C bond formation. The ELF analysis also showed that C–C bond formation during cyclization is very similar for both β-lactams and δ-lactams.

Another frequently used synthetic method for β-lactams is the expansion of cyclopropanones. Several studies have been performed on the expansion of aziridines[37] and hydroxycyclopropylamines.[38,39] Less common synthesis methods have also been investigated theoretically, differing in starting products and subsequent mechanisms. One example is the S_N2 reaction within chloropropionyl amino acids like glycine and alanine[40] or 3-halogen and 3-hydroxy propanamides,[41] leading to formation of β-lactams. Another example is the reaction of photogenerated metallaketenes with imines using Fisher carbene complexes.[42,43]

2.3 Reactivity of β-lactams

Besides the synthesis of β-lactams, their reactivity has been investigated thoroughly. Since the β-lactam ring is the basic skeleton of many antibiotics, their hydrolysis has been investigated extensively both with and without β-lactamase catalysis. A lot of other reactions such as ring expansion, decarbonylation, side-chain reactions and ring cleavage have been investigated since the β-lactam ring strain provides sufficient energy to induce such reactions.[44]

2.3.1 β-lactamases and the hydrolysis of β-lactams

β-lactamases cause a serious threat to β-lactam antibiotics because they hydrolyze the β-lactam moiety of the antibiotic and thus render them inactive. β-lactamases can be divided into four classes, A-D, differing in activity site.[45] Classes A, C and D consist of serine enzymes, which react via nucleophilic attack on the carbon atom of the β-lactam amide, while class B are metalloenzymes, which require zinc ions, to hydrolyze the the β-lactam ring. Many β-lactamase inhibitors contain β-lactam structures, more prone to hydrolyzation than the original antibiotic, thus protecting the antibiotic from being hydrolyzed.[46] Currently marketed β-lactam inhibitors are clavulanic acid **21**, sulbactam **22** and tazobactam **23**.[47]

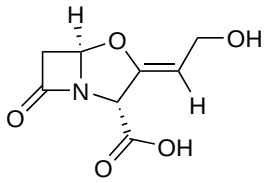

21

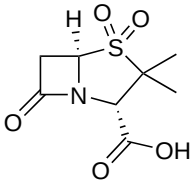

22

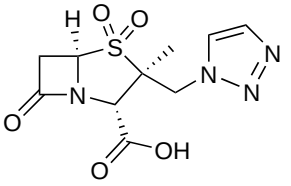

23

Theoretical studies focus on the mechanism of hydrolysis of β-lactams, which can help to produce more potent β-lactam antibiotics. A lot of these studies extensively investigate the hydrolysis of β-lactams by serine residues (β-lactamase classes A, C and D).[48–56] Initial studies focused on the acylation (nucleophilic attack on the β-lactam amide) and deacylation proces (release of the amide) of penicillin. Later, Li *et al.* investigated the reaction after acylation of penicillin[57] and compared this to the results for a sulbactam **22** in their previous study.[58]

B-class β-lactamases have been studied by several groups as well. These enzymes incorporate either one[59] or two[60] zinc ions which catalyze the hydrolysis of the β-lactam ring.

Whereas most theoretical studies focus on the (alkaline) hydrolysis of β-lactams, some try to explain the mechanism of the aminolysis of β-lactams.[61,62]

2.3.2 Other β-lactam reactions

Besides the antibiotic properties of β-lactams, they have also proven to be useful intermediates in organic synthesis.[63] For this purpose, Ojima introduced the term "β-lactam synthon method" in 1987.[6,7] β-lactams can be used in asymmetric synthesis[64] or as useful reactants for the synthesis of different heterocycles.[65] Due to the ring strain of their four-membered rings, β-lactams are very reac-

tive.[44] An overview of possible bond cleavages of β-lactams and corresponding products is given by Alcaide et al.[66] and shown in Figure 2.3. The hydrolysis of β-lactams by cleavage of the N1–C2 bond has already been the subject of the previous section, but many other mechanisms exist. Several theoretical studies have been performed on these synthon methods in order to elucidate their exact, often very complicated, mechanism. The reactions may proceed through ring expansion, decarbonylation, side-chain reactions or ring cleavage. Some examples are explored in the following sections.

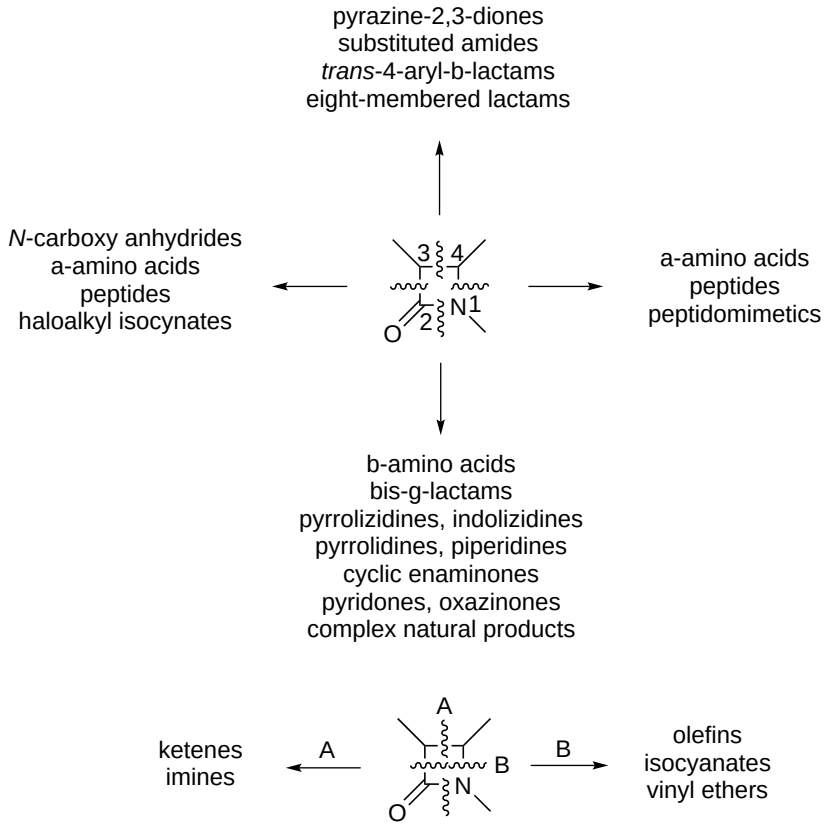

Figure 2.3: β-lactam cleavage possibilities with corresponding products[66]

2.3.2.1 Ring expansion

Ring expansion of β-lactams mostly leads to five- or six-membered rings containing one or two heteroatoms. The strain of the four-membered ring is released and an energetically more favored five- or six-membered ring is formed.[67] A lot of theoretical studies investigate the ring expansion of β-lactams.[11,65,68–72] Two of these studies will be discussed in depth.

Mollet *et al.*[11] investigated the C3–C4 bond cleavage of 3-hydroxy-4-(1,2-dihydroxyethyl) **24** followed by a ring expansion to a six-membered ring. As they aimed to oxidize the hydroxyl group on the side-chain of β-lactams **24**, they stumbled upon the peculiar transformation of **24** to 2-hydroxy-1,4-oxazin-3-ones **29**. Although the $NaIO_4$-mediated oxidation of 3-alkoxy- and 3-phenoxy-4-(1,2-

dihydroxyethyl)-β-lactams led to the expected oxidated β-lactams, the same oxidation conditions caused a ring expansion for the 3-hydroxy-β-lactams **24**, yielding oxazin-3-ones **29**. Altough β-lactams **24** react toward the desired 4-formyl-β-lactams **25**, these products proved to be unstable under the given reaction conditions and reacted further to form the intermediates **26**/**27**. This C3–C4 bond cleavage is facilitated by the OH substituent on the C3 position and will subsequently result in ring closure to selectively form 2-hydroxy-1,4-oxazin-3-ones **29**.

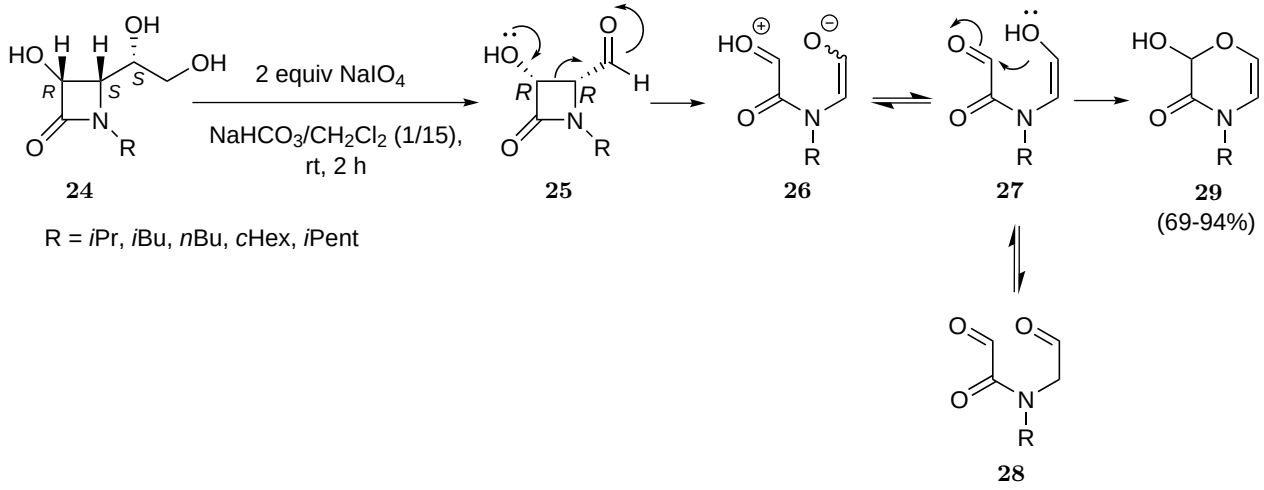

The proposed reaction mechanism for β-lactam **24** with R = Me was further investigated by means of DFT calculations at the M06-2X/6-31+G(d,p)//B3LYP/6-31+G(d,p) level of theory. The solvent (dichloromethane, ϵ=8.93) was taken into account by means of a continuum model (see Solvation, Section 4.1.3). Both systems with and without assistance of a second β-lactam were considered and the obtained Gibbs free energies are shown in Table 2.1.

Without assistance of a second β-lactam **24**, a concerted reaction was found in which β-lactam **25** is directly converted to the intermediate **27** *via* proton transfer. The Gibbs free activation barrier for this reaction is 35.6 kJ.mol^{-1} lower than that for the formation of the zwitterionic intermediate **26**. Subsequent ring closure of intermediate **27** to 2-hydroxy-1-4-oxazin-3-one **29** is highly unfavorable ($\Delta G^{\ddagger}$ =145.6 kJ.mol^{-1}), indicating the model might be inadequate. Another concerted reaction was found, directly converting β-lactam **25** to 2-hydroxy-1-4-oxazin-3-one **29**, altough a very high activation barrier of 167.7 kJ.mol^{-1} makes this reaction unlikely.

To make the model more realistic, a second β-lactam was introduced into the system. In this case, the proton transfer reaction from β-lactam **25** to the intermediate **26** was assisted by the hydroxyl moiety of the second β-lactam, which acts as a proton conduit. This lowered the activation barrier with 13.7 kJ.mol^{-1} compared to the non-assisted case. The most plausible reaction path with β-lactam assistance however, involves conversion of compound **25** to intermediate **27** with subsequent ring closure toward 2-hydroxy-1-4-oxazin-3-one **29**. The Gibbs free activation barrier for the rate

determining first step is 91.1 kJ.mol^{-1} and thus 7.1 kJ.mol^{-1} lower than the non-assisted mechanism. The second step (**27**→**29**) shows the most decrease in Gibbs free activation energy with β-lactam assistance ($\Delta G^{\ddagger}$ =145.6 kJ mol^{-1} without assistance and 84.1 kJ.mol^{-1} with assistance). A third pathway, the simultaneous ring opening and ring closure (**25**→**29**), has a high activation barrier of 140.3 kJ.mol^{-1}, even with β-lactam assistance.

Table 2.1: Free Gibbs activation energies ($\Delta G^{\ddagger}$) for the ring opening of β-lactam to 2-hydroxy-1-4-oxazin-3-one **29** (B3LYP/6-31+G(d,p)//M06-2X/6-31+G(d,p), 298 K, 1 atm, IEF-PCM with CH_2Cl_2)

Reaction	$\Delta G^{\ddagger}$ **(kJ mol^{-1})**	
	without assistance	**with assistance**
25→**26**	133.8	120.1
25→**27**	98.2	91.1
27→**29**	145.6	84.1
25→**29**	158.4	140.3

Thus, the reaction is facilitated by the proton transfer of the hydroxyl group and assistance of the C3 substituded hydroxyl group of a second β-lactam. The $NaIO_4$-mediated oxidation of 3-alkoxy- and 3-phenoxy-β-lactams does not yield 1,4-oxazin-3-ones **29** since these reactants do not have an hydroxyl group on the C3 carbon atom.

Ring expansion to five-membered rings has been studied extensively as well.[69,71,73] Dražić *et al.*[70] investigated the conversion of amino-β-lactams **30** to 2-aminoimidazolones **32** both experimentally and theoretically. They introduced a highly nucleophilic guanidine group at the C3 position of the amino-β-lactams **30** in order to promote the transformation to the five-membered 2-aminoimidazolone ring compounds **31**. The first step of this reaction involves N1–C2 amidolysis of the β-lactam ring and rearrangement to the imidazolones **31**. A base will subsequently eliminate the N1 substituent of the original β-lactams **30** to give rise to the final imidazolone product **32**. If R^1 is a phenyl group, the benzoyl group was cleaved from **32** in the presence of a base. For the theoretical study however, R^1 and R^2 are taken as methyl groups, thus benzoyl cleavage was not investigated.

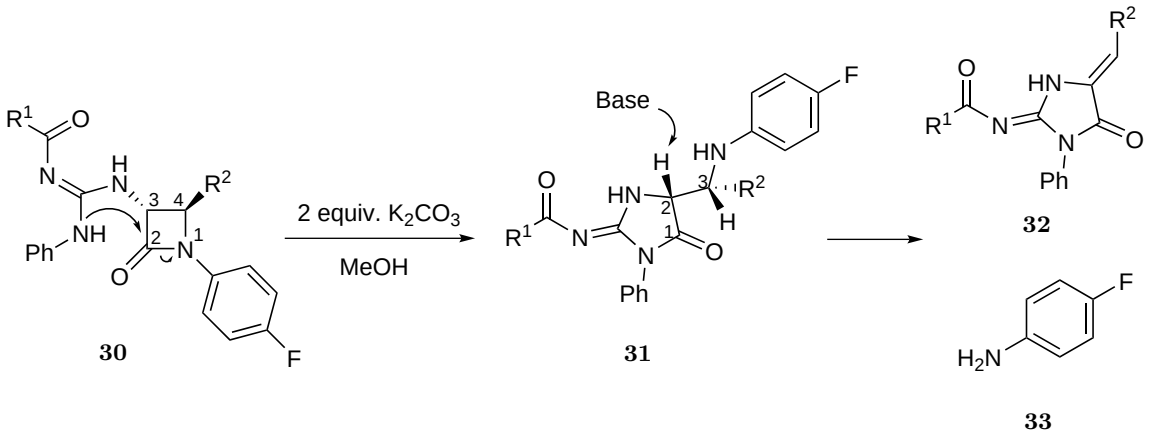

The Gibbs free energy profile for the first step with according molecule geometries is shown in Figure 2.4. During the first step, the guanidine-β-lactam **30** is deprotonated by a base to form the anionic **34** and subsequently undergoes an intramoleculare nucleophlic attack of the guanidinium nitrogen atom on the carbonyl group of the β-lactam ring. The reaction has a Gibbs free activation barrier of 70.6 kJ.mol^{-1} and leads to the formation of the five membered ring, an imidazolon anion **35**. Calculations suggest that the reaction occurs via a bicyclic transition state **TS-D1**.

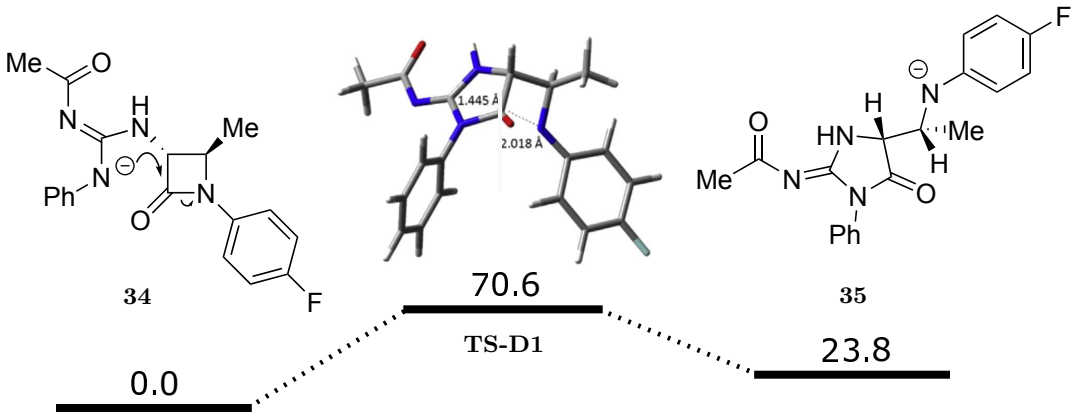

Figure 2.4: Gibbs free energy profile of the first step in the reaction with according reactants and products (MP2//B3LYP/6-31+G(d), 298 K, 1 atm, SMD with MeOH, energies in kJ.mol^{-1})

From this point, two parallel pathways can be followed, differing in the rotation around the C2–C3 bond. The free energy of activation for isomerization is 38.1 kJ.mol^{-1} (reverse barrier 36.8 kJ.mol^{-1}). Before the second step of the reaction can occur, both isomeric anionic imidazolones **35** were protonated again to become neutral and subsequently deprotonated at the carbon atom adjacent to the carbonyl group. This way, a double bond can be formed and the parafluoranilin **33** eliminated. It was expected that this E1cB elimination mechanism would occur spontaneously, but computational analysis showed the need to protonate the nitrogen atom of the amine group first. After protonation, the elimination reaction proceeds via the transition state **TS-D2** leading to the formation of the products **37** and **33**. Figure 2.5 shows the activation barrier for one of the two rotational isomers with according product configurations. The energy barrier for the second isomer is 18.0 kJ.mol^{-1} and the reverse barrier 64.0 kJ.mol^{-1}. The final imidazolone isomers **32** and **37** differ in the orientation of substituents around the newly formed double bond. Since the *cis* isomer **32** is 5.9 kJ.mol^{-1} more stable than the *trans* isomer **32**, only one isomer can be detected in the reaction mixture.

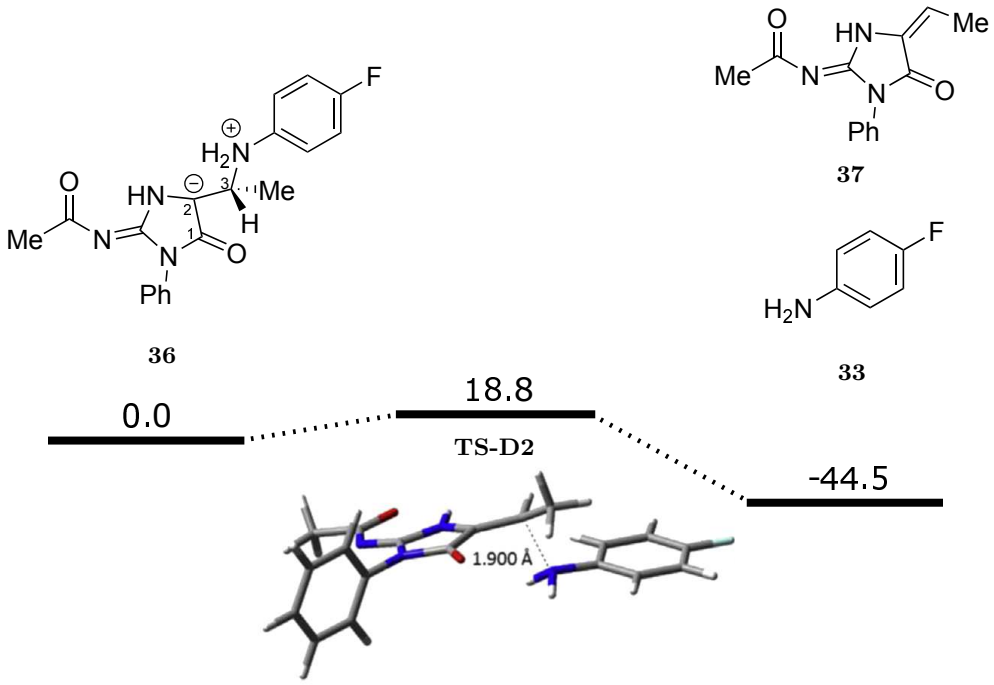

Figure 2.5: Gibbs free energy profile of the first step in the reaction and according reactants an products. Energies in kJ.mol^{-1} (MP2//B3LYP/6-31+G(d), 298 K, 1 atm, SMD with MeOH)

2.3.2.2 Decarbonylation, β-lactam side-chain reactions and ring cleavage

Besides ring expansion, ring cleavage of the β-lactam ring can induce multiple reactions. A possible reaction involves a decarbonylation, the expel of a carbon atom. Thermal decarbonylation of β-lactams was proposed by Wiitala *et al.*[74] for penams, the bicyclic ring structure present in many antibiotics like penicillin **6**.

In some syntheses, it is rather the side-chain of the β-lactam that reacts while the four membered ring induces regio- and stereoselectivity. Since the β-lactam is not actively participating, it is rather the β-lactam, who is acting as the side-chain in these cases.[75–77]

In some reactions, the ring is cleaved without a subsequent rearrangement to a new annular system or side-chain reaction. Pérez-Ruiz *et al.*[78] described the photoinduced electron transfer in β-lactams that leads to N1–C4 bond cleavage with subsequent back electron transfer to the electron donor DABCO (1,4-diazabicyclo[2,2,2]octane), resulting in a C2–C3 bond cleavage. Depending on the side-chains of the β-lactam, several products can be synthesized. With the help of DFT-calculations, they were able to determine the favored pathway.

2.4 Conformational analysis

Computational studies do not only attempt to explain reaction mechanisms.[79–82] DFT calculations can be used to study the conformation of substances and the interactions with their molecular environment. As an example, Tedesco *et al.*[79] performed a conformational analysis on 3-hydroxy-4-aryl-β-lactams. Geometric features of the non-planar β-lactam structure were determined, the flexibility of the substituents at C3 and C4 carbon atoms was analyzed and the additional flexibility due to implicit and explicit solvation was taken into account and compared with experimental results. Soriano-Correa *et al.*[82] performed a DFT study on five different penicillin antibiotics to compare several molecular descriptors such as atomic charges, bond orders, dipole moments, ionization potential, hardness and electrophilicity index. The antibacterial activity of these β-lactam antibiotics can be correlated with the electronic properties of the pharmacophore group and the aminoacyl side-chain.

Chapter 3

Experimental Results

3.1 Results and Discussion

This section discusses the experimental results concerning this Master dissertation. The first part will describe the synthesis of 3-oxo-β-lactams **1**. In a second part, the reactivity of the synthesized azetidine-2,3-diones **1** with respect to primary amines will be investigated. This reaction can result in either formation of α-aminoamides **3**, ethanediamides **4** or 3-imino-β-lactams **5**.

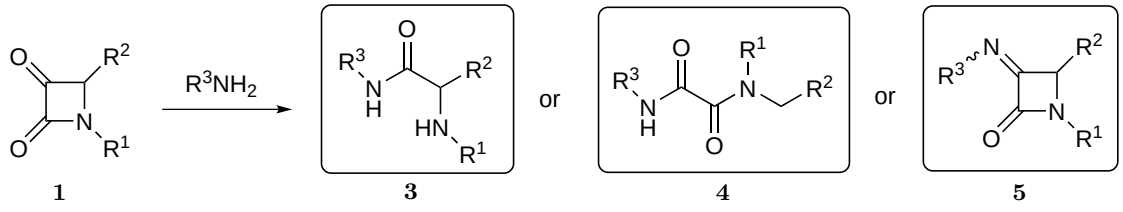

1 **3** **4** **5**

The aim of this study is to investigate the reactivity of 3-oxo-β-lactams **1**, bearing an electron donating (4-methoxyphenyl) or electron withdrawing (4-fluorophenyl) N1 substituent (R^1) in combination with an alkyl (nPr) C4 substituent (R^2), with respect to primary amines. Based on previous research, electron donating N1 substituents are expected to give rise to 3-imino-β-lactams **5**. Meanwhile, for electron withdrawing N1 substituents, formation of α-aminoamides **3** can be expected.[14–16,83]

3.1.1 Synthesis of azetidine-2,3-diones

In order to synthesize azetidine-2,3-diones, 3-acetoxyazetidin-2-ones **38** will be prepared *via* Staudinger synthesis. These will subsequently be deprotected to form 3-hydroxyazetidin-2-ones **39** and oxidized to the desired 3-oxo-β-lactams **1**.

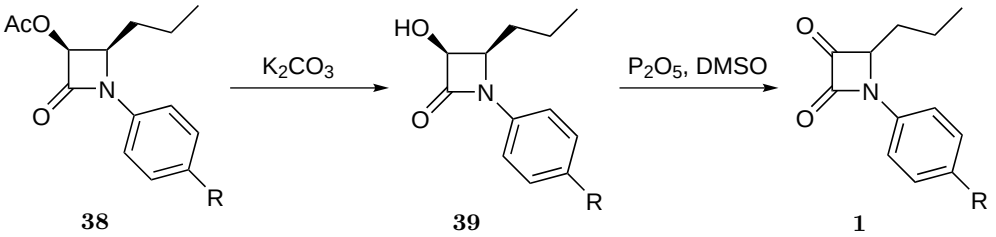

38 **39** **1**

R = OMe, F

3.1.1.1 Synthesis of (*E*)-*N*-(alkylidene)amines

For the synthesis of azetidine-2,3-diones **1**, (*E*)-*N*-(alkylidene)amines **42** were synthesized. The synthesis started with dissolving aldehydes **40** in anhydrous dichloromethane and adding two equivalents of the drying agent magnesium sulphate. After addition of one equivalent of the primairy amine **41**, the mixture was stirred for two hours at 40 °C to obtain the desired imines **42** in a yield of 96-99%. The used substituents and yields for the formation of (*E*)-*N*-(alkylidene)amines **42** are displayed in Table 3.1.

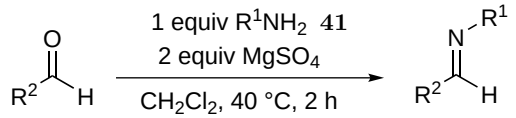

40a–d **42a–d**

Table 3.1: Synthesis of (*E*)-*N*-(alkylidene)amines **42**

Substrate	R^1	R^2	Yield (%)
40a	PMP*	*n*Pr	99
40b	4-FC_6H_4	*n*Pr	99
40c	PMP*	*i*Pr	99
40d	4-FC_6H_4	*i*Pr	96

* PMP=4-methoxyphenyl

3.1.1.2 Synthesis of *cis*-3-acetoxy-4-alkyl-1-arylazetidin-2-ones

The synthesized (*E*)-*N*-(alkylidene)amines **42** were subsequently converted into *cis*-3-acetoxyazetidin-2-ones **44** *via* the Staudinger synthesis (see Chapter 2).

The Staudinger synthesis was performed by dissolving (*E*)-*N*-(alkylidene)amines **42** in anhydrous dichloromethane and adding three equivalents of triethylamine. This mixture was first cooled down to 0 °C in an ice bath. Next, 1.1 equivalent of acetoxyacetyl chloride **43** was added dropwise. The resulting mixture was stirred overnight at room temperature and subsequently purified, using column chromatography on silica gel. When *cis*-3-acetoxy-β-lactams **44** could be isolated (R^2=*i*Pr), an extra recrystallization step was necessary to obtain these compounds in pure form. The *cis*-stereochemistry could be deducted based on the vicinal coupling constant between the C3 and C4 protons in the ^{1}H-NMR-spectra. The synthesized β-lactams showed a coupling constant of 5.2 and 5.3 Hz for C3-C4-proton coupling. Literature reports values of 4.4-5.9 Hz for *cis*-β-lactams,[14,15,84,85] so it can be concluded that indeed *cis*-3-acetoxy-β-lactams **44** were formed. An overview of all substituents and yields can be found in Table 3.2. The last column additionally shows the formed products. Imines **42** are also subject to enamide **45** formation. For imines **42a**,**b**, this leads to a very complex mixture which is why another alkyl side-chain (R^2=*i*Pr) was used. N-(alkylidene)amines **42c** and **42d** still gave rise to 44 and 53% enamide formation, respectively, but at least no complex mixture was obtained.

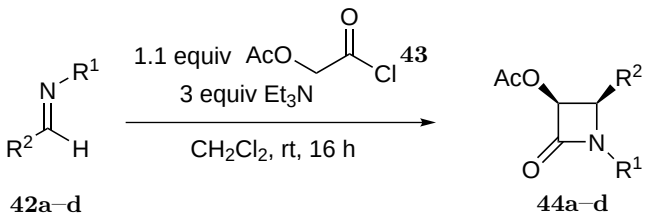

42a–d **44a–d**

Table 3.2: Synthesis of *cis*-3-acetoxy-4-alkyl-1-arylazetidin-2-ones **44**

Substrate	R^1	R^2	Yield (%)	Products
42a	PMP	*n*Pr	-	complex mixture
42b	4-FC_6H_4	*n*Pr	-	complex mixture
42c	PMP	*i*Pr	44[(1)]	56% **44c**, 44% **45c**[(2)]
42d	4-FC_6H_4	*i*Pr	21[(1)]	47% **44d**, 53% **45d**[(2)]

[(1)] After column chromatography (SiO_2) and recrystalization from hexane/EtOAc
[(2)] Percentages based on LC-MS analysis of the crude reaction mixture

For imines **42c**,**d**, the enamide formation is shown below. Nucleophilic addition of imines **42c**,**d** across the acid chloride **43** and subsequent α-deprotonation with respect to the *in situ* formed iminium moiety **46** can account for the formation of the observed enamides **45c**,**d**. Since two hydrogen atoms can be abstracted in case R^2 = *n*Pr, this reactant is very submissive to enamide formation, which can lead to a complex mixture of products. Hence, using an *i*Pr side-chain instead of an *n*Pr one, conversion toward enamides is reduced, probably due to the fact that only one hydrogen atom can be abstracted by the base together with the fact that this group induces steric hindrance. Nevertheless, still 44 and 53 % of the reactant is converted to the corresponding enamide **45c** and **45d**, respectively. Laborious procedure optimization will be needed to avoid enamides **45a**,**b** formation.

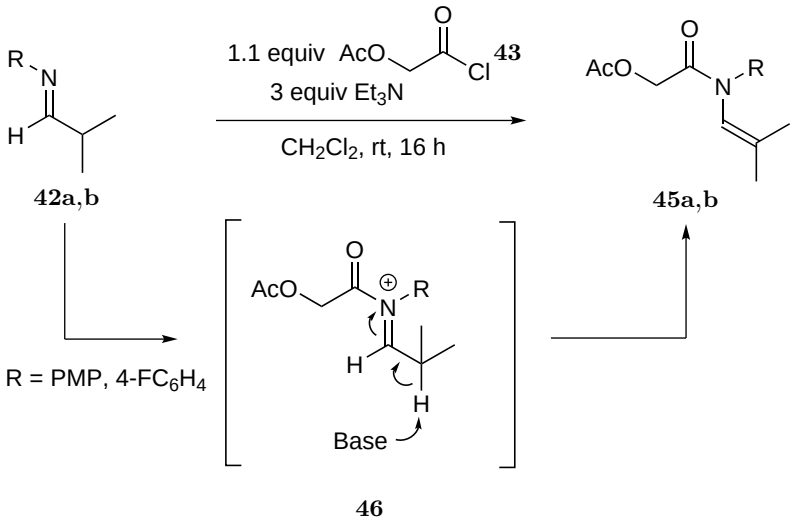

3.1.1.3 Synthesis of *cis*-1-aryl-3-hydroxy-4-isopropylazetidin-2-ones

The synthesized *cis*-3-acetoxy-4-isopropylazetidin-2-ones **44c**,**d**, synthesized in the previous step, were hydrolysed to the corresponding *cis*-3-hydroxyazetidin-2-ones **47a**,**b**. β-Lactams **44** were dissolved in MeOH, a MeOH/H_2O (1/1) mixture or *i*PrOH in addition with 2 equivalents of potassium carbonate. Stirring for a certain time gave rise to *cis*-3-hydroxyazetidin-2-ones **47**. Several conditions were examined for the conversion of the 3-acetoxyazetidin-2-ones **44** and are summarized in Table 3.3.

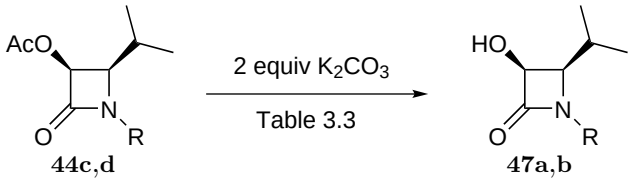

Table 3.3: Synthesis of *cis*-1-aryl-3-hydroxy-4-isopropylazetidin-2-ones **47**

Trial	R	Reaction conditions	Product*
1	PMP	MeOH/H_2O (1/1), rt, 1 h	no conversion
2	PMP	MeOH, rt, 2 h	100% **47a**, yield=55%
3	4-FC_6H_4	MeOH/H_2O (1/1), rt, 1 h	no conversion
4	4-FC_6H_4	MeOH/H_2O (1/1), 0 °C, 1 h	no conversion
5	4-FC_6H_4	MeOH, 0 °C, 15 min	no conversion
6	4-FC_6H_4	MeOH, rt, 3 h	37% **47b**, 63% reactant **44d**
7	4-FC_6H_4	MeOH, 0 °C, 1 h	76% **47b**, 24% reactant **44d**
8	4-FC_6H_4	*i*PrOH, rt, 1 h	76% **47b**, 24% reactant **44d**
9	4-FC_6H_4	*i*PrOH, rt, 12 h	100% **47b**, yield=19%

* Determined by means of LC-MS

Although complete conversion of 3-acetoxyazetidin-2-ones **44** toward 3-hydroxyazetidin-2-ones **47** was observed in trial 2 and 9, the isolated yields are rather low, which could be attributed to the poor work-up method. The multiple washing and extraction stages account for foaming and therefore product loss. Inquiries for work-up optimization should be carried out, but was not possible within

the time frame of this thesis.

3.1.1.4 Synthesis of 1-aryl-4-isopropylazetidine-2,3-diones

The last step in the synthesis of 3-oxoazetidin-2-ones **1** involves an oxidation of the synthesized *cis*-3-hydroxyazetidin-2-ones **47**. A variety of oxidation methods for the oxidation of 3-hydroxyazetidin-2-ones **47** exists. Commonly used methods are the Swern oxidation, Albright-Onodera oxidation, Corey-Kim oxidation and Collins oxidation.[86–89] Based on previous research,[14,15] the Albright-Onodera oxidation was carried out for the oxidation of *cis*-3-hydroxyazetidin-2-ones **47**. This reaction oxidizes hydroxyazetidin-2-ones **47** to azetidine-2,3-diones **1** when the Albright-Onodera reagent, consisting of a P_2O_5 **50** solution in DMSO **48**, is added.[87,90] In this perspective, the reaction is also called the "Fosforpentoxide-aided Moffatt oxidation". P_2O_5 **50** and DMSO **48** generate *in situ* the active oxidans $Me_2{}^+SO(P_2O_5)^-$ **51**. 3-Hydroxy-β-lactams **47** perform a nucleophilic substitution on the activated complex **51** after which the $PO_3{}^-$ anion is eliminated. It is this $PO_3{}^-$ anion that acts as a base for the formation of sulfurylide **53**, which is subsequently transformed into the contemplated azetidine-2,3-diones **1**.

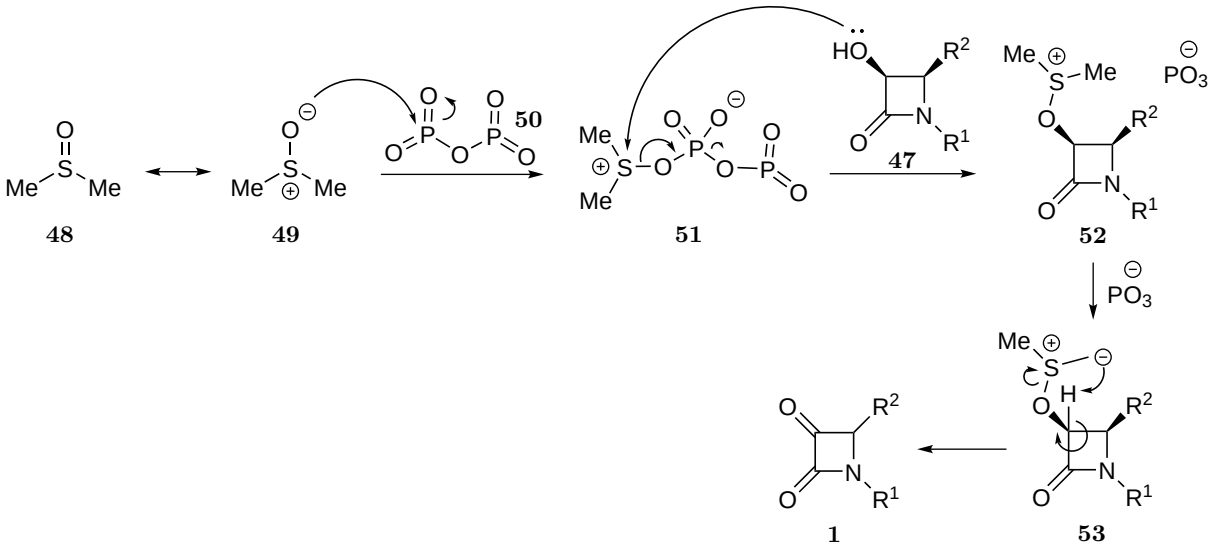

Practically, DMSO and 1.5 equivalents of P_2O_5 were mixed and stirred for ten minutes to activate DMSO. *Cis*-3-hydroxyazetidin-2-ones **47** were dissolved in DMSO and added dropwise to the activated DMSO-complex **51**. The resulting mixture was stirred for 72 hours at 150 °C. In order to remove traces of dimethylsulfoxide, the product was purified by means of column chromatography on silica gel, giving rise to pure 4-isopropylazetidine-2,3-diones **54** at 73-84% yield. Since azetidine-2,3-diones **54** are unstable compounds, they can not be conserved long and should be stored at low temperature (-18 °C) to avoid degradation.

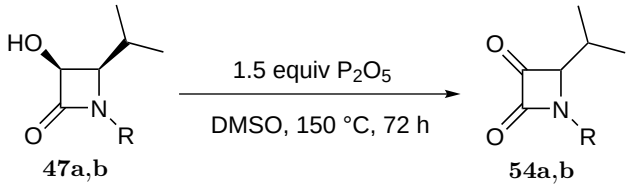

Table 3.4: Synthesis of 4-isopropylazetidin-2,3-diones **54**

Substrate	R	Yield (%)*
47a	PMP	73
47b	4-FC_6H_4	84

* After column chromatography (SiO_2)

3.1.2 Reactivity of azetidine-2,3-diones

The reactivity of azetidine-2,3-diones **1** with respect to primary amines was investigated. Literature and preliminary research at the SynBioC Research Group (Department of Sustainable Organic Chemistry and Technology, Faculty of Bio science Engineering, Ghent University) has shown imination of azetidine-2,3-diones **1** to occur in a complex way. Depending on the substituents (R^1, R^2 and R^3) of azetidine-2,3-diones **1** and the primary amine, the reaction might lead to the formation of other (ring opening) products than the expected 3-iminoazetidin-2-ones **5**. An overview of all reaction pathways and investigated azetidine-2,3-diones **1** of earlier research are shown below.[14–16,83,91]

L. Demeurisse investigated the importance of the C4 aryl substituent for the formation of ethanediamides **4** *via* a C3-C4 ring opening reaction.[15] A final conclusion can be given when alkyl side-chains will be introduced at the C4 carbon atom in combination with an electron donating substituent at the N1 nitrogen atom, showing no ethanediamide **4** formation. In this light, experiments were be carried out to see if 4-isopropyl-1-(4-methoxyphenyl)azetidine-2,3-dione **54a** would react toward the corresponding 3-iminoazetidin-2-one **5**.

Alcaide *et al.* were the first to describe a carbon monoxide elimination reaction in which the N1–C2 and C2–C3 bond of the β-lactam break.[16] Ever since, research by L. Crul and L. Demeurisse has tried to mimic the specific reaction conditions of this article but only traces of the α-aminoamides **3** have been found.[14,15] In this light, the reactivity of 1-(4-fluorophenyl)-4-isopropylazetidine-2,3-dione **54b** with respect to primary amines was tested in order to elucidate the remarkable inconsistency with the literature. On the one hand, the formation of ethanediamides **4** is not expected, since the C4 carbon atom bears no aryl group. The anion stabilizing N1 substituent, on the other hand, makes this β-lactam **54b** a suitable substrate for α-aminoamide **3** formation.

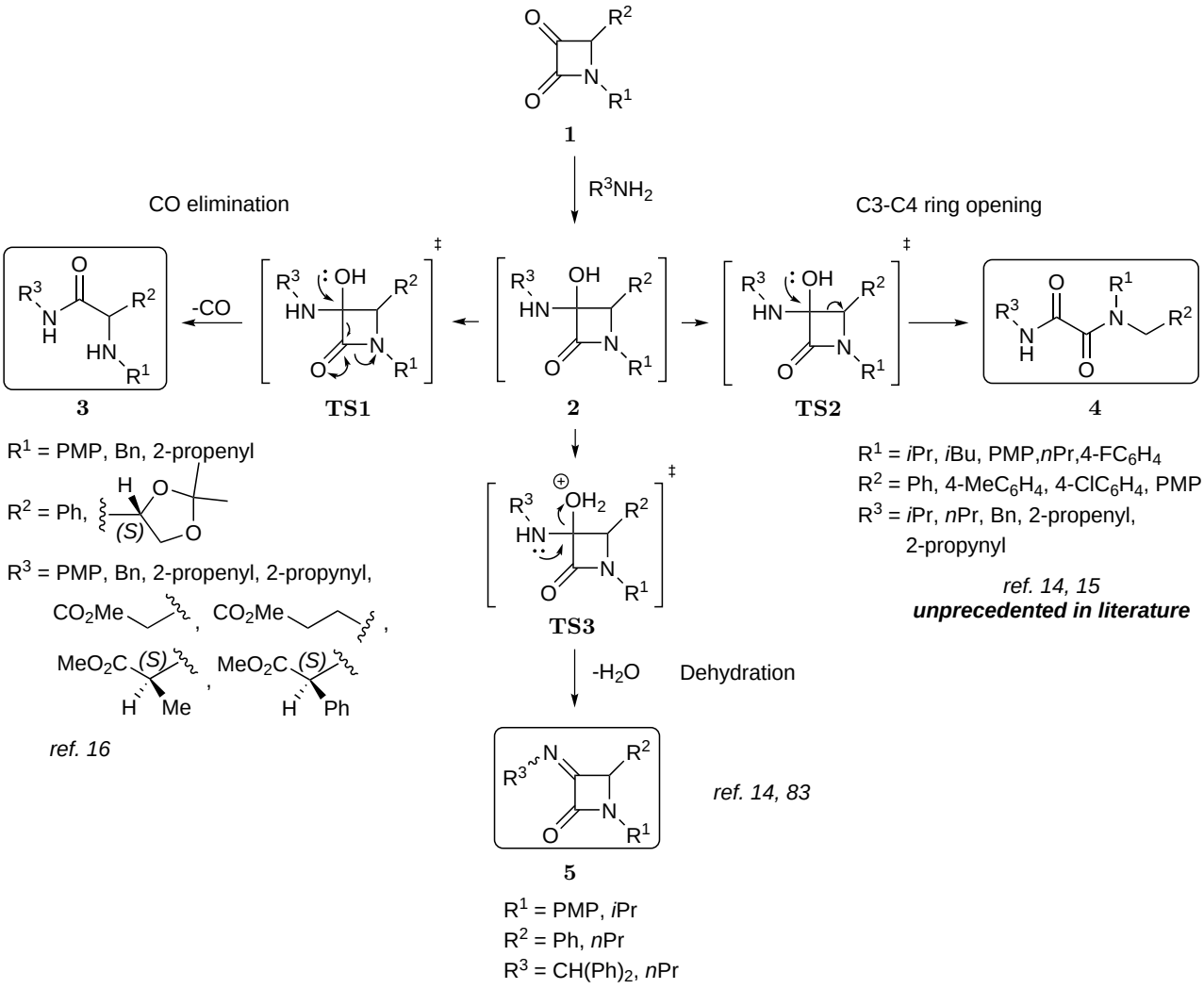

3.1.2.1 Imination of 3-oxoazetidin-2-ones

The reactivity of 1-aryl-4-isopropylazetidin-2,3-diones **54** was explored by adding isopropylamine and two equivalents of magnesium sulphate as drying agent to a solution of azetidine-2,3-diones **54** in dry dichloromethane. Several conditions have been tested to convert 4-isopropylazetidine-2,3-diones **54** and are summarized in Table 3.5.

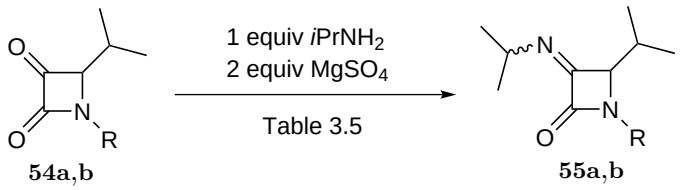

Both **54a** and **54b** explicitly led to the formation of the corresponding 3-isopropylimino-azetidin-2-ones **55**. The synthesized imine compounds **55** proved to be both base and acid stable during washing with 1N sodium hydroxide and column chromatography on silica gel.

Table 3.5: Reaction conditions for reaction of 3-oxo-β-lactams **54** with isopropylamine

Trial	R	x equiv *i*PrNH$_2$	Reaction conditions	Product[(1)]
1	PMP	1	CH_2Cl_2, rt, 2 h	no conversion
2	PMP	10	CH_2Cl_2, rt, 24 h	no conversion
3	PMP	10	THF, Δ, 16 h	no conversion
4	PMP	10	CH_2Cl_2, Δ, 24 h	91% **54a**, 9% **55a**
5	PMP	10	CH_2Cl_2, MW, 60 °C, 2 h	82% **54a**, 18% **55a**
6	PMP	10	CH_2Cl_2, MW, 60 °C, 12 h	29% **54a**, 71% **55a**
7	PMP	10	CH_2Cl_2, MW, 60 °C, 30 h	100% **55a**, yield=95%[(2)]
8	4-FC_6H_4	1	CH_2Cl_2, rt, 2 h	no conversion
9	4-FC_6H_4	10	CH_2Cl_2, rt, 24 h	81% **54b**, 19% **55b**
10	4-FC_6H_4	10	CH_2Cl_2, MW, 60 °C, 18 h	100% **55b**, yield=76%[(2)]

[(1)] Determined by means of LC-MS
[(2)] Yield after four extractions with NaOH

Table 3.6 summarizes the characteristic spectral values for azetidine-2,3-diones **54** and 3-isopropyliminoazetidin-2-ones **55**. Proof for the conversion of azetidine-2,3-diones **54** is deducted from this table in occurrence of new $CH(CH_3)_2$ signals for both ^{1}H-NMR and ^{13}C-NMR, showing introduction of an extra isopropyl group into the molecule. Moreover, the C_3=O signal in the ^{13}C-NMR spectrum of the azetidine-2,3-diones **54** could not be retrieved in the 3-isopropyliminoazetidin-2-ones **55** ^{13}C-NMR spectra, while C=N signals were exclusively retrieved in the latter, showing complete transformation of azetidine-2,3-diones **54**. Proof of 3-isopropylaminoazetidin-2-ones **55** formation was finally deducted *via* LC-MS analysis in which only the mass of the 3-imino-β-lactam was retrieved in the signals and in the absence of characteristic signals in both LC-MS and NMR spectra for α-aminoamides **3** and ethanediamides **4**.

Table 3.6: Characteristic spectral values for azetidine-2,3-diones **54** and 3-isopropyliminoazetidin-2-ones **55**

Compound	^{1}H-NMR (ppm, $CDCl_3$)	^{13}C-NMR (ppm, $CDCl_3$)		
	$C\underline{H}(CH_3)_2$	$\underline{C}H(CH_3)_2$	C_3=O	C_3=N
54a	2.49 (septet x d)	27.2	195.3	-
55a	2.43 (septet x d)	26.8	160.3	156.0
	4.71 (septet)	53.0		
54b	2.49 (septet x d)	27.3	195.1	-
55b	2.44 (septet x d)	26.8	160.0	156.1
	4.70 (septet)	53.2		

3.1.3 Conclusion and outlook

Alkyl chains at the C4 carbon atom and both electron donating (PMP) and withdrawing (4-FC_6H_4) aromatic substituents at the N1 nitrogen atom gave rise to the formation of 3-imino-β-lactams **5**. Hence it can be assumed, taking into account the earlier research concerning the reactivity of 3-oxo-β-

lactams with respect to primary amines, that the only prerequisite for the C3-C4 ring opening reaction is an aromatic C4-substituent.[14,15]

The combination of an alkyl C4 substituent with an electron withdrawing N1 substituent on the azetidine-2,3-dione **54** was expected to give rise to selective α-aminoamide **3** formation.[15] The discrepancy between research by Alcaide *et al.* and other research groups could thus not be explained since the α-aminoamides **3** were never selectively formed in any experiment, but only traces detected.

Computational analysis in the next chapter will attempt to find an explanation for the discrepancy in the literature. The three pathways were investigated with several substituents to find underlying mechanisms for selective formation of α-aminoamides **3**, ethanediamides **4** and 3-imino-β-lactams **55**.

3.2 Materials and methods

3.2.1 Analysing methods

3.2.1.1 Thin-layer chromatography

For the determination of R_f-values, thin-layer chromatography was applied with experimentally determined eluent. Pre-coated silicate plates (Merck Silicagel 60 F_{254}, 0.25 mm thickness) were used for this matter. Detection of non-volatile compounds was performed by using ultraviolet light and/or potassium permanganate.

3.2.1.2 Column chromatography

Purification of reaction mixtures and compounds was performed by means of column chromatography with silica gel as stationary phase (Davisil® Chromatographic Silica Media, 70-200 μm diameter and ca. 4 nm pore diameter). The diameter of the glass column used was adjusted to the amount of product to be purified. The appropriate eluent was determined on the basis of thin-layer chromatography. Elution speed of the reaction mixture to be purified was approximately 5 cm.min^{-1}.

3.2.1.3 Liquid chromatography-Mass spectroscopy

Analysis of both crude reaction mixtures and purified end products was performed by means of liquid chromatography-mass spectroscopy (LC-MS) with an Agilent 1200 series LC/MSD SL apparatus. The apparatus was equipped with a Supelco Ascentic Express C18 column (3 cm length, 4.6 mm internal

diameter), a UV detector, an electrospray ionisation mass spectrometer (ESI, 70 eV) and a quadrupole detector. The applied solvent mixture contained acetonitrile and water.

3.2.1.4 NMR spectroscopy

For ^{1}H-NMR, ^{13}C-NMR and ^{19}F-NMR spectra recordings, a Bruker Avance Nanobay III (400 MHz, 100 MHz, 376 MHz) high resolution NMR-spectrometer was used with a 5 mm BBFO Z-gradient high resolution probe at room temperature. The compounds were solved in deuterated solvent ($CDCl_3$) with tetramethylsilane (TMS) as internal standard. The chemical shift was reported as δ-value in ppm and peaks assigned with the aid of 2D-COSY and HSQC experiments.

3.2.1.5 Mass spectroscopy

Low resolution mass spectroscopic analysis was carried out using an Agilent 1100 Series VL mass spectrometer which is equipped with an electrospray ionization geometry (ES, 70 eV). Detection was performed by a mass selective quadrupole detector.

3.2.1.6 Melting point determination

Using a Kofler-melting point apparatus, type WME Heizbank of Wagner and Munz, the melting point of solid compounds could be determined. The melting apparatus has a temperature gradient of 50 to 260 °C. The apparatus is calibrated first, using different standards, each having a specific melting point. After calibration, the crystals are put on the cold side of the melting bench and are moved slowly to the warmer side until the crystals melt. This is the component's melting point.

3.2.2 Microwave reactor

Microwave reactions were carried out in a CEM Discover Benchmate microwave reactor, provided with a Synergy-software, which made it possible to set a specific time and temperature. Special thick-walled vials and septum were used to carry out the reactions in this reactor.

3.2.3 Dry solvents

Dichloromethane (CH_2Cl_2) was dried by distillation in the presence of calcium hydride. Tetrahydrofuran (THF) was distilled as well, using sodium fiber in the presence of benzophenone as water indicator for the drying process.

3.2.4 Safety

3.2.4.1 General safety features

In the context of safety and health, every aspect in this Master dissertation was carried out in agreement with the 'Internal guidelines' and 'Safety instructions' provided by the SynBioC research group (Department of Sustainable Organic Chemistry and Technology, Faculty of Bio science Engineering, Ghent University). Before commencement of the experiments, the Material Safety Data Sheet (MSDS) for every used reagent and solvent was consulted. Moreover, special precautions were taken in case of handling hazardous devices or reagents to guarantee optimal safety. Maximal investment in personal protection and security of close-by workers was provided.

3.2.4.2 Specific safety risks

Prepatory to setting up reactions, safe alternatives to harmful chemicals and solvents were always sought for. For some cases, it seemed inevitable to avoid the use of certain chemicals, thus handling them under every needed precaution. The most important risky reagents and solvents are listed below with according chemical, physical and environmental effects.

Acetoxyacetyl chloride

Acetoxyacetyl chloride is known as very corrosive and irritating. It should be kept away from any water and may cause burns to skin or irritation to eyes and inhalation tissue. Regarding the high volatility and utmost damaging health effects, complete personal protection in a ventilated space (fume hood) is necessary when handling this substance.

Isopropylamine

Isopropylamine possesses extremely flamable and hygroscopic properties with a strong ammonia odor. Extra precautions when heating have to be respected as this may cause release of poisonous nitrogen oxides and hydrogen cyanide. A face mask and protection gloves should be worn and residues of the compound collected in separate waste containers in view of toxicity for the environment.

Phosphorus pentoxide (P_2O_5)

Phosphorus pentoxide reacts exothermically with water and has corrosive and irritating properties. The reagent can cause severe burns if contacted with skin due to formation of phosphoric acid. There-

fore, protection golves are mandatory when handling phosphorous pentoxide.

Dichloromethane (CH_2Cl_2

) Dichloromethane may cause cancer as well as eye and skin irritation. When inhaled, respiratory tract irritation could occur. It reacts vigorously with active metals such as lithium, sodium and potassium, and with strong bases such as potassium tert-butoxide.

Siliciumdioxide (SiO_2)

Silica gel is used as chromatographic solid phase and bears irritating properties for both eyes and respiratory ways. Complete personal protection is necessary.

3.2.5 Experiments description

3.2.5.1 Synthesis of *cis*-3-acetoxy-1-aryl-4-isopropylazetidin-2-ones 44

The synthesis of *cis*-3-acetoxy-4-isopropyl-1-(4-methoxyphenyl)azetidin-2-one **44c** serves as an example for the synthesis of *cis*-3-acetoxy-1-aryl-4-isopropylazetidin-2-ones **44**.
In a flask of 250 mL, 8.86 g (50 mmol) (*E*)-*N*-(alkylidene)amine **42c** is dissolved in 50 mL anhydrous CH_2Cl_2 with subsequent addition of 15.18 g (150 mmol; 3 equiv) triethylamine. After cooling down the reaction mixture to 0 °C in an ice bath, a solution of 7.51 g (55 mmol; 1.1 equiv) acetoxyacetyl chloride in 10 mL anhydrous CH_2Cl_2 is added dropwise. After stirring for 16 hours at room temperature, the reaction mixture was poured into water (30mL) and extracted with CH_2Cl_2 (10mL). The organic phase was subsequently poured into HCl (30mL) and extracted again with CH_2Cl_2 (10mL). The organic phase is dried ($MgSO_4$), filtered of the drying agent and the solvent removed *in vacuo*. This is further purified by means of column chromatography with petroleumether/ethyl acetate eluent (7/2) and recrystallized from ethyl acetate/hexane (5/1), which afforded 6.09 g (44%) *cis*-3-acetoxy-4-isopropyl-1-(4-methoxyphenyl)azetidin-2-one **xiia**.

***Cis*-3-acetoxy-4-isopropyl-1-(4-methoxyphenyl)azetidin-2-one 44c**

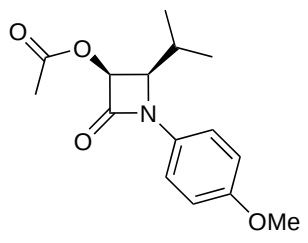

^{1}**H-NMR** (400 MHz, $CDCl_3$): δ 0.97 and 1.00 (2 x 3H, 2 x d, J = 6.9 Hz, $CH(C\underline{H}_3)_2$); 2.18-2.29 (1H, m, $C\underline{H}(CH_3)_2$); 2.18 (3H, s, $CH_3C{=}O$); 3.79 (3H, s, CH_3O); 4.22 (1H, ~t, J = 5.4 Hz, CHN); 6.04 (1H, d, J = 5.4 Hz, CHO); 6.88 (2H, d, J = 9.0 Hz, $CH_3O(C\underline{H}_{arom})_{ortho}$); 7.34 (2H, d, J = 9.0 Hz, $CH_3O(C\underline{H}_{arom})_{meta}$). ^{13}**C-NMR** (100 MHz, $CDCl_3$): δ 18.83 and 18.84 ($CH(\underline{C}H_3)_2$); 20.7 ($\underline{C}H_3C{=}O$); 28.4 ($\underline{C}H(CH_3)_2$); 55.5 (CH_3O); 62.7 (CHN); 73.9 (CHO); 114.4 ($CH_3O(H\underline{C}_{arom})_{ortho}$); 119.8 ($CH_3O(H\underline{C}_{arom})_{meta}$); 130.6 ($NC_{arom,quat}$);

156.8 ($CH_3O\underline{C}_{arom,quat}$); 162.9 and 169.6 (NC=O, $CH_3\underline{C}$=O). **MS** (70 eV): m/z (%) 278 (M^++1, 44). Light-brown crystals. R_f = 0.25 (PE/EtOAc 7/2). Yield after column chromatography (SiO_2) and recrystallization (EtOAc/PE 5/1): 44%. T_m = 84°C.

***Cis*-3-acetoxy-1-(4-fluorophenyl)-4-isopropylazetidin-2-one 44d**

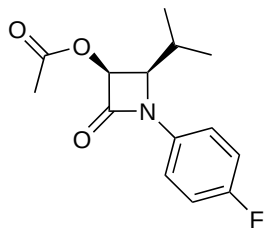

^{1}H-NMR (400 MHz, $CDCl_3$): δ 0.98 and 1.01 (2 x 3H, 2 x d, J = 6.9 Hz, $CH(C\underline{H}_3)_2$); 2.19-2.31 (1H, m, $C\underline{H}(CH_3)_2$); 2.19 (3H, s, CH_3C=O); 4.24 (1H, ~t, J = 5.5 Hz, CHN); 6.07 (1H, d, J = 5.5 Hz, CHO); 7.05 (2H, ~t, J = 8.7 Hz, $F(CH_{arom})_{ortho}$); 7.39 (2H, d x d, J = 8.7, 4.6 Hz, $F(CH_{arom})_{meta}$). **^{19}F-NMR** (376 MHz, $CDCl_3$): δ (-116.66)-(-116.60) (m, FC_{quat}). **^{13}C-NMR** (100 MHz, $CDCl_3$): δ 18.8 and 18.9 ($CH(\underline{C}H_3)_2$); 20.7 ($\underline{C}H_3C$=O); 28.4 ($\underline{C}H(CH_3)_2$); 62.8 (CHN); 73.8 (CHO); 116.0 (d, J = 22.8 Hz, $F(HC_{arom})_{ortho}$); 119.8 (d, J = 8.0 Hz, $F(HC_{arom})_{meta}$); 133.5 (d, J = 2.8 Hz, $NC_{arom,quat}$); 159.6 (d, J = 244.9 Hz, FC_{quat}); 163.1 and 169.5 (NC=O, $CH_3\underline{C}$=O). **MS** (70 eV): m/z (%) 266 (M^++1, 41). White crystals. R_f = 0.25 (PE/EtOAc 4/1). Yield after column chromatography (SiO_2) and recrystallization (EtOAc/PE 5/1): 21%. T_m = 84°C.

3.2.5.2 Synthesis of *cis*-1-aryl-3-hydroxy-4-isopropylazetidin-2-ones 47

The synthesis of *cis*-3-hydroxy-4-isopropyl-1-(4-methoxyphenyl)azetidin-2-one **47a** serves as an example for the synthesis of *cis*-1-aryl-3-hydroxy-4-isopropylazetidin-2-ones **47**.

In a flask of 250 mL, 13.85 g (50 mmol) *cis*-3-acetoxy-4-isopropyl-1-(4-methoxyphenyl)azetidin-2-one **44c** is dissolved in 50 mL *i*PrOH. 13.82 g (100 mmol; 2 equiv) K_2CO_3 is added to the reaction mixture and stirred at room temperature for 24 hours. The solvent is removed *in vacuo* and the residue redissolved in diethyl ether (20 mL). The organic fraction is washed twice with water (50 mL) and afterwards, the water fraction is extracted twice with diethyl ether (50 mL). The combined organic fractions are dried with $MgSO_4$, filtered of the drying agent and the solvent removed *in vacuo*. The recrystallization in a mixture of ethyl acetate/hexane (30/1) afforded 6.47 g (55%) *cis*-3-hydroxy-4-isopropyl-1-(4-methoxyphenyl)azetidin-2-one **47a**.

***Cis*-3-hydroxy-4-isopropyl-1-(4-methoxyphenyl)azetidin-2-one 47a**

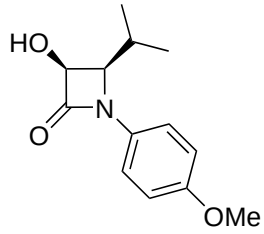

^{1}H-NMR (400 MHz, $CDCl_3$): δ 1.04 and 1.08 (2 x 3H, 2 x d, J = 6.9 Hz, $CH(C\underline{H}_3)_2$); 2.32 (1H, ~octet, J = 6.9 Hz, $C\underline{H}(CH_3)_2$); 3.79 (3H, s, CH_3O); 4.07 (1H, d x d, J = 6.9, 5.6 Hz, CHN); 4.32 (1H, d, J = 5.6 Hz, OH); 5.08 (1H, ~t, J = 5.6 Hz, CHO); 6.86 (2H, d, J = 9.0 Hz, $CH_3O(C\underline{H}_{arom})_{ortho}$); 7.33 (2H, d, J = 9.0 Hz, $CH_3O(C\underline{H}_{arom})_{meta}$). **^{13}C-NMR** (100 MHz, $CDCl_3$): δ 19.0 and 19.6 ($CH(\underline{C}H_3)_2$); 28.7 ($\underline{C}H(CH_3)_2$); 55.5 (CH_3O); 64.1 (CHN); 75.3 (CHO); 114.3 ($CH_3O(H\underline{C}_{arom})_{ortho}$); 120.0 ($CH_3O(H\underline{C}_{arom})_{meta}$); 130.9 ($NC_{arom,quat}$); 156.6 ($CH_3O(\underline{C}_{arom,quat})$; 168.1 (C=O). **MS** (70 eV): m/z (%) 236 (M^++1, 100). White crystals. Yield

after recrystallization from EtOAc/hexane (30/1): 55%. T_m = 170°C.

***Cis*-1-(4-fluorophenyl)-3-hydroxy-4-isopropylazetidin-2-one 47b**

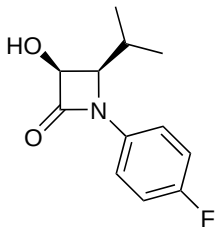

^{1}**H-NMR** (400 MHz, $CDCl_3$): δ 1.05 and 1.09 (2 x 3H, 2 x d, J = 6.9 Hz, $CH(C\underline{H}_3)_2$); 2.32 (1H, ~octet, J = 6.9 Hz, $C\underline{H}(CH_3)_2$); 3.14 (1H, d, J = 6.2 Hz, OH); 4.08 (1H, d x d, J = 6.9, 5.5 Hz, CHN); 5.08 (1H, d x d, J = 6.2, 5.5 Hz, CHO); 7.03 (2H, ~t, J = 8.8 Hz, $F(CH_{arom})_{ortho}$); 7.38 (2H, d x d, J = 8.8, 4.7 Hz, $F(CH_{arom})_{meta}$). ^{19}**F-NMR** (376 MHz, $CDCl_3$): δ (-117.15)-(-117.08) (m, FC_{quat}). ^{13}**C-NMR** (100 MHz, $CDCl_3$): δ 19.0 and 19.5 ($CH(\underline{C}H_3)_2$); 28.6 ($\underline{C}H(CH_3)_2$); 64.1 (CHN); 75.4 (CHO); 115.9 (d, J = 22.7 Hz, $F(HC_{arom})_{ortho}$); 119.9 (d, J = 8.0 Hz, $F(HC_{arom})_{meta}$); 133.7 (d, J = 2.8 Hz, $NC_{arom,quat}$); 159.5 (d, J = 244.3 Hz, FC_{quat}); 168.2 (C=O). **MS** (70 eV): m/z (%) 224 (M^++1, 100). White crystals. Yield after recrystallization from EtOAc/hexane (30/1): 21%. T_m = 162°C.

3.2.5.3 Synthesis of 1-aryl-4-isopropylazetidine-2,3-diones 54

The synthesis of 4-isopropyl-1-(4-methoxyphenyl)azetidine-2,3-dione **54a** serves as an example for the synthesis of 1-aryl-4-isopropylazetidine-2,3-diones **54**.

In a flask of 100 mL, 35 mL dimethylsulphoxide and 2.13 g P_2O_5 (7.5 mmol; 1.5 equiv) are mixed. After ten minutes of stirring at room temperature, a solution of 1.18 g *cis*-3-hydroxy-4-isopropyl-1-(4-methoxyphenyl)azetidin-2-one **47a** (5 mmol; 1 equiv) in 20 mL dimethylsulphoxide is added dropwise. After stirring for 72 hours at 150 °C, the reaction mixture was allowed to cool to room temperature and then neutralized with saturated $NaHCO_3$ solution (20 mL). The mixture is extracted four times with ethyl acetate (20 mL) and the combined organic fractions washed with brine (50 mL) and distilled water (50 mL). After drying with $MgSO_4$, filtering of the drying agent and evaporation of the solvent *in vacuo*, the mixture is purified by means of column chromatography with ethyl acetate/petroleum ether eluent (2/5) to give rise to 851 mg (73%) 4-isopropyl-1-(4-methoxyphenyl)azetidine-2,3-dione **54a**.

4-Isopropyl-1-(4-methoxyphenyl)azetidine-2,3-dione 54a

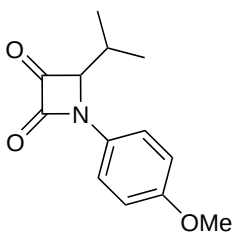

^{1}**H-NMR** (400 MHz, $CDCl_3$): δ 0.91 and 1.19 (2 x 3H, 2 x d, J = 7.0 Hz, $CH(C\underline{H}_3)_2$); 2.49 (1H, septet x d, J = 7.0, 4.0 Hz, $C\underline{H}(CH_3)_2$); 3.84 (3H, s, CH_3O); 4.60 (1H, d, J = 4.0, CHN); 6.96 (2H, d, J = 9.1 Hz, $CH_3O(C\underline{H}_{arom})_{ortho}$); 7.52 (2H, d, J = 9.1 Hz, $CH_3O(C\underline{H}_{arom})_{meta}$). ^{13}**C-NMR** (100 MHz, $CDCl_3$): δ 16.3 and 18.5 ($CH(\underline{C}H_3)_2$); 27.2 ($\underline{C}H(CH_3)_2$); 55.6 (CH_3O); 76.5 (CHN); 114.8 ($CH_3O(H\underline{C}_{arom})_{ortho}$); 119.3 ($CH_3O(H\underline{C}_{arom})_{meta}$); 130.0 ($NC_{arom,quat}$); 158.0 and 159.9 ($CH_3O\underline{C}_{arom,quat}$, NC=O); 195.3 ($CH\underline{C}$=O). **MS** (70 eV): m/z (%) 234 (M^++1, 100). Yellow crystals. R_f = 0.30 (PE/EtOAc 5/2). Yield after column chromatography (SiO_2): 73%. T_m = 96°C.

1-(4-Fluorophenyl)-4-isopropylazetidine-2,3-dione 54b

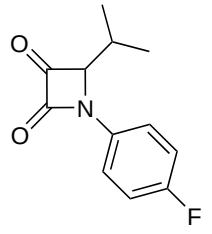

^{1}**H-NMR** (400 MHz, $CDCl_3$): δ 0.92 and 1.20 (2 x 3H, 2 x d, J = 6.9 Hz, $CH(C\underline{H}_3)_2$); 2.49 (1H, septet x d, J = 6.9, 4.1 Hz, $C\underline{H}(CH_3)_2$); 4.63 (1H, d, J = 4.1 Hz, CHN); 7.15 (2H, d x d, J = 9.0, 8.3 Hz, $F(CH_{arom})_{ortho}$); 7.57 (2H, d x d, J = 9.0, 4.7 Hz, $F(CH_{arom})_{meta}$). ^{19}**F-NMR** (376 MHz, $CDCl_3$): δ (-113.86)-(-113.80) (m, FC_{quat}). ^{13}**C-NMR** (100 MHz, $CDCl_3$): δ 16.3 and 18.5 ($CH(\underline{C}H_3)_2$); 27.3 ($\underline{C}H(CH_3)_2$); 76.6 (CHN); 116.6 (d, J = 22.9 Hz, $F(HC_{arom})_{ortho}$); 119.4 (d, J = 8.1 Hz, $F(HC_{arom})_{meta}$); 132.8 (d, J = 2.9 Hz, $NC_{arom,quat}$); 160.1 (NC=O); 160.5 (d, J = 247.4 Hz, FC_{quat}); 195.1 ($CH\underline{C}$=O). **MS** (70 eV): m/z (%) 239 (M^++NH_4, 31). Yellow crystals. R_f = 0.24 (PE/EtOAc 5/2). Yield after column chromatography (SiO_2): 84%. T_m = 102°C.

3.2.5.4 Synthesis of 1-aryl-4-isopropyl-3-isopropylimino-azetidin-2-ones 55

The synthesis of 4-isopropyl-3-isopropylimino-1-(4-methoxyphenyl)azetidin-2-one **55a** serves as an example for the synthesis of 1-aryl-4-isopropyl-3-isopropylimino-azetidin-2-ones **55**.

In a microwave vial, 47 mg (0.2 mmol) 4-isopropyl-1-(4-methoxyphenyl)azetidine-2,3-dione **54a** is dissolved in 20 mL anhydrous CH_2Cl_2 and mixed with 48 mg (0.4 mmol; 2 equiv) magnesium sulphate. After addition of 0.16 mL isopropylamine, the mixture is put in the microwave at 60 °C for 30 hours. After reaction, the mixture is filtered of the drying agent and the solvent evaporated *in vacuo*. The product is washed four times with 1N NaOH (10mL) and ethyl acetate (10 mL). After evaporation of the solvent *in vacuo*, 55.9 mg (95%) 4-isopropyl-3-isopropylimino-1-(4-methoxyphenyl)azetidin-2-one **55a** was isolated.

4-Isopropyl-3-isopropylimino-1-(4-methoxyphenyl)azetidin-2-one 55a

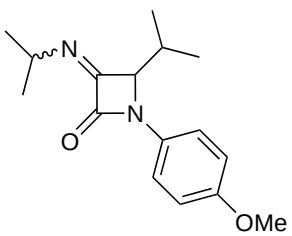

^{1}**H-NMR** (400 MHz, $CDCl_3$): δ 0.90 and 1.16 (2 x 3H, 2 x d, J = 6.9 Hz, $CHCH(C\underline{H}_3)_2$); 1.246 and 1.254 (2 x 3H, 2 x d, J = 6.3 Hz, $NCH(C\underline{H}_3)_2$); 2.43 (1H, septet x d, J = 6.9, 3.5 Hz, $CHC\underline{H}(CH_3)_2$); 3.81 (3H, s, CH_3O); 4.49 (1H, d, J = 3.5 Hz, CHN); 4.71 (1H, septet, J = 6.3 Hz, $NC\underline{H}(CH_3)_2$); 6.92 (2H, d, J = 9.0 Hz, $CH_3O(C\underline{H}_{arom})_{ortho}$); 7.43 (2H, d, J = 9.0 Hz, $CH_3O(C\underline{H}_{arom})_{meta}$). ^{13}**C-NMR** (100 MHz, $CDCl_3$): δ 15.0 and 17.4 ($CHCH(\underline{C}H_3)_2$); 23.0 and 23.4 ($NCH(\underline{C}H_3)_2$); 26.8 ($CH\underline{C}H(CH_3)_2$); 53.0 ($N\underline{C}H(CH_3)_2$)); 54.5 (CH_3O); 67.4 (CHN); 113.6 ($CH_3O(H\underline{C}_{arom})_{ortho}$); 118.0 ($CH_3O(H\underline{C}_{arom})_{meta}$); 129.5 ($NC_{arom,quat}$); 155.96 and 155.99 ($CH_3O\underline{C}_{arom,quat}$, C=N); 160.3 (C=O). **MS** (70 eV): m/z (%) 275 (M^++1, 100). Yellow oil. R_f = 0.25 (PE/EtOAc 5/1). Yield: 95%.

1-(4-Fluorophenyl)-4-isopropyl-3-(isopropylimino)azetidin-2-one 55b

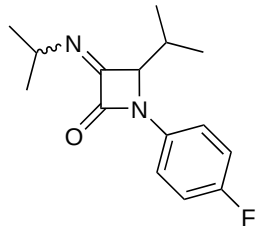

^{1}**H-NMR** (400 MHz, $CDCl_3$): δ 0.91 and 1.17 (2 x 3H, 2 x d, J = 6.9 Hz, $CHCH(C\underline{H}_3)_2$); 1.25 and 1.26 (2 x 3H, 2 x d, J = 6.3 Hz, $NCH(C\underline{H}_3)_2$); 2.44 (1H, septet x d, J = 6.9, 3.6 Hz, $CHC\underline{H}(CH_3)_2$); 4.51 (1H, d, J = 3.6 Hz, CHN); 4.70 (1H, septet, J = 6.3 Hz, $NC\underline{H}(CH_3)_2$); 7.09 (2H, d x d, J = 9.0, 8.5 Hz, $F(C\underline{H}_{arom})_{ortho}$); 7.47 (2H, d x d, J = 9.0, 4.7 Hz, $F(C\underline{H}_{arom})_{meta}$). ^{19}**F-NMR** (376 MHz, $CDCl_3$): δ (-116.16)-(-116.09) (m, FC_{quat}). ^{13}**C-NMR** (100 MHz, $CDCl_3$): δ 14.9 and 17.4 ($CHCH(\underline{C}H_3)_2$); 22.9 and 23.4 ($NCH(\underline{C}H_3)_2$); 26.8 ($CH\underline{C}H(CH_3)_2$); 53.2 ($N\underline{C}H(CH_3)_2$)); 67.5 (CHN); 115.2 (d, J = 22.8 Hz, $F(HC_{arom})_{ortho}$); 118.1 (d, J = 8.0 Hz, $F(HC_{arom})_{meta}$); 132.3 (d, J = 2.8 Hz, $NC_{arom,quat}$); 156.1 (C=N); 158.7 (d, J = 245.2 Hz, FC_{quat}); 160.0 (C=O). **MS** (70 eV): m/z (%) 263 (M^++1, 100). Yellow oil. R_f = 0.27 (PE/EtOAc 5/1). Yield: 76%.

Chapter 4

Computational Results

In this chapter, molecular modeling will be used to further investigate the different reaction pathways, introduced in Chapter 1. This field has been developed over the last 35 years and was introduced as a new section of chemistry called theoretical or computational chemistry.[92] Physical and chemical properties of microscopic molecular systems can be calculated and subsequently used to predict macroscopic properties of the systems. Hence, theoretical chemistry hands the chemist an extra tool to rationalize experimental results or even predict the experimental outcome with sophisticated computer-based simulations. First, the computational methods used in this work will be discussed. These techniques will afterwards be used to investigate the reactivity of 3-oxo-β-lactams and results reported and discussed.

4.1 Computational methods

Molecular modeling techniques can be divided into three categories: ab initio methods, semi-empirical methods and molecular mechanics. Ab initio methods, which are based on quantum mechanics, are often the most accurate models but they have a high computational cost. Semi-emperical methods on the other hand are based on both quantum mechanics and empirical data, reducing the computational effort. The last class, molecular mechanics, differs from the previous techniques since it is based on classical physics with relative simple equations to significantly reduce the computational cost compared to ab initio and semi-emperical methods. In this dissertation, only the first approach, ab initio calculations, will be performed. The class of ab initio methods consists of three different methods: Hartree-Fock methods, post-Hartree-Fock methods and Density Functional Theory.

4.1.1 (Post-) Hartree-Fock Method (HF)

The Hartree-Fock (HF) theory is a many-body technique in which the electronic wave function is written as a Slater determinant of one electron orbitals called molecular orbitals (MO). Writing the electronic wave function as a Slater determinant satisfies the exclusion principle (anti-symmetry) as introduced by Pauli which states that two identical particles cannot occupy the same quantum state, i.e. cannot have the four same quantum numbers. Within, the Hartree-Fock method, the set of molecular orbitals that minimizes the ground state energy of the system is determined. These molecular orbitals are expressed as a linear combination of a set of given basis functions, usually atom-centered Gaussian type functions, also called "atomic orbitals". Furthermore, each atomic orbital is written as a linear combination of Gaussian type orbitals (GTOs).[93]

In order to obtain the lowest energy electronic wave function, the coefficients of these linear combinations are varied. This iterative optimization is a self-consistent field (SCF) method and gives the HF wave function and energy.[94] HF is a fast calculation method but is not as accurate as the other ab initio calculations.

Post-Hartree-Fock methods differ from HF because they add electron-electron correlations in the Hamiltonian. In this case, the electronic wave function is written as a linear combination of multiple Slater determinants.[95] This makes this method more accurate but requires a lot more computational effort. A common method is the Møller-Plesset perturbation theory in which the eigenfunctions and eigenvalues are written as power series in undisturbed HF-functions and energies. This series can be trucated after a given number of terms, giving rise to MPn methods (MP2, MP3).[96,97]

4.1.2 Density Functional Theory (DFT)

The most popular molecular modeling method today is Density Functional Theory (DFT). This theory differs from previously mentioned theories because it is based on the electron density instead of wave functions of many-body systems. This approach is more useful for bigger systems since post-HF-systems are computationally too expensive. Hohenberg and Kohn provided a good foundation for this theory with two theorems.[98,99] The first Hohenberg-Kohn theorem states that the electron density uniquely determines the Hamiltonian operator and thus all the properties of the system. The second Hohenberg-Kohn theorem states that the energy as a functional of the density only attains its minimum value when the input density is that of the ground state. Hence, DFT is only applicable to ground

states and not to excited states, but its applicability ranges from atoms, molecules and solids to nuclei and quantum and classical fluids. Since the exact form of this functional is not known, a lot of different functionals have been proposed over the years. Each of these has a different applicability and provides accurate energies and/or geometries for a limited set of systems.

DFT-methods are able to make very accurate predictions of molecular energies and activation barriers. On top of that, they are more time efficient than post-HF methods. This makes DFT the method of choice to study a variety of ground state molecular properties like vibrational frequencies, atomization and ionization energies, electronic and magnetic properties, etc.[100]

Since DFT is computationally less demanding than post-HF methods and provides reliable energies and geometries, this will be the only method used in this work. All geometry optimizations and energy calculations are performed with the M06-2X functional and the 6-31+G(d,p) basis set. This functional is accurate for main group thermochemistry, kinetics and non-covalent interactions.[101]

4.1.3 Solvation

The solvent environment can be introduced into the calculations by means of two possible solvation methods: explicit solvation or implicit solvation. Explicit solvation on one hand is used when the solvent molecules are known to be able to interact explicitly with the substrate. The discrete solvent molecules are placed around the chemically active species to form a so-called "supermolecule" structure.[27] In implicit solvation on the other hand, the solvent is modeled as a continuous medium instead of individual explicit solvent molecules.

When using implicit solvation, the system under study is placed in a cavity in an continuous medium, characterized by a dielectric constant (ϵ). The advantage of this method is that it takes into account potential long-range interactions with the solvent environment. Nevertheless, it fails to account for the local fluctuations in solvent density around a solute molecule called first-solvation-shell effects.[102] The solvent molecules in the region close to the solute posses different properties (bulk-dielectric treatment, dispersion interaction, hydrogen bonding, charge transfer and the hydrophobic effect) than those in the bulk. These properties are difficult to take into account when using implicit solvation.[103]

The electrostatic interaction of a solute with the solvent depends upon the charge distribution and polarizability of the solute. The induced polarization of the molecule in the continuum creates a reaction field which changes the wave function and can be solved by self-consistent reaction field

(SCRF). The polarized continuum model (PCM) is the nowadays frequently used method.[104] A PCM variant will be used throughout this work called integral equation formalism PCM (IEF-PCM).[105,106]

Besides explicit and implicit solvation, a mixed implicit/explicit solvation model can be used. This model was first proposed by Frisch *et al.* and concerns a layer or sphere of solvent molecules around the solute, while modeling the bulk with an implicit solvent.[107] The implicit solvation can be taken into account during the geometry optimization with explicit solvent molecules or when calculating the energy of a geometry that was previously optimized. Using this mixed solvation model, both short- and long-term interactions are taken into account.

4.2 Computational methodology

All geometry optimizations and frequency caluclations were performed with the DFT functional M06-2X[101] with a 6-31+G(d,p) basis set. Stationary points were characterized as either minima, in the case of stable reactants and products, or first-order saddle points, in the case of transition states, by means of frequency calculations. When the transition state of a certain reaction was found, it was connected with the corresponding reactants and products *via* intrinsic reaction coordinate (IRC) calculations[108] followed by full geometry optimizations. For calculations including a solvent environment, IEF-PCM implicit solvation was used. All Gibbs free energies are reported with respect to separate reactants. The pre-reactive complex, which is the configuration of the reactants before onset of the reaction, will be denoted by its abbreviation PRC.

The DFT calculations were performed with the Gaussian 09[109] program package. Visualization of geometries was done with the Cylview[110] freeware package.

4.3 Results and discussion

Scheme 1.1 in Chapter 1 gives an overview of the possible reactions of 3-oxo-β-lactams **1** with respect to primary amines. The first step involves the amination of 3-oxo-β-lactams **1** to form 3-amino-3-hydroxy-β-lactams **2**. In the second step, multiple reactions can occur. In the first reaction path, the carbon monoxide elimination reaction yields α-aminoamides **3** by eliminating carbon monoxide. The second reaction path, the C3–C4 ring opening reaction cleaves the β-lactam ring at the C3-C4 bond to form ethanediamides **4**. In the last reaction path, H_2O is expelled to form 3-imino-β-lactams **5**, during the dehydration reaction. The amination step in combination with the dehydration reaction is also known as the imination reaction of 3-oxo-β-lactams **1**. The reaction path that will be followed, is dependent on the 3-oxo-β-lactam **1** substituents. The aim of this theoretical study is primarly to find the exact mechanism of the three reactions. Secondly, computational results will be compared to experimental results to validate the model.

To start with, a simple system was chosen in order to locate the different pathways. The N1 and C4 atoms of the 3-oxo-β-lactam **1a** are methylated and methylamine **56** was chosen as a simple primary amine ($R^1 = R^2 = R^3 = Me$ in Scheme 1.1). Later on, these methyl groups will be replaced by more realistic ones to make the comparison with experimental results possible.

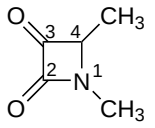

1a

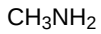

56

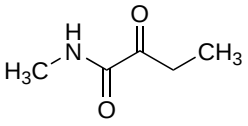

57

4.3.1 Amination

The first step in the reaction of 3-oxo-β-lactams **1** involves their amination, yielding 3-amino-3-hydroxy-β-lactams **2**. In order to investigate the influence of a β-lactam ring during the amination reaction, this reaction was compared to the amination of the corresponding acyclic compound **57**, which is formed by opening the 3-oxo-β-lactam **1a** ring at the N1–C4 bond. Both reactions were studied computationally *in vacuo* and the Gibbs free energy profiles shown in Figure 4.1. The Gibbs free activation barriers are 134.2 and 125.6 kJ.mol^{-1} for the acyclic compound **57** and the 3-oxo-β-lactam **1a**, respectively. From these calculations, it can be concluded that there is no preference for amination of 3-oxo-β-lactam **1a** over the acyclic compound **57**. Later on, calculations in the solvent environment will be discussed and compared to these *in vacuo* results.

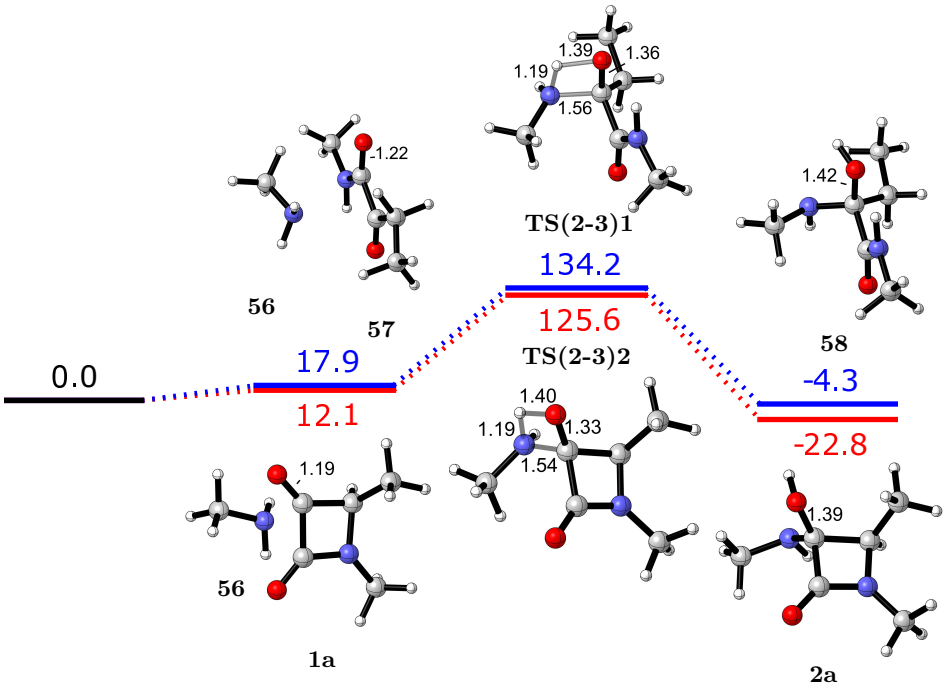

Figure 4.1: Gibbs free energy profiles for the amination of 3-oxo-β-lactam **1a** **(red)** and N-methyl-2-oxo-butanamide **57** **(blue)** *in vacuo* (M06-2X/6-31+G(d,p), 298 K, 1 atm, energies in kJ.mol^{-1}, bond lengths in Å)

In the following, the subsequent reactions from 3-amino-3-hydroxy-β-lactams **2** to either α-aminoamide **3**, ethanediamides **4** or 3-imino-β-lactam **5** will be investigated. First, calculations without the aid of a second molecule will be discussed, followed by the calculations with assisting molecules. Next, the influence of the solvent is explored.

4.3.2 Calculations without the aid of an extra molecule

First of all, interactions with other molecules will not be taken into account. The three reactions will be investigated and according transition states will be discussed.

4.3.2.1 Carbon monoxide elimination reaction

The carbon monoxide elimination reaction as introduced by Alcaide *et al.*[16] is shown in Figure 4.2. This reaction involves simultaneous bond breaking and atom transfer. The N1–C2 and the C2–C3 bonds of the β-lactam ring must be broken and a hydrogen atom abstraction from the hydroxyl group and a hydrogen addition at the ring's nitrogen atom (N1) have to occur. Furthermore, formation of a double bond at the oxygen atom that was initially part of the hydroxyl group takes place. Since only one reactant molecule was taken into account in these calculations, the hydrogen atom transfer has to

occur intramolecularly from the hydroxyl group to the N1 nitrogen atom.

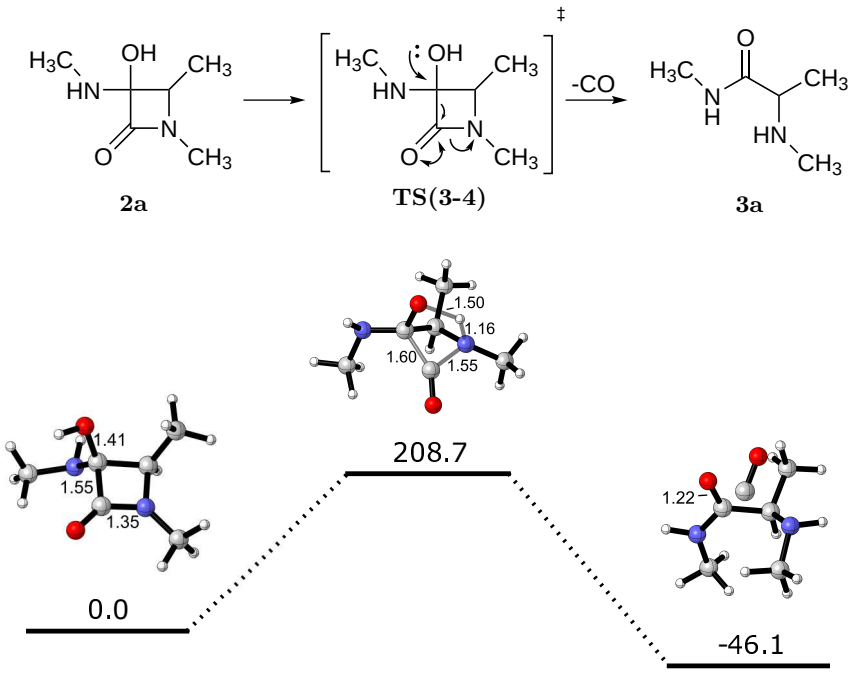

Figure 4.2: Gibbs free energy profile for the carbon monoxide elimination reaction. (M06-2X/6-31+G(d,p), 298 K, 1 atm, energies in kJ.mol^{-1}, bond lengths in Å)

The Gibbs free energy profile is displayed in Figure 4.2 and shows a single step pathway with an activation barrier of 208.7 kJ.mol^{-1}. The N1–C2 and the C2–C3 bonds break with simultaneous proton transfer from the hydroxyl group to the N1 nitrogen atom in a single step. The products are 46.1 kJ.mol^{-1} lower in energy than the reactants, indicating an exergonic reaction ($\Delta G_{rxn}<0$). The hydroxyl hydrogen atom has approached the N1 nitrogen atom at 1.16 Å in the transition state, showing the ongoing hydrogen transfer. The N1–C2 and C2–C3 bond lenghts are 1.55 and 1.60 Å, respectively. Comparing these distances to the the bond lengths in the stable reactant (1.35 and 1.55 Å, respectively), the N1–C2 has elongated 0.20 Å while the C3–C4 has only elongated 0.05 Å at **TS(3-4)**. The C3-O bond in the reactant is 1.41 Å compared to 1.22 Å in the product, indicating double bond formation. Thus the N1–C2 and C2–C3 bond breaking indicate an early transition state but the advancing hydrogen transfer indicates a late transition state. Therefore, **TS(3-4)** is an asynchronous transition state.

Experiments have shown that the carbon monoxide elimination reaction occurs at room temperature and 1 atm (standard conditions, STP).[16] Although it has to be taken into account that different side-chains can influence the reaction energy, the calculated activation barrier is very high. Therefore, this single step mechanism involving an intramolecular hydrogen transfer without the aid of other molecules is probably not the correct mechanism.

4.3.2.2 C3-C4 ring opening reaction

The C3-C4 ring opening reaction is shown in Figure 4.3. The reaction involves C3–C4 bond breakage and formation of a C3-O double bond. The Gibbs free energy profile for the single step reaction mechanism is shown in Figure 4.3.

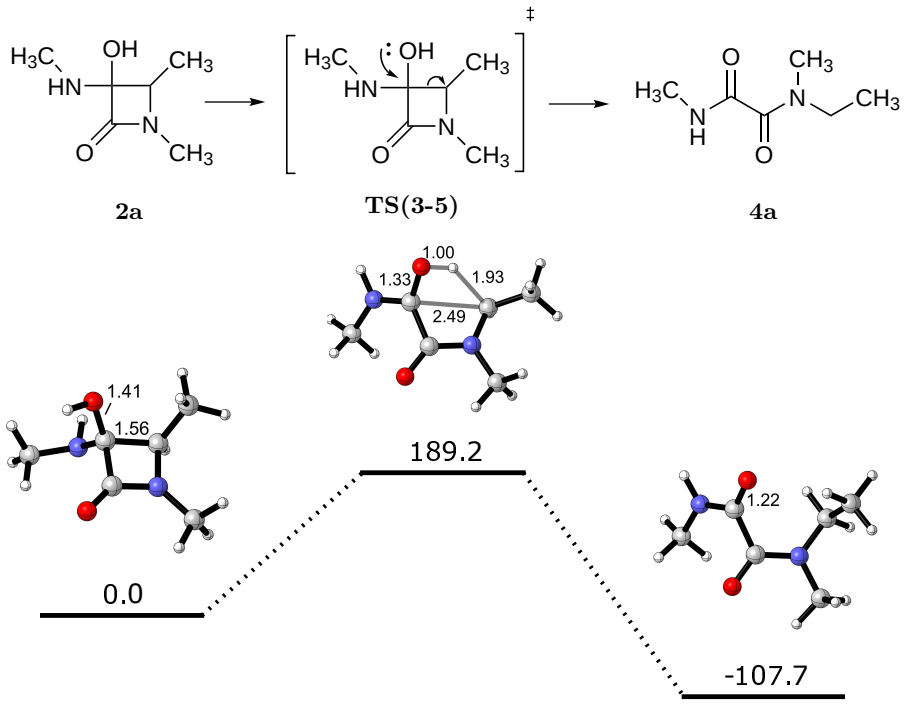

Figure 4.3: Gibbs free energy profile for the C3-C4 ring opening reaction. (M06-2X/6-31+G(d,p), 298 K, 1 atm, energies in kJ.mol^{-1}, bond lengths in Å)

The activation barrier of this single step reaction is 189.2 kJ.mol^{-1}. The products are 107.7 kJ.mol^{-1} lower in energy than the reactants, indicating that this reaction is exergonic. The C3–C4 bond has elongated while the hydroxyl's proton is transferred to the C4 carbon atom. At the transition state, the C3–C4 bond length is 2.49 Å compared to a bond length of 1.56 Å in the reactant. Hence, the bond has elongated almost 1 Å by the time the transition state is reached, indicating a late transition state. The hydroxyl hydrogen atom is oriented toward the C4 carbon atom of the ring at **TS(3-5)** in order to make the transfer. The O–H bond is 1.00 Å while the C4–H bond is 1.93Å, suggesting an early transition state when based on the hydrogen transfer. The C3-O bond in the reactant is 1.56 Å compared to 1.22 Å in the product and 1.33 Å at **TS(3-5)**, showing ongoing double bond formation.

Experiments have shown that the C3-C4 ring opening reaction occurs at STP.[14,15] Since the activation barrier for this single step intermolecular reaction without the aid of an extra molecule is high, this mechanism is probably not the correct mechanism for this reaction.

4.3.2.3 Dehydration reaction

The dehydration reaction of 3-amino-β-lactams **2** involves the C3–N double bond formation with expel of H_2O to form 3-imino-β-lactams **5** and is shown in Figure 4.4. This single step reaction involves a hydrogen transfer from the C3 substituted nitrogen atom to the hydroxyl group with simultaneous expel of H_2O.

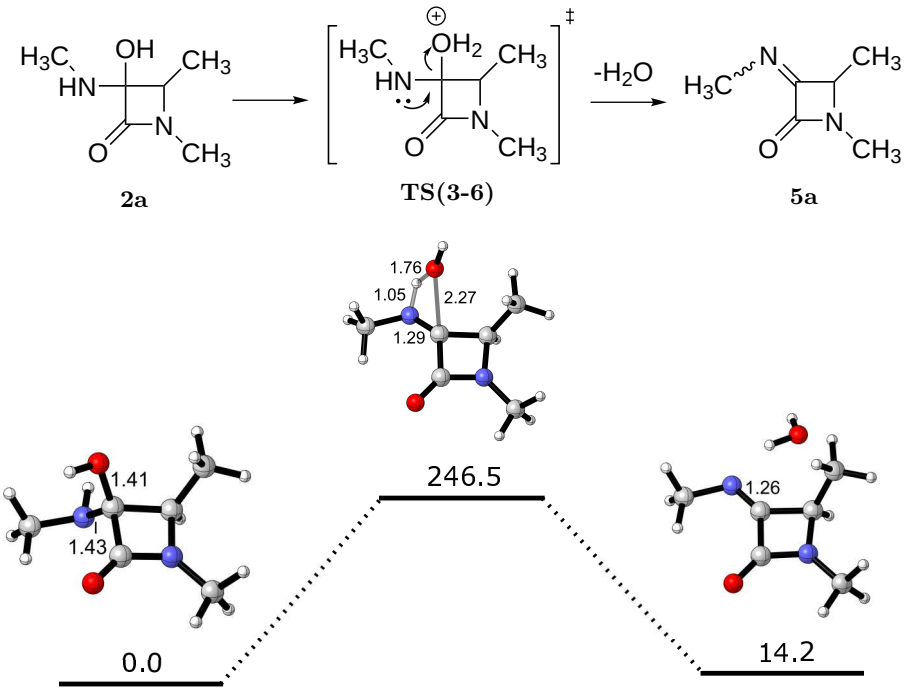

Figure 4.4: Gibbs free energy profile for the dehydration reaction. (M06-2X/6-31+G(d,p), 298 K, 1 atm. Energies in kJ.mol^{-1}, bond lengths in Å)

Figure 4.4 shows the Gibbs free energy profile for this reaction. An activation barrier of 246.5 kJ.mol^{-1} was found. The product is 14.2 kJ.mol^{-1} higher in energy compared to the reactant, showing an endergonic energy profile. The C3-N bond is 1.29 Å in **TS(3-6)** and 1.43 Å in the reactant, showing ongoing double bond formation. The nitrogen substituent on the C3 carbon atom has oriented its hydrogen atom toward the leaving hydroxyl group in order to transfer the proton to form the H_2O molecule (N–H = 1.05 Å and O–H = 1.76 Å). The C3 carbon atom and the leaving H_2O molecule are at a distance of 2.27 Å, indicating **TS(3-6)** is a late transition state.

Experiments have shown that the dehydration reaction can occur at STP.[83] Since the barrier for this reaction is very high and the reaction proceeds endergonically, this single step intramolecular hydrogen transfer reaction without the aid of a second molecule is probably not the correct mechanism for this reaction. The endergonic behavior of this reaction might be attributed to the *in vacuo* calculations. However, during experimental imination of 3-oxo-β-lactams **1**, magnesium sulphate is added to the

reaction mechanism to absorb water, thus preventing the reverse reaction.[14,15]

For all three reactions under study, the single step reaction mechanisms without the aid of an extra molecule show very high Gibbs free activation barriers. The C3-C4 ring opening reaction shows the lowest activation barrier of 189.2 kJ.mol^{-1}. This activation barrier is 37.8 and 57.3 kJ.mol^{-1} lower than the carbon monoxide elimination and the dehydration reaction, respectively. Both the carbon monoxide elimination reaction and the C3-C4 ring opening reaction show an exergonic Gibbs free energy profile while the dehydration proceeds endergonically.

Since experimental results have shown that the reactions under study take place at standard conditions, other mechanisms than these single step intramolecular hydrogen transfer reactions without the aid of an extra molecule are most probably taking place. The presence of a solvent, other reactants or reaction products could have a catalytic effect on these reactions and might thus lower the activation barriers. Reactant or product molecules could facilitate the proton transfer in the three reactions, which will be investigated in the following.

4.3.3 Calculations with the aid of an extra molecule

For the single step intramolecular hydrogen transfer reactions in the previous sections, the high barriers indicate that the systems under study were insufficient for the formation of the ring opening products **3** and **4** or the imines **5**. In this section, other molecules will be introduced into the system, which can interact with the reactant to facilitate hydrogen transfers and bond breakings.

Since plenty of reactant molecules are present at the start of a reaction, it is plausible that these these molecules influence the reaction mechanism. Therefore, for each of the three reaction pathways under study, a second 3-amino-3-hydroxy-β-lactam **2** was added to the reactants environment (4.3.3.1).

Once product molecules are formed, they could also have a catalytic effect on the reaction. Therefore, the product molecules for each reaction path were added to the reactant's environment and the influence on the pathways was investigated (4.3.3.2).

4.3.3.1 Assistance of a reactant molecule

Since all three reactions under study involve a hydrogen transfer, suitable proton accepting and donating sites on the reactant were searched for. In this light, the proton affinity of several reactant sites of the reactant molecule **2** were assessed. It was tested which 3-amino-3-hydroxy-β-lactam reactant **2a** is most stable when an extra hydrogen atom is added on a certain position. The energies of the different protonated reactants **2a** were compared and the results are shown in Table 4.1. Reactant **2a** with protonation at the hydroxyl group is found to be the most stable, followed by protonation at the nitrogen atom in the side-chain of the ring (N2). Besides their good proton accepting behavior, these two atoms possess a proton and are therefore suitable donors of protons during the reaction as well. Protonation at the N1 nitrogen atom is found to be the least preferred, followed by protonation at the carbonyl oxygen atom.

Table 4.1: Gibbs Free energies (kJ.mol^{-1}) of protonated reactants **2a**

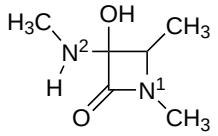

2a

Protonation site	**ΔG**
OH	0.0
O	72.2
N1 (from upper site)	90.0
N1 (from lower site)	97.8
N2	30.2

$\Delta G = G - G_{OH}$

For the three reactions under study, several different mechanisms were investigated where a second reactant assists by means of its hydroxyl group or N2 nitrogen atom. As mentioned earlier, there is a hydrogen atom present at these two sites, which enables a direct accepting and donating mechanism (direct proton shuttle). Nevertheless, pathways involving donation of the hydrogen atom (either from O-H or N2-H) and acceptance of a hydrogen atom on another site of the assisting reactant (indirect proton shuttle) were investigated as well.

Carbon monoxide elimination reaction

Since the carbon monoxide elimination reaction involves a hydrogen transfer from the hydroxyl moiety to the N1 nitrogen atom, a second reactant might assist by accepting the hydrogen atom from the hydroxyl group while simultaneously donating a hydrogen atom to the N1 nitrogen atom. A first pathway was investigated, involving a direct proton shuttle with assistance of the hydroxyl group of the second reactant. The Gibbs free energy profile is shown in Figure 4.5. The reaction proceeds *via* a stepwise mechanism to form the α-aminoamide **3a**. The first step involves a hydrogen transfer from

the hydroxyl group toward the N1 nitrogen atom and elongation of the N1–C2 and C2–C3 bonds to the intermediate complex **59**. The activation barrier for this step is 126.0 kJ.mol^{-1} (**TS(3-4)1a**). The intermediate complex **59** is 113.2 kJ.mol^{-1} higher in energy when compared to the separate reactants. In the second step, were the CO is expelled, the assisting reactant has been reoriented (**TS(3-4)1b**). This second step occurs barrierless and gives rise to the α-aminoamide **3** with recuperation of the 3-amino-3-hydroxy-β-lactam **2a**. The reaction energy for the complete reaction is 41.5 kJ.mol^{-1}, indicating an exergonic pathway.

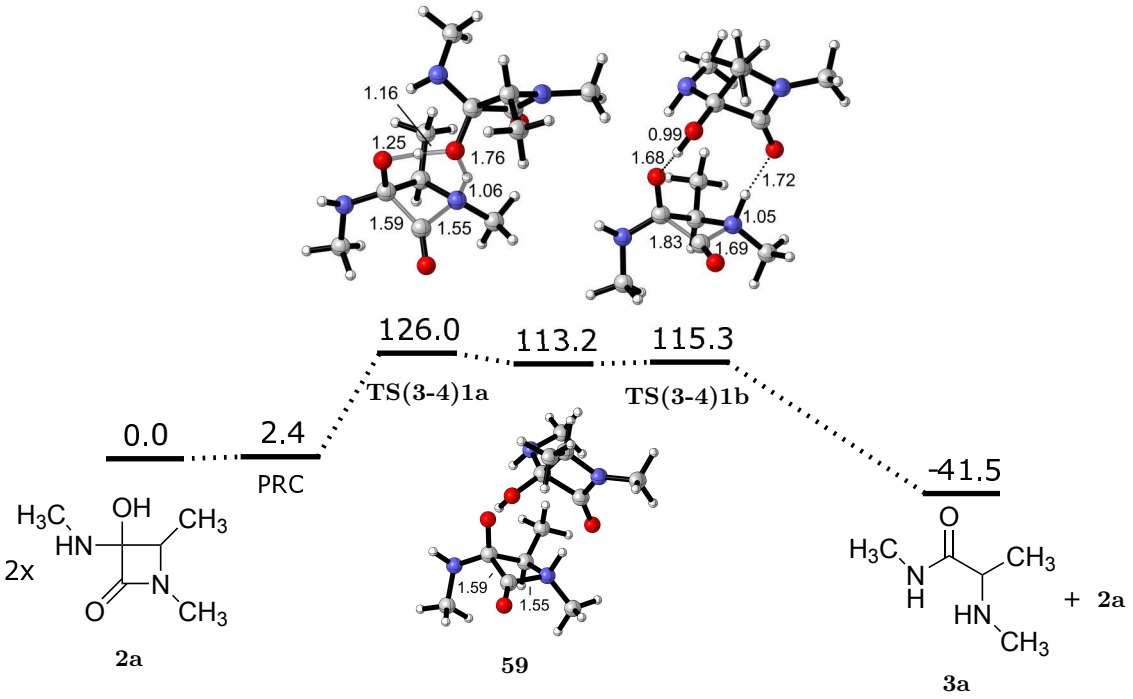

Figure 4.5: Gibbs free energy profile for the carbon monoxide elimination reaction **with assistance of a reactant 2a in a direct proton shuttle** (M06-2X/6-31+G(d,p), 298 K, 1 atm. Energies in kJ.mol^{-1}, bond lengths in Å, PRC = pre-reactive complex)

The direct proton shuttle with assistance of the N2 site of the assisting reactant could not be located. It is expected that this pathway would give rise to a higher activation barrier since it was demonstrated earlier that the N2 site shows less proton affinity than the OH site. Nevertheless, to make sure such pathway can be ruled out, it should be investigated in the future.

Besides this direct proton shuttle, an indirect proton shuttle has been investigated as well. Two sites of the assisting reactant could be donating the hydrogen atom (OH and N2) and several sites of the assisting reactant could be accepting the hydrogen atom of which the OH, N2 and carbonyl site are the most probable based on the proton affinity, calculated in Table 4.1. One pathway was located where the hydroxyl moiety of the assisting reactant serves as the hydrogen donor for the N1 nitrogen atom and the carbonyl oxygen atom of the assisting reactant acts as the proton acceptor for the hydroxyl proton and is shown in Figure 4.6. In this reaction pathway, the indirect hydrogen transfer and the

emission of carbon monoxide take place in one step. This leads to the formation of the intermediate complex **60** which is readily converted to the product complex via simple internal proton transfer in the assisting reactant. The Gibbs free energy profile is shown in Figure 4.6. The activation barrier is 160.9 kJ.mol^{-1}, giving rise to the intermediate complex **60** and after internal proton transfer to the product **3a** and the assisting reactant **2a**. This product complex is 21.5 kJ.mol^{-1} lower in energy than the separate reactants.

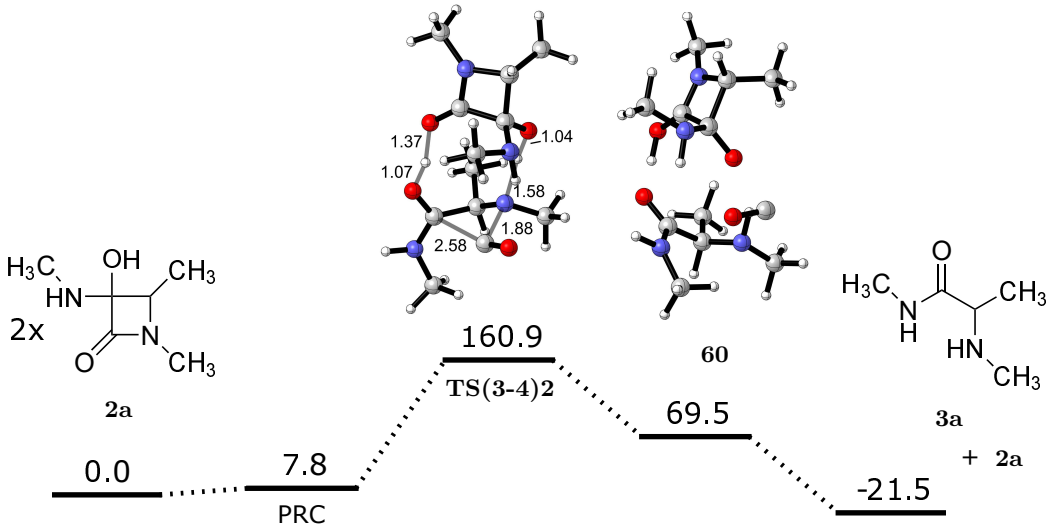

Figure 4.6: Gibbs free energy profile for the carbon monoxide elimination reaction **with assistance of a reactant 2a in an indirect proton shuttle** (M06-2X/6-31+G(d,p), 298 K, 1 atm. Energies in kJ.mol^{-1}, bond lengths in Å, PRC = pre-reactive complex)

Although only one indirect proton transfer pathway was located, several other could take place. It is remarkable that the indirect proton shuttle pathway above, where the OH site of the assisting reactant is the proton donor with a carbonyl proton acceptor site, was found rather than a N2 proton acceptor site, since the latter showed better proton affinity in Table 4.1. This will be investigated in more detail in the future.

It can be concluded that the direct proton shuttle with OH assistance is preferred over the indirect proton shuttle with hydroxyl and carbonyl assistance since the activation barrier is 34.9 kJ.mol^{-1} lower for the former. Comparing these reactant assisted carbon monoxide elimination reaction pathways to the single step pathway without assistance ($\Delta G^{\ddagger}$ = 208.1 kJ.mol^{-1}), it can be concluded that the assistance clearly lowers the activation barriers. The direct proton shuttle reactant assisting pathway can thus be considered as the most appropriate pathway for the carbon monoxide elimination reaction.

C3-C4 ring opening reaction

Similar to the carbon monoxide elimination reaction, both direct proton and indirect proton shuttle

pathways with an assisting reactant molecule have been investigated. Two pathways were investigated with a direct proton shuttle, one interacting with the hydroxyl moiety and one interacting with the N2 nitrogen atom of the assisting reactant. The Gibbs free energy profiles for both reactions are shown in Figure 4.7. Both pathways proceed in a single step with activation barriers of 167.6 and 179.7 kJ.mol^{-1} for interaction at the assisting reactant's hydroxyl group and N2 atom, respectively. They both proceed exergonically giving rise to ethanediamide **4a** with recuperation of reactant **2a**. The product complexes are 96.6 and 75.2 kJ.mol^{-1} lower in energy than the separate reactants, for **TS(3-5)1** and **TS(3-5)2**, respectively.

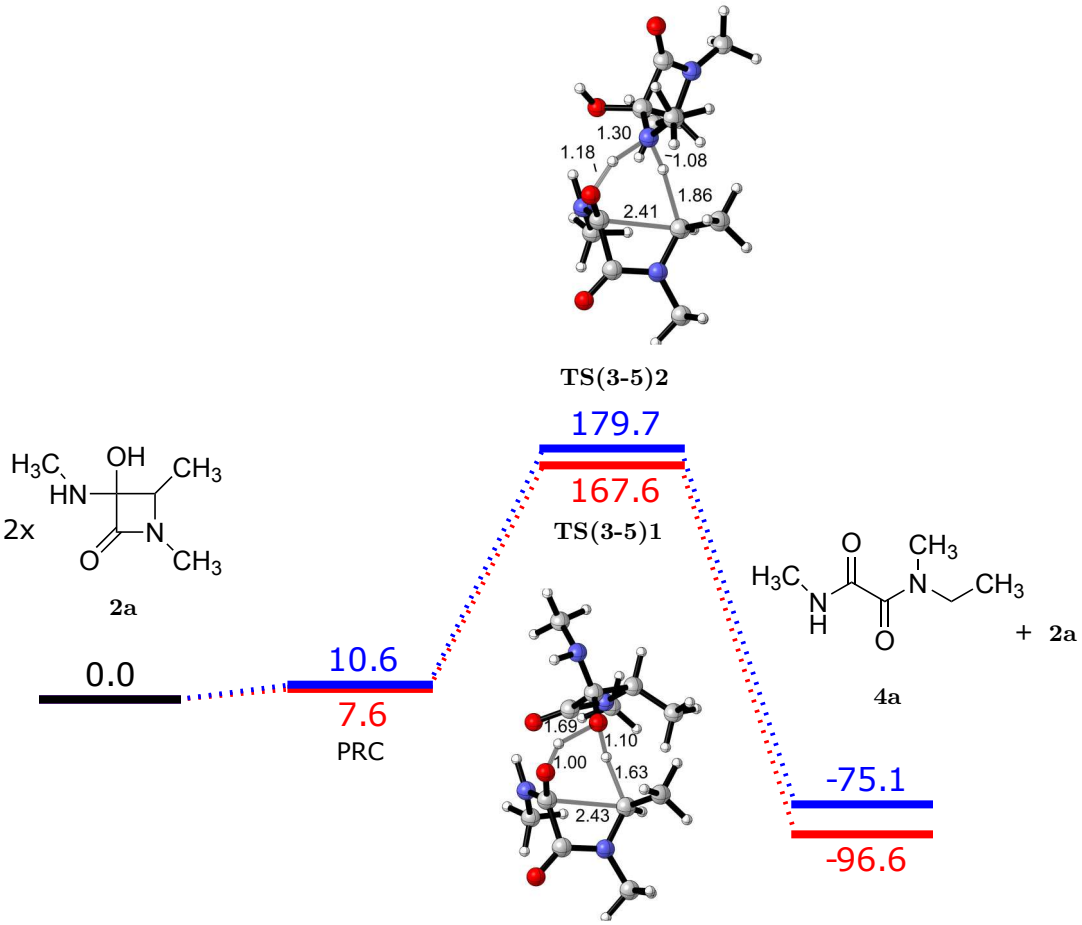

Figure 4.7: Gibbs free energy profile for the C3-C4 ring opening reaction **with assistance of a reactant 2a** at the OH **(red)** and NH **(blue)** **in a direct proton shuttle** (M06-2X/6-31+G(d,p), 298 K, 1 atm. Energies in kJ.mol^{-1}, bond lengths in Å, PRC = pre-reactive complex)

Besides the direct proton shuttle pathways, two indirect proton shuttle pathways have been investigated. The Gibbs free energy profiles of the two pathways are shown in Figure 4.8. The red pathway shows interaction of the hydroxyl group of the assisting reactant by protonating the C4 carbon while its carbonyl moiety accepts the hydroxyl hydrogen atom of the reactant. The blue pathway shows interaction at the N2 nitrogen atom of the assisting reactant as proton donor and the carbonyl oxygen atom as proton acceptor. The red pathway is the preferred pathway with an activation barrier of 138.4 kJ.mol^{-1}, while the blue pathway has an activation barrier of 184.0 kJ.mol^{-1}. Both pathways

initially lead to the formation of the intermediate complexes **61** and **62**, which readily convert to the product complexes **4a** via internal proton transfers or tautomerization. The product complexes are 71.7 and 96.6 kJ.mol^{-1} more stable when compared to the separate reactants, indicating exergonic reaction pathways.

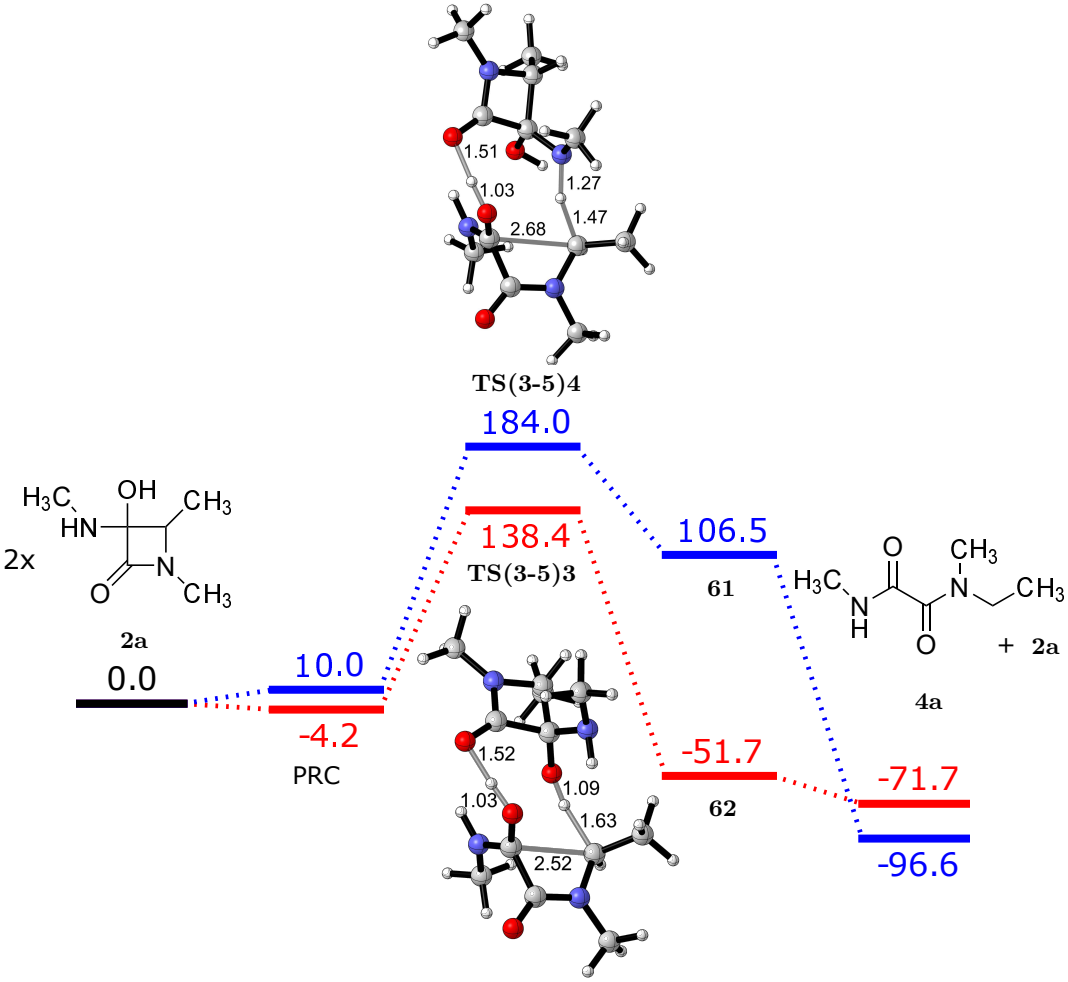

Figure 4.8: Gibbs free energy profile for the C3-C4 ring opening reaction **with assistance of a reactant 2a** at the OH **(red)** and NH **(blue)** **in a indirect proton shuttle** (M06-2X/6-31+G(d,p), 298 K, 1 atm. Energies in kJ.mol^{-1}, bond lengths in Å, PRC = pre-reactive complex)

The indirect pathways initially lead to the intermediate complexes **61** and **62**. Figure 4.9 shows the configurations of both intermediate complexes **61** and **62**. In product complex **61**, the product is accompanied by a zwitterionic assisting reactant. Internal proton transfer in the assisting reactant gives rise to the stable ethanediamide **4a**. In **62**, the hydroxyl hydrogen atom of the reactant is not transferred to the carbonyl moiety of the assisting reactant. Moreover, the hydroxyl group of the assisting reactant (which donated its hydrogen atom) has abstracted the N2 substituted hydrogen atom of the reactant to form a hydroxyl again. Investigation of the optimization trajectory showed initial indirect proton transfers after which the hydrogen atom that was transferred from the reactant to the assistant reactant is transferred back. Subsequent reorientation of the assisting reactant in **62** leads to the abstraction of the N2 hydrogen atom by the hydroxyl oxygen atom of the reactant, giving rise to a imine bond in the formed C3-C4 ring opening intermediate. Figure 4.8 shows that

this intermediate complex **62** is 53.8 kJ.mol^{-1} more stable than the intermediate complex **61**. This is due to the recuperation of the stable assisting reactant **2a** in **62**, while the transferred proton in **61** resides on the carbonyl of the assisting proton, which is an unstable residing place. Nevertheless, tautomerization of the intermediate complex **61** gives rise to 20.0 kJ.mol^{-1} more stable product **4a**. This notable pathway could be further investigated in the future for a direct proton shuttle from the N2 site to the C4 carbon atom by the assistant reactant's hydroxyl group.

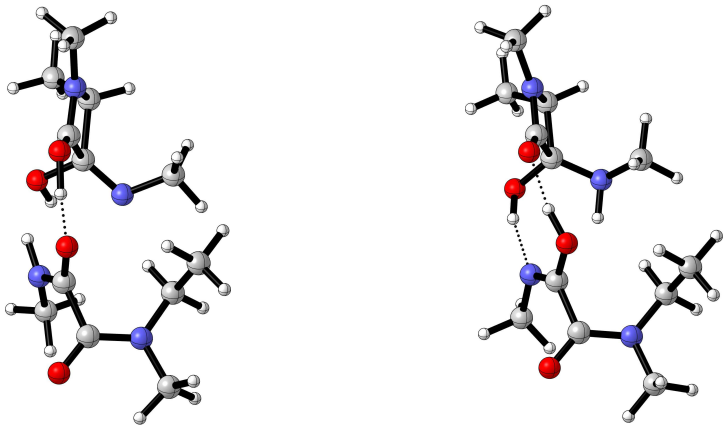

61 **62**

Figure 4.9: Unstable intermediates of the blue pathway **61** and the red pathway **62** in Figure 4.8 (M06-2X/6-31+G(d,p), 298 K, 1 atm).

Although only two indirect proton transfer pathway were located, several other reactant interactions could take place. In the two indirect pathways above, the carbonyl site of the assisting reactant acts as a proton acceptor. Yet, Table 4.1 showed the poor proton affinity of the carbonyl site. The indirect proton shuttles with N2 and OH assistance (one donating, one accepting) could in the future be located but were not found within the time frame of this dissertation.

Comparing the two direct and the two indirect proton shuttle reactant assisting C3-C4 ring opening pathways, the indirect proton shuttle with OH and carbonyl assistance shows the lowest activation barrier of 138.4 kJ.mol^{-1}. This activation barrier is 29.2 and 41.3 kJ.mol^{-1} lower than the direct proton shuttle pathways and 45.6 kJ.mol^{-1} lower than the other indirect proton shuttle pathway. Moreover, the activation barrier is 50.8 kJ.mol^{-1} lower than the single step reaction pathway without assistance, showing the catalytic effect of the assisting reactant for the C3-C4 ring opening reaction. It can thus be concluded that the indirect proton shuttle with OH and carbonyl reactant assistance is presumably the correct pathway for this reaction.

Dehydration reaction

For the dehydration pathway, two direct proton shuttles and two indirect proton shuttles were investigated as well. The assisting reactant can aid the proton transfer from the N2 nitrogen atom to

the hydroxyl group in order to expel H_2O and form the C3–N imine double bond.

The Gibbs free energy profiles for the direct proton shuttles with assistance at the OH (red pathway) and N2 site (blue pathway) are shown in Figure 4.10. The activation barriers for the single step pathways are 147.8 and 198.1 kJ.mol^{-1} for OH assistance and N2 assistance, respectively. The formed 3-imino-β-lactams **5a** are 23.3 and 24.1 kJ.mol^{-1} higher in energy when compared to the separate reactants, indicating endergonic pathways.

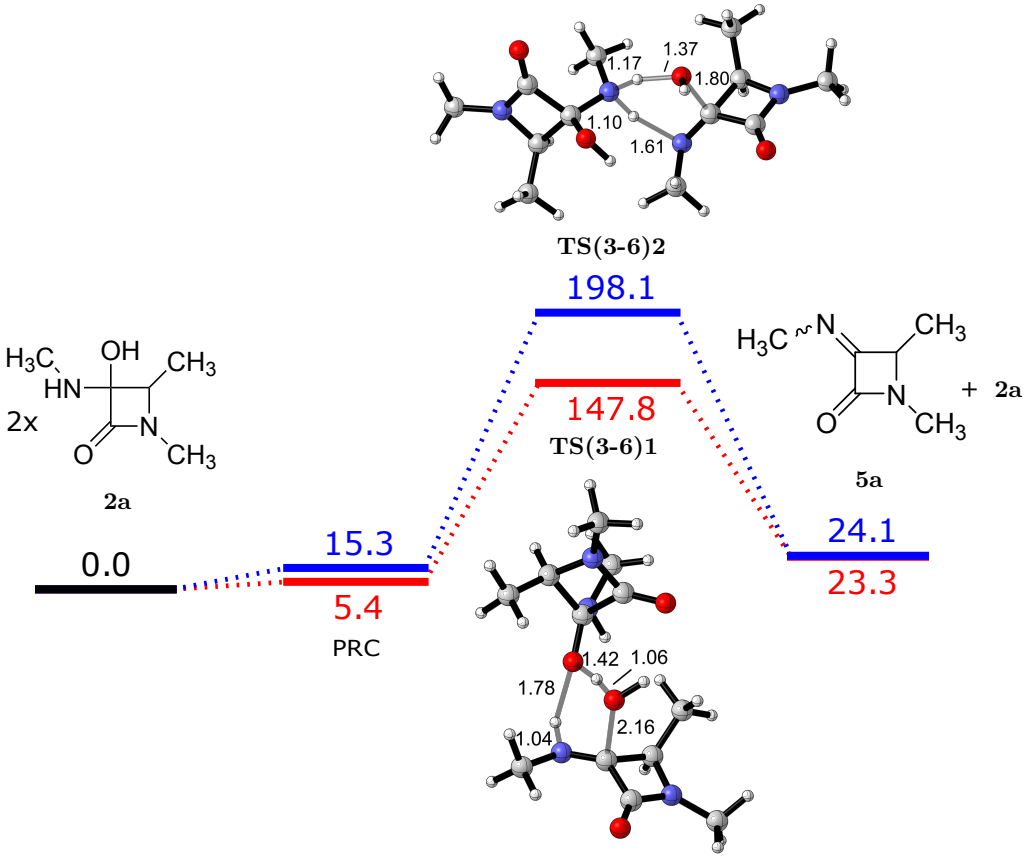

Figure 4.10: Gibbs free energy profile for the dehydration reaction **with assistance of a reactant 2a** at the OH **(red)** and NH **(blue)** **in a direct proton shuttle** (M06-2X/6-31+G(d,p), 298 K, 1 atm. Energies in kJ.mol^{-1}, bond lengths in Å, PRC = pre-reactive complex)

The Gibbs free energy profiles for two indirect proton shuttles are shown in Figure 4.11. The red pathway shows the simultaneous hydrogen transfer and expel of H_2O by interaction with the hydroxyl and carbonyl groups of the assisting reactant. This reaction leads to the formation of the intermediate complex **63**, which is readily converted to the product complex **5a** via simple internal proton transfer in the assisting reactant. The blue pathway shows the reaction by interaction with the hydroxyl and N2 site of the assisting reactant. This reaction leads to the formation of the intermediate complex **63**, which is readily converted to the product complex **5a** via simple internal proton transfer in the assisting reactant as well. The activation barriers are 120.1 and 140.1 kJ.mol^{-1} for the OH and N2 assistance, respectively. Both reactions lead to the 3-imino **5a** and the assisting reactant **2a**. The product complexes are 14.2 kJ.mol^{-1} higher in energy than the separate reactants.

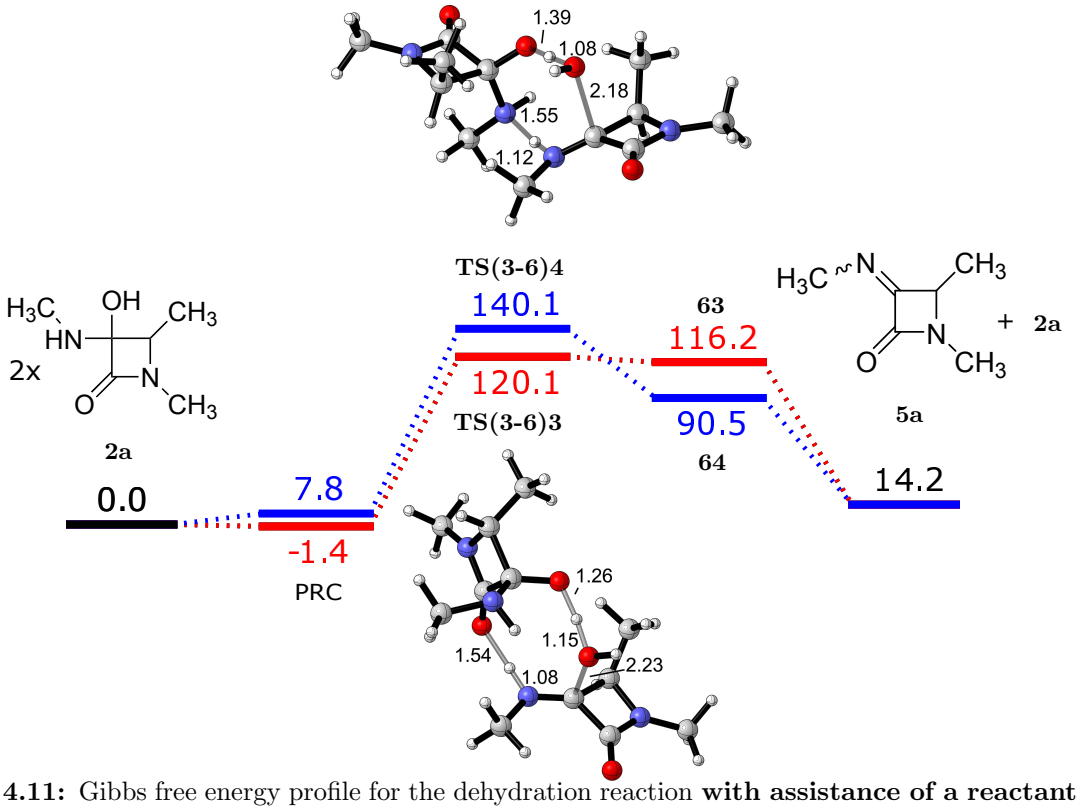

Figure 4.11: Gibbs free energy profile for the dehydration reaction **with assistance of a reactant 2a** at the OH **(red)** and NH **(blue)** **in an indirect proton shuttle** (M06-2X/6-31+G(d,p), 298 K, 1 atm. Energies in kJ.mol^{-1}, bond lengths in Å, PRC = pre-reactive complex)

Besides the two indirect proton shuttles as discussed above, two other pathways could be investigated as well. The N2 site of the assisting reactant could be donating a proton while the OH or carbonyl site could be accepting the proton. These pathways could not be located within the time frame of this dissertation.

Comparing the reactant assisting dehydration pathways, it can be concluded that indirect proton shuttle pathways show the lowest activation barriers and are thus preferred over direct proton shuttle pathways. The OH assisted indirect proton shuttle shows the lowest activation barrier (120.1 kJ.mol^{-1}). This activation barrier is 20 kJ.mol^{-1} lower than for the N2 assisted indirect proton shuttle pathway and 27.7 and 78.0 kJ.mol^{-1} lower than for the two direct proton shuttle pathways. Moreover, comparing this pathway to the single step dehydration pathway without assistance, the activation barrier is 40.8 kJ.mol^{-1} lower, showing the catalytic effect of the reactant assistance for the dehydration reaction.

An overview of the Gibbs free activation energies ($\Delta G^{\ddagger}$) and Gibbs free reaction energies (ΔG_{rxn}) for all reactant assisting pathways are given in Table 4.2. It can be concluded that a direct proton shuttle is most likely (lowest activation barrier) for the carbon monoxide elimination pathway while an indirect proton shuttle with OH assistance is most likely for the C3-C4 ring opening and the dehydration reaction.

Table 4.2: Gibbs free activation energies ($\Delta G^{\ddagger}$ in kJ.mol^{-1}) and Gibbs free reaction energies (ΔG_{rxn} in kJ.mol^{-1}) for all pathways involving **reactant interaction** *in vacuo*. ($R^1 = R^2 = R^3 = Me$, energies with respect to the separate reactants, M06-2X/6-31+G(d,p), 298 K, 1 atm)

Reaction	**Proton shuttle**	$\Delta G^{\ddagger}$	ΔG_{rxn}
CO elimination	Direct	126.0*	-41.5
	Indirect	160.9	-21.5
C3-C4 ring opening	Direct (with OH)	167.6	-96.6
	Direct (with N2)	179.7	-75.1
	Indirect (with OH)	138.4	-71.1
	Indirect (with N2)	184.0	-96.6
Dehydration	Direct (with OH)	147.8	23.3
	Direct (with N2)	198.1	24.1
	Indirect (with OH and CO)	120.1	14.2
	Indirect (with OH and N2)	140.1	14.2

* $\Delta G^{\ddagger}$ for the rate determining (first) step

The lowest barrier (120.1 kJ.mol^{-1}) is found for the dehydration reaction with an indirect proton shuttle with OH and carbonyl assistance. Altough, the dehydration reaction was calculated to be endergonic, the experimental imination of 3-oxo-β-lactams **1** (amination + dehydration reaction) proceeds with magnesium sulphate which acts as water adsorbent (see Chapter 3). Hence, this reagent prevents the reverse dehydration reaction, giving rise to 3-imino-β-lactams **5**. It can thus be expected that a methylated 3-oxo-β-lactam would give rise to 3-imino-β-lactam **5a** formation when reacting with a primary amine.

4.3.3.2 Product interaction

Besides interaction of an assisting reactant, the reaction product could influence the reaction as well. The product molecule can facilitate the proton transfer on the condition that it has a site that can easily be deprotonated. In the reaction products of the three reactions shown below, the 3-imino-β-lactam product **5a** of the dehydration reaction does not possess NH or OH groups and hence cannot facilitate proton transfer. The α-aminoamide **3a**, which is the product of the carbon monoxide elimination reaction, bears two NH-groups. It is expected that the amide nitrogen atom will be a better proton donor than the other N atom since it can delocalize its π-electrons in the amide bond when the proton is abstracted (amide-iminol tautomerism).[111,112] Ethanediamide **4a**, which is the product of the C3-C4 elimination reaction, contains one NH group that can facilitate a proton transfer.

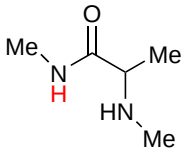

3a

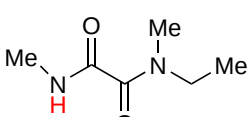

4a

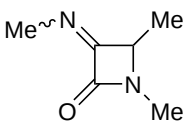

5a

Carbon monoxide elimination reaction

Two pathways, involving a direct and an indirect proton shuttle with α-aminoamide **3a** assistance were located for the carbon monoxide elimination reaction. The Gibbs free energy profiles for both pathways are shown in Figure 4.12. The red pathway is the single step direct proton shuttle where the NH moiety of the assisting product donates its hydrogen to the reactant N1 nitrogen atom while accepting the hydrogen atom from the hydroxyl group. Both the proton transfer and N1–C2 and C2–C3 bond breakings occur simultaneously, giving rise to a very high activation barrier of 205.1 kJ.mol^{-1}, leading to the formation of two α-aminoamides **3a**. The blue pathway shows the product assisted indirect proton shuttle in which the product donates its free hydrogen atom to the N1 nitrogen atom of the reactant while abstracting the hydroxyl hydrogen atom at its carbonyl site. This pathway has an activation barrier of 159.0 kJ.mol^{-1} and leads to the formation of an intermediate complex **65**, which is readily converted toward two α-aminoamides **3a** *via* intrinsic proton transfer.

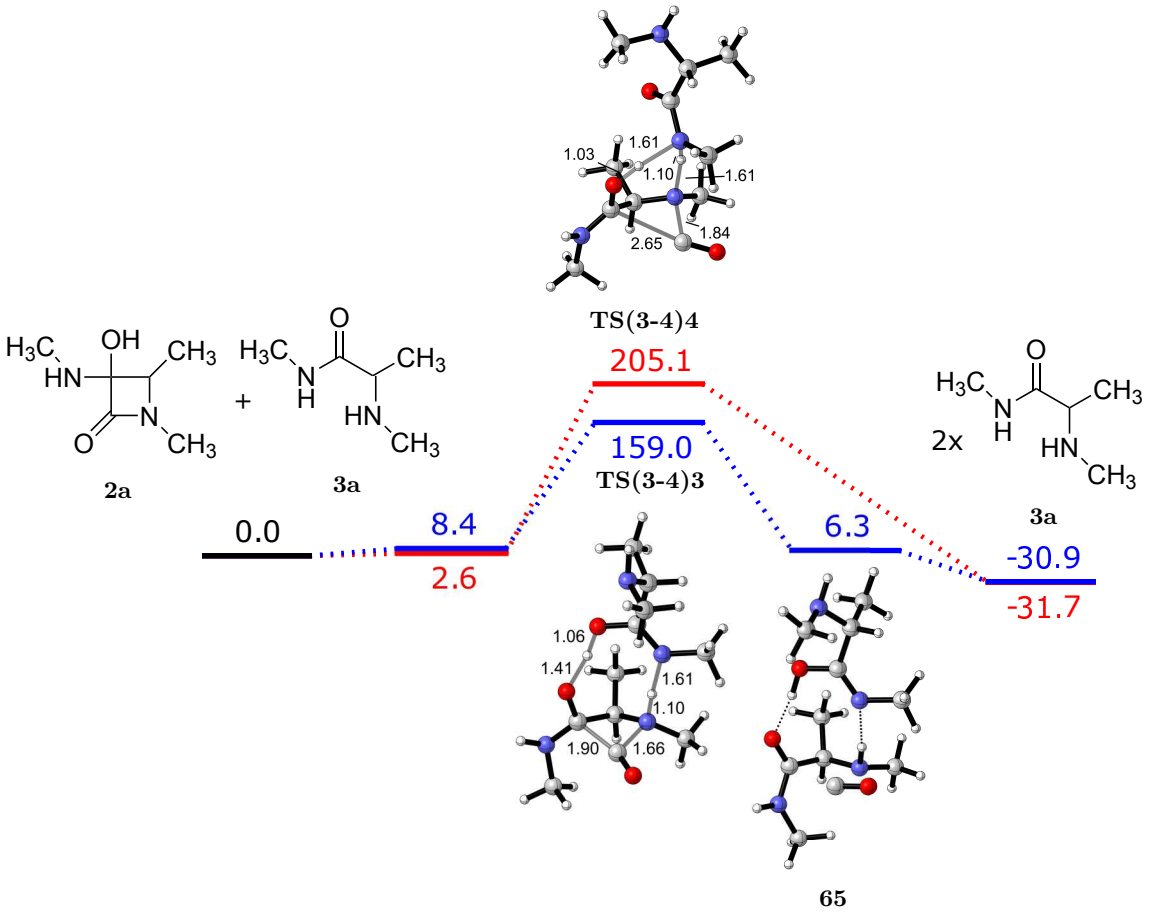

Figure 4.12: The intermolecular carbon monoxide elimination reaction with Free Gibbs reaction energies (in kJ.mol^{-1}) and according geometries and bond lengths (in Å) **with assistance of an according product molecule 3a**. (M06-2X/6-31+G(d,p), 298 K, 1 atm)

When comparing the most plausible product assisting pathway with the most plausible reactant assisting pathway (direct proton shuttle, $\Delta G^{\ddagger}$ = 126.0 kJ.mol^{-1}), it can be concluded that product assistance has a lower catalytic activity than the reactant. The reactant assisting direct proton shut-

tle remains the best pathway for the carbon monoxide elimination reaction.

Another plausible pathway, which could not be investigated within the time frame of this dissertation, concerns an indirect proton transfer in which the second NH site serves as a proton accepting place instead of the carbonyl in the mechanism above.

C3-C4 ring opening reaction

Two pathways, involving a direct and an indirect proton shuttle with ethanediamide **4a** assistance were located for the C3-C4 elimination reaction. The Gibbs free energy profiles for both pathways are shown in Figure 4.13. The red pathway is the direct proton shuttle leading to the formation of two molecules ethanediamide **4a** and has an activation barrier of 237.2 kJ.mol^{-1}. The blue pathway is the indirect proton shuttle with an activation barrier of 267.1 kJ.mol^{-1}, initially leading to the formation of the intermidate complex **66** which is readily converted to two molecules ethanediamide **4a** *via* internal proton transfer.

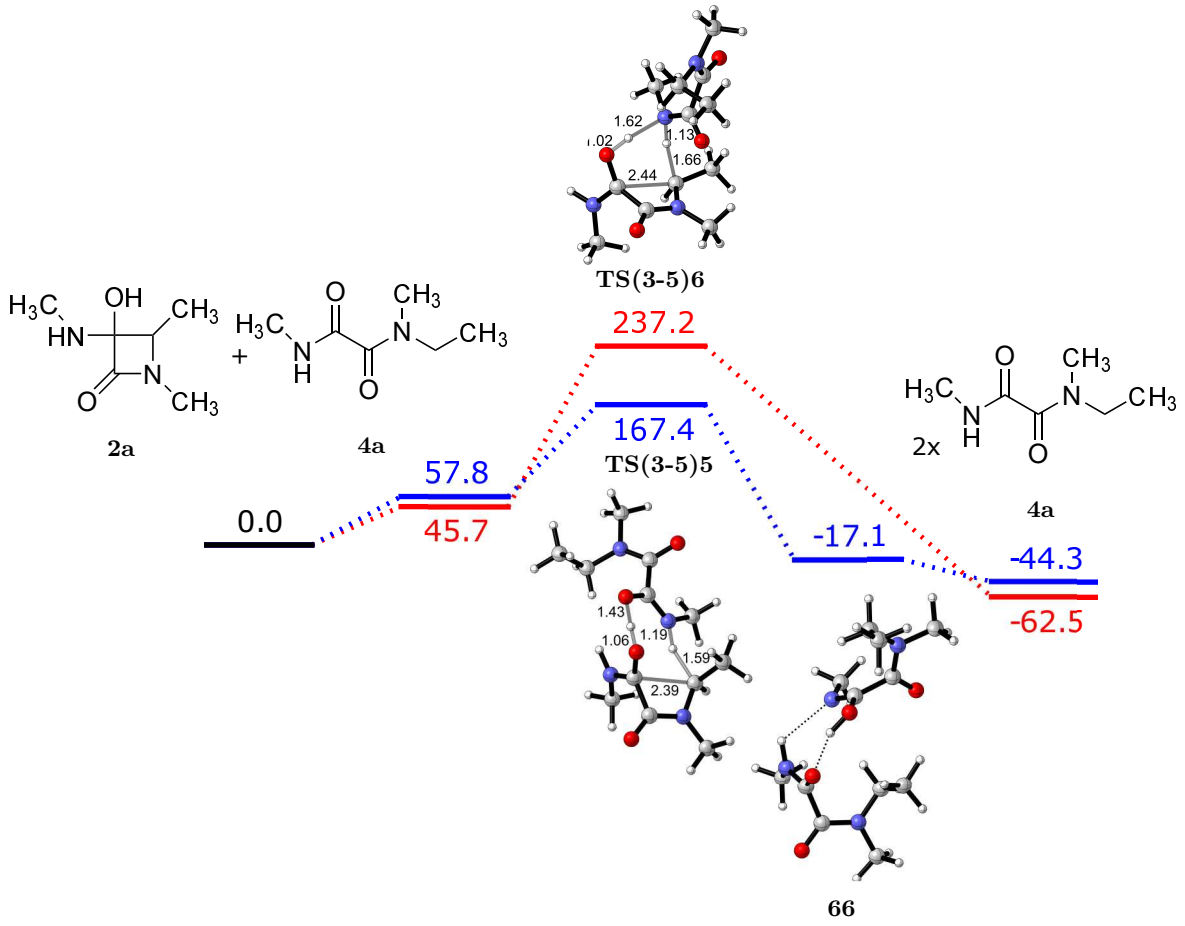

Figure 4.13: The intermolecular C3-C4 ring opening reaction with Free Gibbs reaction energies (in kJ.mol^{-1}) and according geometries and bond lengths (in Å) **with assistance of an according product molecule 4a** (M06-2X/6-31+G(d,p), 298 K, 1 atm)

As well as for the carbon monoxide elimination reaction with product assistance, the single proton

shuttle for the C3-C4 elimination reaction (**TS(3-5)6**) has a much higher activation barrier than the double proton shuttle (**TS(3-5)5**). When comparing these barriers to the most plausible reactant assisted pathway (indirect proton shuttle with OH assistance, $\Delta G^{\ddagger}$ = 138.4 kJ.mol^{-1}), it can be concluded that product assistance is not favored for the C3-C4 ring opening reaction either.

4.3.3.3 Solvent interaction

Lab experiments involving the three reactions under study, were performed in solvents such as dichloromethane (CH_2Cl_2, $\epsilon = 8.93$) and tetrahydrofuran (THF, $\epsilon = 7.4257$).[14–16] All theoretical calculations above were carried out *in vacuo*, hence without taking into account any solvation effects. Therefore, in this section, a solvent environment will be added to the systems under study.

Both reactions with and without assistance of a second reactant have been investigated in a solvent environment (IEF-PCM, see Section 4.1.3), as well as the first step, amination of 3-oxo-β-lactam **1a** and the acyclic compound **57**. The amination and the three intramolecular proton transfer pathways have been investigated in dichloromethane. Two reactant assisted pathways, the direct and indirect pathway of the carbon monoxide elimination reaction, have been calculated in dichloromethane and tetrahydrofuran. Hence, the influence on both intramolecular and intermolecular hydrogen transfers by the solvent was investigated. The Gibbs free activation energies ($\Delta G^{\ddagger}$) and Gibbs free reaction energies (ΔG_{rxn}) for calculation with and without solvent environment are shown in Table 4.3.

Taking into account the solvent environment slightly increases the activation barrier for direct and indirect proton shuttles and decreases the activation barrier for intramolecular proton transfer reactions. Nevertheless, these effects do not influence the trends as determined before. The carbon monoxide elimination and C3-C4 ring opening reaction are exergonic and the dehydration reaction is endergonic in the solvent environment as well. The effect of CH_2Cl_2 and THF is comparable, which was expected since their dielectric constants, on which implicit solvation is based, are comparable.

As mentioned earlier, the amination reaction for 3-oxo-β-lactam **1a** is slightly preferred over the amination of the acyclic compound **57** *in vacuo*. Since this is also the case for calculations with dichloromethane, it can be concluded that amination of 3-oxo-β-lactam **1a** is preferred over the amination of acyclic compound **57**.

Table 4.3: Gibbs free activation energies ($\Delta G^{\ddagger}$ in kJ.mol^{-1}) and Gibbs free reaction energies (ΔG_{rxn} in kJ.mol^{-1}) for calculation with and without the solvent environment. ($R^1 = R^2 = R^3 = Me$, energies with respect to the separate reactants, M06-2X/6-31+G(d,p), 298 K, 1 atm, IEF-PCM with CH_2Cl_2 ($\epsilon = 8.93$) and THF ($\epsilon = 7.4257$))

Reaction	**Proton shuttle**	**Solvation**	$\Delta G^{\ddagger}$	ΔG_{rxn}
Amination of 3-oxo-β-lactam	Intramolecular	-	125.6	-22.8
		CH_2Cl_2	114.8	-11.14
Amination of acyclic **57**	Intramolecular	-	134.2	-4.3
		CH_2Cl_2	127.7	-4.1
CO elimination	Intramolecular	-	208.7	-46.1
		CH_2Cl_2	198.2	-43.9
	Direct	-	126.0 and 115.3*	-41.5
		CH_2Cl_2	137.1 and 135.8*	-14.1
		THF	142.2 and 130.1*	-24.2
	Indirect	-	160.9	-21.5
		CH_2Cl_2	164.9	-10.5
		THF	164.9	-16.3
C3-C4 ring opening	Intramolecular	-	189.2	-107.7
		CH_2Cl_2	189.8	-101.9
Dehydration	Intramolecular	-	252.6	14.2
		CH_2Cl_2	240.7	11.0

* Stepwise mechanism with two activation barriers

4.3.4 Comparison with experimental results

Since experimental results[14–16] have shown the preferential formation of C3-C4 ring opening products in case of an aryl R^2 substituent, a 3-oxo-β-lactam with R^2 = Ph was studied computationally as well. The amination step and all reactant assisting pathways were calculated for this 3-oxo-β-lactam **1b**, both *in vacuo* and with dichloromethane, using IEF-PCM. Since rather high activation barriers were found for interaction at NH for the methylated 3-oxo-β-lactam **1a**, these pathways were not investigated.

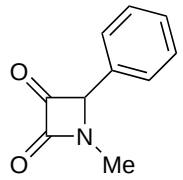

1b

The Gibbs free activation energies are summarized in Table 4.4. The activation barriers for the amination, carbon monoxide elimination and dehydration reaction are comparable for β-lactams **1a** and **1b**. The activation barriers for the C3-C4 ring opening reaction are much lower for R^2 = Ph. The indirect proton shuttle for this reaction shows the lowest activation barrier of 81.6 kJ.mol^{-1}

in vacuo and 95.3 kJ.mol^{-1} with CH_2Cl_2, which is 56.8 kJ.mol^{-1} lower than for the methylated β-lactam **1a**. This shows the preferential formation of the ethanediamide **4b** in case an aromatic R^2-substituent is present. It can thus be concluded that the computational results are in accordance with the experimental results.

Table 4.4: Gibbs free activation energies ($\Delta G^{\ddagger}$ in kJ.mol^{-1}) and Gibbs free reaction energies (ΔG_{rxn} in kJ.mol^{-1}) for the amination and relevant reactant assisting pathways. (R^1 = R^3 = Me and R^2 = Ph/Me, energies with respect to the separate reactants, M06-2X/6-31+G(d,p), 298 K, 1 atm, IEF-PCM with CH_2Cl_2 (ϵ = 8.93))

Reaction	**Proton shuttle**	**Solvation**	**(R^2 = Ph)**		**(R^2 = Me)**
			ΔG_{rxn}	$\Delta G^{\ddagger}$	$\Delta G^{\ddagger}$
Amination	-	-	-16.9	125.1	134.2
CO-elimination	Direct (at OH)	-	-39.4	125.4	126.0
		CH_2Cl_2		139.9	137.1
	Indirect (at OH)	-		159.5	160.9
		CH_2Cl_2	-9.3	168.0	164.9
C3-C4 ring opening	Direct (at OH)	-	-105.9	134.2	167.6
		CH_2Cl_2	-81.3	150.4	-
	Indirect (at OH)	-	-62.3	81.6	138.4
		CH_2Cl_2	-40.7	95.3	-
Dehydration	Direct (at OH)	-	8.18	135.1	147.8
		CH_2Cl_2	23.2	143.9	-
	Indirect (at OH)	-	9.6	122.3	120.1
		CH_2Cl_2	45.0	133.2	-

Additionally, it can be seen in Table 4.4 that for β-lactams **1a** and **1b**, a direct proton shuttle is preferred for the carbon monoxide elimination reaction and an indirect proton shuttle for the C3-C4 ring opening and dehydration reaction. Furthermore, calculations including implicit solvation with dichloromethane slightly increase the activation barrier for the direct and indirect proton shuttles.

In order to further compare with experimental results, two β-lactams with the same substituents as these from lab experiments were analyzed computationally (Table 4.5). In case 1, the 3-amino-3-hydroxy-β-lactam **2** carries *i*Pr and *n*Pr side-chains, which experimentally gave rise to 3-imino-β-lactam **5** formation in dichloromethane, following the dehydration reaction. Case 2 involves 3-amino-3-hydroxy-β-lactam **2**, of which the 3-oxo-β-lactam **54** was synthesized during this dissertation (chapter 3). This reaction led to 3-imino-β-lactam **5** formation in dichloromethane as well.

Table 4.5: Investigated 3-amino-3-hydroxy-β-lactams **2** with according substituents

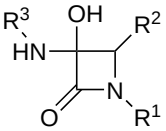

2

Case	**R^1**	**R^2**	**R^3**	**Solvent**	**Product**
1	*i*Pr	*n*Pr	*n*Pr	CH_2Cl_2	**5**[14]
2	$MeOC_6H_4$	*i*Pr	*i*Pr	CH_2Cl_2	**5** (this work)

Both reactions have been investigated computationally and the results for the most plausible pathways are summarized in Table 4.5. Based on the activation barriers of the pathways of case 1, the dehydration reaction is preferred. For case 2, the dehydration reaction is not preferred over the carbon monoxide elimination reaction. It can thus be concluded that for case 1, the computational result are in line with experimental results, although this is not the case for case 2. A possible explanation for this disagreement is that the reaction proceeded under 60 °C in a microwave, while these calculations were carried out under STP. It can thus be concluded that further investigation of these pathways is necessary in combination with new cases.

Table 4.6: Gibbs free activation energies ($\Delta G^{\ddagger}$ in kJ.mol^{-1}) and Gibbs free reaction energies (ΔG_{rxn} in kJ.mol^{-1}) for the two cases of Table 4.5. Energies with respect to the separate reactants, M06-2X/6-31+G(d,p), 298 K, 1 atm)

Case	**Reaction**	**Interaction (proton donor)**	$\mathbf{\Delta G^{\ddagger}}$	$\mathbf{\Delta G_{rxn}}$
1	CO elimination	Direct proton shuttle	164.8[(2)]	-38.5
	C3-C4 ring opening	Indirect proton shuttle (with OH)	148.5	-48.2
	Dehydration	Indirect proton shuttle (with OH and CO)	121.7	24.8
		Indirect proton shuttle (with OH and N2)	119.2	24.8
2	CO elimination	Direct proton shuttle	135.1[(1)]	
	C3-C4 ring opening	Indirect proton shuttle (with OH)	161.4	-28.3
	Dehydration	Indirect proton shuttle (with OH and CO)	139.2	39.5
		Indirect proton shuttle (with OH and N2)	141.9	39.5

[(1)] single step reaction barrier
[(2)] $\Delta G^{\ddagger}$ for the rate determining (first) step

Chapter 5

Summary and conclusion

The discovery of penicillin in 1929 has led to a broad spectrum of β-lactam antibiotics. Besides their application as antibacterials, β-lactams have been proven to contain many other pharmaceutical activities. From a chemical perspective, referring to the "β-lactam synthon method", azetidin-2-ones can be transformed toward a broad variety of potential bioactive products by cleaving the highly strained β-lactam ring. In this Master dissertation, the reactivity of 3-oxo-β-lactams **i** with respect to primary amines was investigated. Previous experiments have shown that reaction of primary amines with 3-oxo-β-lactams **i** leads to the formation of either α-aminoamides **ii**, ethanediamides **iii** or 3-imino-β-lactams **iv**. On one hand, experimental practices involving 3-oxo-β-lactam synthesis by means of Staudinger synthesis with subsequent imination was carried out. On the other hand, a theoretical approach of the three pathways, leading to the three different reaction products, was performed.

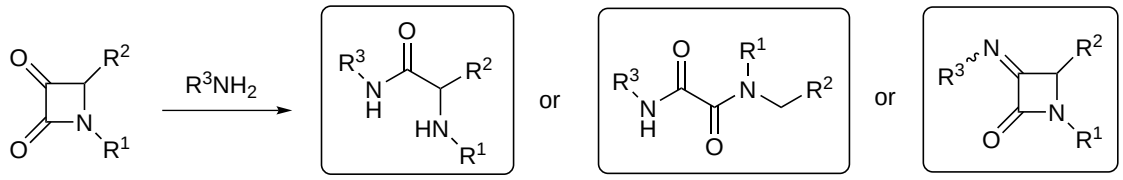

i **ii** **iii** **iv**

5.1 Summary

For the synthesis of 3-oxo-β-lactams **ix**, (*E*)-*N*-(alkylidene)amines **vi** were used, synthesized *via* imination of isobutyraldehyde **v**. Imines **vi** were subsequently transformed toward *cis*-3-acetoxy-β-lactams **vii**, using the Staudinger synthesis. Hydrogenolysis of these *cis*-3-acetoxy-β-lactams **vii** yielded *cis*-3-hydroxyazetidin-2-ones **viii**, after which these were oxidized toward the contemplated

3-oxo-β-lactams **ix**.

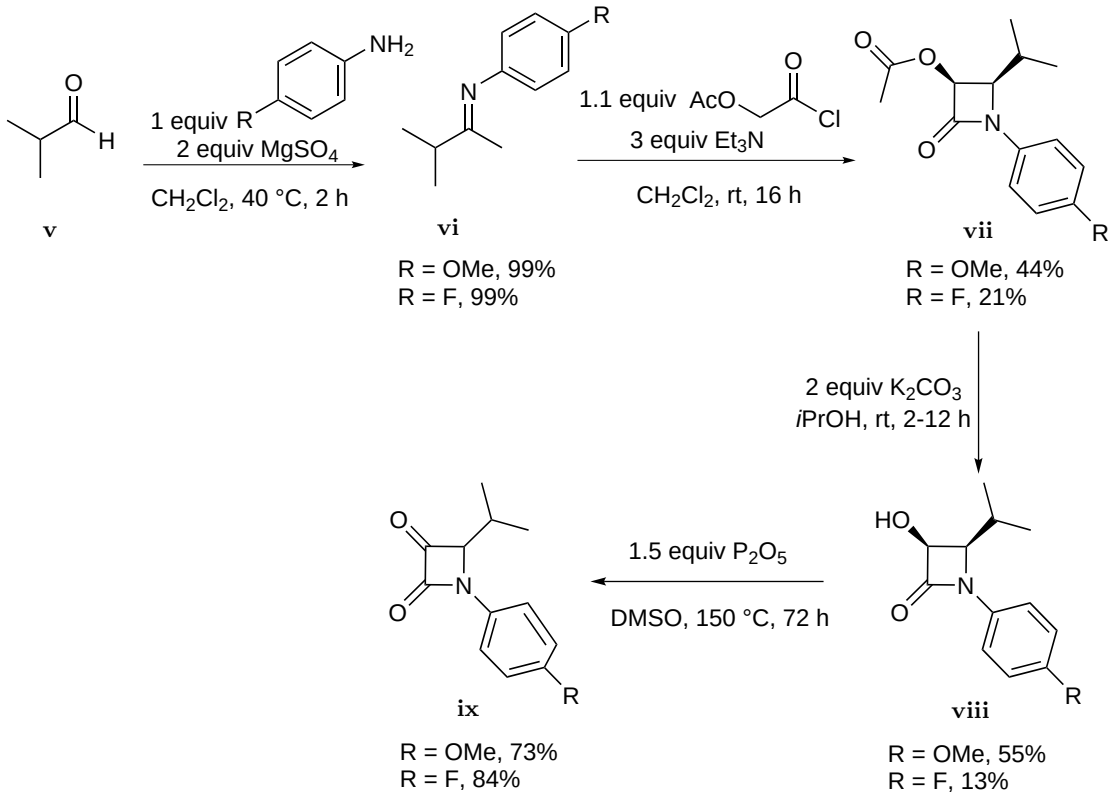

The reactivity of 3-oxo-β-lactams **ix** with respect to primary amines was subsequently tested. Both 3-oxo-β-lactams **ix** gave rise to 3-imino-β-lactams **x** formation.

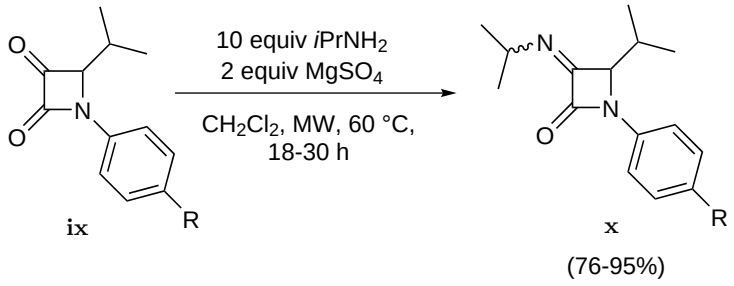

In the computational study, the reaction paths from 3-oxo-β-lactam **i** toward α-aminoamides **ii**, ethanediamides **iii** and 3-imino-β-lactams **iv** were investigated.

To start with, a simple system was chosen with $R^1 = R^2 = R^3 = Me$ in order to locate the different pathways and were at first investigated *in vacuo*. The first step involves the amination of 3-oxo-β-lactams **ix** toward 3-amino-3-hydroxy-β-lactams **xi**, which proved to be slightly favored compared to the amination of an acyclic carbonyl component. For the reaction paths from 3-amino-3-hydroxy-β-lactam **xi** toward the three different products (**ii**, **iii** and **iv**), reaction mechanisms with and without assistance of an extra molecule were investigated. The most plausible pathways are summarized in Table 5.1

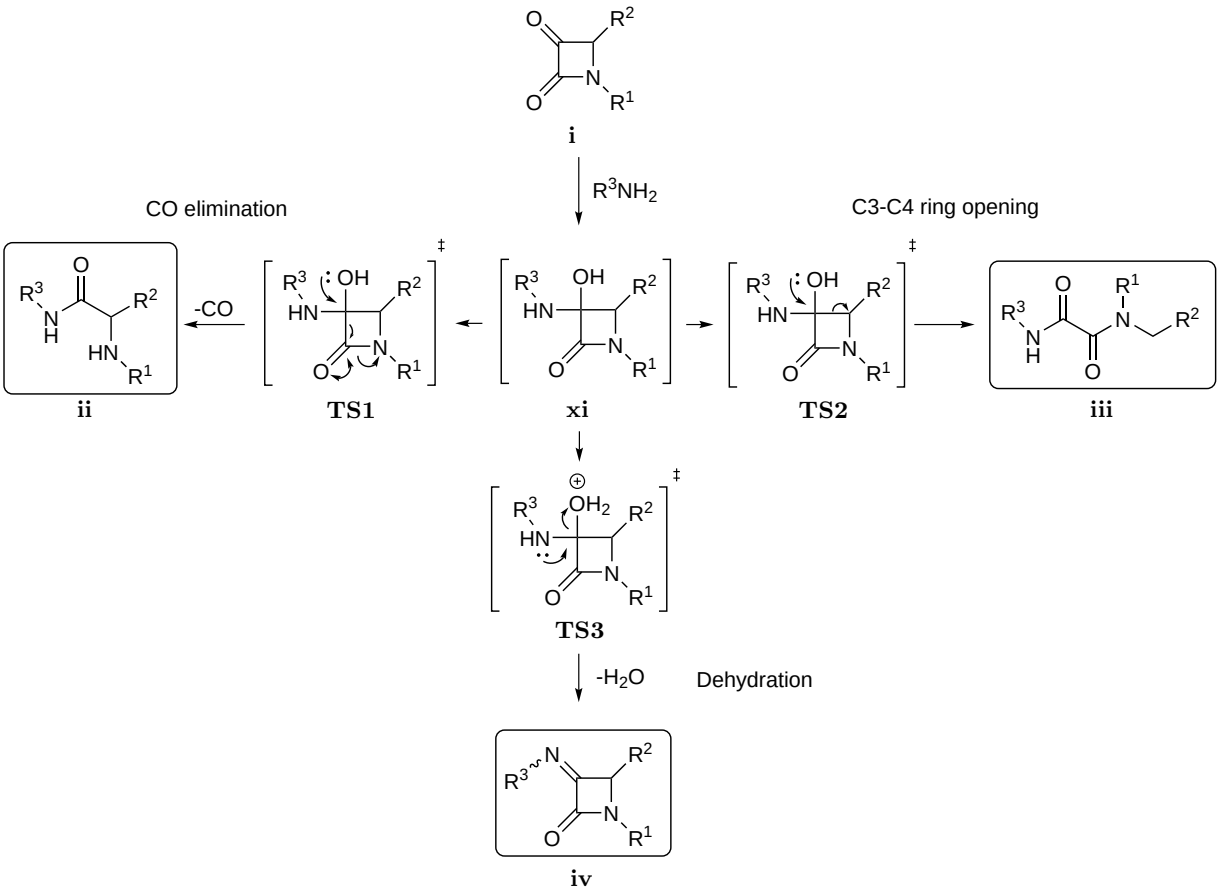

Table 5.1: Gibbs free activation energies ($\Delta G^{\ddagger}$ in kJ.mol^{-1}) for the most plausible pathways (R^1 = R^3 = Me and R^2=Me/Ph, energies with respect to the separate reactants, M06-2X/6-31+G(d,p), 298 K, 1 atm, IEF-PCM with CH_2Cl_2 (ϵ=8.93))

Reaction	**Proton shuttle**	$\Delta G^{\ddagger}$ **(R^2 = Me)**		$\Delta G^{\ddagger}$ **(R^2 = Ph)**
		in vacuo	**with CH_2Cl_2**	**with CH_2Cl_2**
CO-elimination	Intramolecular	208.7	198.2	-
	Direct	126.0	137.1	139.9
C3-C4 ring opening	Intramolecular	189.2	189.8	-
	Indirect	138.4	-	95.3
Dehydration	Intramolecular	252.6	240.7	-
	Indirect	120.1	-	133.2

The carbon monoxide elimination reaction involves simultaneous hydrogen transfer from the hydroxyl site toward the nitrogen atom of the ring and N1–C2 and C2–C3 bond breakings, leading to α-aminoamides **ii**. During the C3-C4 ring opening reaction, the C3–C4 bond breaks with simultaneous hydrogen transfer from the hydroxyl site toward the C4 carbon atom, leading to the formation of ethanediamides **iii**. The dehydration reaction involves the hydrogen transfer from the nitrogen atom in the side-chain toward the hydroxyl site with subsequent expel of H_2O, leading to 3-imino-β-lactams **iv** formation.

Without assistance, all three pathways followed a single step intramolecular proton transfer mechanism with very high activation barriers (Table 5.1). With assistance of a reactant, a stepwise direct proton shuttle pathway was preferred for the carbon monoxide elimination reaction, while the C3-C4 ring opening and dehydration reaction preferred an indirect proton shuttle pathway. All reactant assisting pathways showed a significant activation barrier decrease while product assistance could not further lower the activation barriers for any of the three reaction paths.

The solvent environment was taken into account by using an implicit solvation model (IEF-PCM). The solvent slightly increases the activation barrier for direct and indirect proton shuttles and decreases the activation barrier for intramolecular proton transfer reactions (see Table 5.1).

The influence of a C4 substituted aryl was investigated by replacing the methyl side-chain on the C4 carbon atom by a phenyl group (R^2 = Ph). This lowered the C3-C4 ring-opening reaction barrier significantly, while the carbon-monoxide elimination and dehydration reactions showed no significant differences when compared to the methylated β-lactam. Hence, the computational results are in accordance to experimental results.

In order to compare theoretical and experimental results more closely, two 3-amino-3-hydroxy-β-lactams **xi** were investigated with the substituents used in the experimental designs. The appropriate solvent was taken into account using an implicit solvation model and the most plausible pathways were investigated. For one case, the computational results were in line with experimental outcome, while for the other case, differences were found that could be attributed to the circumstances in which the reaction experimentally occured. More thorough investigation is necessary in the future.

5.2 Conclusion and outlook

The formation of 3-imino-β-lactams **x** for both electron withdrawing and electron accepting N1 substituents in combination with an alkyl C4 substituent leads to two conclusions. On one hand, this confirms the importance of an aryl substituent on the C4 position (R^2 = aryl) for ethanediamide **iii** formation, since the alkyl C4 substituents do not give rise to these compounds. On the other hand, it was expected that an alkyl C4 substituent with an electron withdrawing N1 substituent (4-FC_6H_4) on the 3-oxo-β-lactam **i** would give rise to selective α-aminoamide **3** formation, but 3-imino-β-lactams **x** were formed.[15] Thus the discrepancy in literature concerning the formation of α-aminoamides **ii** could not be explained.

The theoretical work of this dissertation provided the basis of the reactivity of 3-oxo-β-lactams with respect to primary amines **i**. The most plausible pathways were found for the three reaction paths. The influence of a C4 aryl substituent to favor C3-C4 ring opening reactions was determined. Furthermore, two experimental designs have been calculated in order to validate the model with experimental results. The reaction condition were exactly adopted for one case and the model proved to be in agreement to the experimental results.

The reactions under study need to be further investigated in the future. Suggestions for new cases are shown in Table 5.2.

Table 5.2: Suggestions for further theoretical research

$\mathbf{R^1}$	$\mathbf{R^2}$	$\mathbf{R^3}$	**Solvent**	**Product**
$MeOC_6H_4$	Ph	Bn	THF	**ii**[16] or **iii**[14]
*i*Bu	MeC_6H_4	*n*Pr	CH_2Cl_2	**iii**[14]
$MeOC_6H_4$	2,2-dimethyl-1,3-dioxolane	Bn	THF	**ii**[16]

Bibliography

[1] Fleming, A. *Br. J. Exp. Pathol.* **1929**. *10*, 226.

[2] Finlay, J., Miller, L. & Poupard, J. A. *J. Antimicrob. Chemother.* **2003**. *52*, 18.

[3] Levy, S. B. & Marshall, B. *Nat. Med.* **2004**. *10*, S122.

[4] Mehta, P. D., Sengar, N. & Pathak, A. *Eur. J. Med. Chem.* **2010**. *45*, 5541.

[5] Alcaide, B. & Almendros, P. *Curr. Med. Chem.* **2004**. *11*, 1921.

[6] Ojima, I. *Acc. Chem. Res.* **1995**. *28*, 383.

[7] Ojima, I., Shimizu, N., Qiu, X., Chen, H. & Nakahashi, K. *Bull. Soc. Chim. Fr.* **1987**, 649.

[8] Kamath, A. & Ojima, I. *Tetrahedron* **2012**. *68*, 10640.

[9] Van Brabandt, W., Dejaegher, Y., Van Landeghem, R. & De Kimpe, N. *Org. Lett.* **2006**. *8*, 1101.

[10] Alcaide, B., Almendros, P., Cabrero, G., Callejo, R., Ruiz, M. P., Arnó, M. & Domingo, L. R. *Adv. Synth. Catal.* **2010**. *352*, 1688.

[11] Mollet, K., Goossens, H., Piens, N., Catak, S., Waroquier, M., Törnroos, K. W., Van Speybroeck, V., D'hooghe, M. & De Kimpe, N. *Chem. Eur. J.* **2013**. *19*, 3383.

[12] Almendros, P., Aragoncillo, C., Cabrero, G., Callejo, R., Carrascosa, R., Luna, A., del Campo, T. M., Pardo, M. C., Teresa, M. & Ruiz, M. P. *Arkivoc* **2010**. *III*, 74.

[13] Graf, R., Lohaus, G., Börner, K., Schmidt, E. & Bestian, H. *Angew. Chem. Int. Ed. Engl.* **1962**. *1*, 481.

[14] Crul, L. *Synthese en reactiviteitsstudie van 3-iminoazetidin-2-onen.* Master's thesis, Universiteit Gent, **2014**.

[15] Demeurisse, L. *Studie van 3-iminoazetidin-2-onen als bouwstenen in de organische chemie.* Master's thesis, Universiteit Gent, **2015**.

[16] Alcaide, B., Almendros, P. & Aragoncillo, C. *J. Org. Chem.* **2002**. *8*, 3646.

[17] Staudinger, H. *Justus Liebigs Ann. Chem.* **1907**. *356*, 51.

[18] Palomo, C., Aizpurua, J. M., Ganboa, I. & Oiarbide, M. *Eur. J. Org. Chem.* **1999**, 3223.

[19] Liu, C., Xie, Z., Li, Y., Zhao, G. & Liu, F. *Chin. J. Appl. Chem.* **2005**. *22*, 1042.

[20] Shaikh, A. L., Puranik, V. G. & Deshmukh, A. *Tetrahedron Lett.* **2006**. *47*, 5993.

[21] Van Driessche, B., Van Brabandt, W., D'hooghe, M., Dejaegher, Y. & De Kimpe, N. *Tetrahedron* **2006**. *62*, 6882.

[22] Arrieta, A., Lecea, B. & Cossío, F. P. *J. Org. Chem.* **1998**. *63*, 5869.

[23] Xu, J. *Arkivoc* **2009**. *4*, 21.

[24] Jiao, L., Liang, Y. & Xu, J. *J. Am. Chem. Soc.* **2006**. *128*, 6060.

[25] Cossio, F. P., Ugalde, J. M., Lopez, X., Lecea, B. & Palomo, C. *J. Am. Chem. Soc.* **1993**. *115*, 995.

[26] Arrieta, A., Ugalde, J. M., Cossío, F. P. & Lecea, B. *Tetrahedron Lett.* **1994**. *35*, 4465.

[27] Cooper, R., Daugherty, B. & Boyd, D. *Pure Appl. Chem.* **1987**. *59*, 485.

[28] Sordo, J., Gonzalez, J. & Sordo, T. *J. Am. Chem. Soc.* **1992**. *114*, 6249.

[29] Wei, D., Zhu, Y., Zhang, C., Sun, D., Zhang, W. & Tang, M. *J. Mol. Catal. A: Chem.* **2011**. *334*, 108.

[30] Anand, N., Shah, B. A., Kapoor, M., Parshad, R., Sharma, R. L., Hundal, M. S., Pannu, A. P., Bharatam, P. V. & Taneja, S. C. *J. Org. Chem.* **2011**. *76*, 5999.

[31] Arrieta, A., Cossío, F. P. & Lecea, B. *J. Org. Chem.* **2000**. *65*, 8458.

[32] Li, X., Jin, X. & Xu, J. *J. Org. Chem.* **2015**. *80*, 6976.

[33] Domingo, L. R. & Sáez, J. A. *RSC Adv.* **2014**. *4*, 58559.

[34] Moore, H. W. & Hughes, G. *Tetrahedron Lett.* **1982**. *23*, 4003.

[35] Brady, W. T. & Shieh, C. *J. Org. Chem.* **1983**. *48*, 2499.

[36] Pilmé, J., Renault, E., Ayed, T., Montavon, G. & Galland, N. *J. Chem. Theory Comput.* **2012**. *8*, 2985.

[37] Ardura, D., López, R. & Sordo, T. L. *J. Org. Chem.* **2006**. *71*, 7315.

[38] Campomanes, P., Menéndez, M. I., Cárdenas-Jirón, G. I. & Sordo, T. L. *J. Phys. Chem. A* **2005**. *109*, 7822.

[39] Campomanes, P., Menéndez, M. I. & Sordo, T. L. *J. Org. Chem.* **2003**. *68*, 6685.

[40] Pérez-Faginas, P., Alkorta, I., García-López, M. T. & González-Muñiz, R. *Tetrahedron Lett.* **2008**. *49*, 215.

[41] Campomanes, P., Menéndez, M. I. & Sordo, T. L. *J. Phys. Chem. A* **2004**. *108*, 11109.

[42] Arrieta, A., Cossío, F. P., Fernández, I., Gómez-Gallego, M., Lecea, B., Mancheño, M. J. & Sierra, M. A. *J. Am. Chem. Soc.* **2000**. *122*, 11509.

[43] Fernández, I., Sierra, M. A., Mancheno, M. J., Gómez-Gallego, M. & Cossio, F. P. *J. Am. Chem. Soc.* **2008**. *130*, 13892.

[44] Novak, I. & Chua, P. J. *J. Phys. Chem. A* **2006**. *110*, 10521.

[45] Ambler, R. *Philos. Trans. R. Soc. London, Ser. B* **1980**. *289*, 321.

[46] Drawz, S. M. & Bonomo, R. A. *Clin. Microbiol. Rev.* **2010**. *23*, 160.

[47] Ehmann, D. E., Jahić, H., Ross, P. L., Gu, R.-F., Hu, J., Kern, G., Walkup, G. K. & Fisher, S. L. *Proc. Natl. Acad. Sci. USA* **2012**. *109*, 11663.

[48] Díaz, N., Suárez, D., Sordo, T. L. & Merz, K. M. *J. Phys. Chem.* **2001**. *105*, 11302.

[49] Fujii, Y., Hata, M., Hoshino, T. & Tsuda, M. *J. Phys. Chem.* **2002**. *106*, 9687.

[50] Gherman, B. F., Goldberg, S. D., Cornish, V. W. & Friesner, R. A. *J. Am. Chem. Soc.* **2004**. *126*, 7652.

[51] Hata, M., Tanaka, Y., Fujii, Y., Neya, S. & Hoshino, T. *J. Phys. Chem.* **2005**. *109*, 16153.

[52] Hermann, J. C., Hensen, C., Ridder, L., Mulholland, A. J. & Höltje, H.-D. *J. Am. Chem. Soc.* **2005**. *127*, 4454.

[53] Hermann, J. C., Ridder, L., Mulholland, A. J. & Höltje, H.-D. *J. Am. Chem. Soc.* **2003**. *125*, 9590.

[54] Alvarez-Idaboy, J., González-Jonte, R., Hernández-Laguna, A. & Smeyers, Y. *J. Mol. Struct. THEOCHEM* **2000**. *504*, 13.

[55] Coll, M., Frau, J., Vilanova, B., Donoso, J., Munoz, F. & Blanco, F. G. *J. Phys. Chem.* **2000**. *104*, 11389.

[56] Garcıa, R. C., Coll, M., Donoso, J., Muñoz, F. et al. *Chem. Phys. Lett.* **2003**. *372*, 275.

[57] Li, R., Feng, D. & Zhu, F. *Int. J. Quantum Chem.* **2007**. *107*, 2032.

[58] Zhu, F., Li, R., Feng, D., He, M. & Cai, Z. *Int. J. Quantum Chem.* **2007**. *107*, 1925.

[59] Xu, D., Zhou, Y., Xie, D. & Guo, H. *J. Med. Chem.* **2005**. *48*, 6679.

[60] Xu, D., Guo, H. & Cui, Q. *J. Am. Chem. Soc.* **2007**. *129*, 10814.

[61] Lopez, R., Menendez, M., Diaz, N., Suarez, D., Campomanes, P., Ardura, D. & Sordo, T. *Curr. Org. Chem.* **2006**. *10*, 805.

[62] Xie, M., Fu, Y. & Chen, Q. *J. Mol. Struct. THEOCHEM* **2008**. *855*, 111.

[63] Alcaide, B., Almendros, P. & Aragoncillo, C. *Chem. Rev.* **2007**. *107*, 4437.

[64] Ojima, I. & Delaloge, F. *Chem. Soc. Rev.* **1997**. *26*, 377.

[65] Mollet, K., Catak, S., Waroquier, M., Van Speybroeck, V., D'hooghe, M. & De Kimpe, N. *J. Org. Chem.* **2011**. *76*, 8364.

[66] Alcaide, B. & Almendros, P. *Synlett* **2002**, 381.

[67] Mollet, K., D'hooghe, M. & De Kimpe, N. *Mini-Rev. Org. Chem.* **2013**. *10*, 1.

[68] Alajarín, M., Sánchez-Andrada, P., Cossío, F. P., Arrieta, A. & Lecea, B. *J. Org. Chem.* **2001**. *66*, 8470.

[69] Alcaide, B., Almendros, P., Luna, A., Cembellín, S., Arnó, M. & Domingo, L. R. *J. Org. Chem.* **2011**. *17*, 11559.

[70] Dražić, T., Vazdar, K., Vazdar, M., Daković, M., Mikecin, A.-M., Kralj, M., Malnar, M., Hećimović, S. & Habuš, I. *Tetrahedron* **2015**. *71*, 9202.

[71] Domingo, L. R., Aurell, M. J. & Arnó, M. *Tetrahedron* **2009**. *65*, 3432.

[72] Ardura, D. & López, R. *J. Org. Chem.* **2007**. *72*, 3259.

[73] Li, G.-Q., Dai, L.-X. & You, S.-L. *Org. Lett.* **2009**. *11*, 1623.

[74] Wiitala, K. W., Tian, Z., Cramer, C. J. & Hoye, T. R. *J. Org. Chem.* **2008**. *73*, 3024.

[75] Vazdar, K. & Vazdar, M. *Tetrahedron Lett.* **2015**. *56*, 6908.

[76] Alcaide, B., Almendros, P., Martínez del Campo, T., Soriano, E. & Marco-Contelles, J. L. *Chem. Eur. J.* **2009**. *15*, 1909.

[77] Alcaide, B., Almendros, P., Carrascosa, R., López, R. & Menéndez, M. I. *Tetrahedron* **2012**. *68*, 10748.

[78] Pérez-Ruiz, R., Sáez, J. A., Jiménez, M. C. & Miranda, M. A. *Org. Biomol. Chem.* **2014**. *12*, 8428.

[79] Tedesco, D., Zanasi, R., Guerrini, A. & Bertucci, C. *Chirality* **2012**. *24*, 741.

[80] Pena-Gallego, A., Cabaleiro-Lago, E., Fernández-Ramos, A., Hermida-Ramón, J. & Martınez-Núñez, E. *J. Mol. Struct. THEOCHEM* **1999**. *491*, 177.

[81] Kovač, V., Radolović, K., Habuš, I., Siebler, D., Heinze, K. & Rapić, V. *Eur. J. Inorg. Chem.* **2009**, 389.

[82] Soriano-Correa, C., Sanchez Ruiz, J. F., Raya, A. & Esquivel, R. O. *Int. J. Quantum Chem.* **2007**. *107*, 628.

[83] Cainelli, G., Giacomini, D., Trere, A. & Boyl, P. P. *J. Org. Chem.* **1996**. *61*, 5134.

[84] Barrow, K. & Spotswood, T. *Tetrahedron Lett.* **1965**. *6*, 3325.

[85] Alcaide, B., Almendros, P., Rodríguez-Vicente, A. & Ruiz, M. P. *Tetrahedron* **2005**. *61*, 2767.

[86] Omura, K. & Swern, D. *Tetrahedron* **1978**. *34*, 1651.

[87] Onodera, K., Hirano, S. & Kashimura, N. *Carbohydr. Res.* **1968**. *6*, 276.

[88] Corey, E. J. & Kim, C. *J. Am. Chem. Soc.* **1972**. *94*, 7586.

[89] Collins, J., Hess, W. & Frank, F. *Tetrahedron Lett.* **1968**. *9*, 3363.

[90] Albright, J. D. & Goldman, L. *J. Am. Chem. Soc.* **1965**. *87*, 4214.

[91] Kametani, T., Huang, S.-P., Honda, T. et al. *Heterocycles* **1985**. *23*, 2693.

[92] Tsuneda, T. *Density functional theory in quantum chemistry.* Springer, **2014**.

[93] Sherrill, C. D. *School of Chemistry and Biochemistry, Georgia Institute of Technology* **2000**.

[94] Hertsen, D., Catak, S., Waroquier, M., D'hooghe, M., De Kimpe, N. & Van Speybroeck, V. In *Quantum Chemistry in Belgium, 10th edition.*

[95] Cramer, C. J. *Essentials of computational chemistry: theories and models.* John Wiley & Sons, **2013**.

[96] Møller, C. & Plesset, M. S. *Phys. Rev.* **1934**. *46*, 618.

[97] Goossens, H., Catak, S., D'hooghe, M., De Kimpe, N. & Van Speybroeck, V. *Inzicht in de vorming van 3-methoxy-3-methylazetidinen: Rationalisering van het reactiemechanisme via kwantummechanische berekeningen.* Master's thesis, Universiteit Gent, **2010**.

[98] Hohenberg, P. & Kohn, W. *Phys. Rev.* **1964**. *136*, B864.

[99] Kohn, W. & Sham, L. J. *Phys. Rev.* **1965**. *140*, A1133.

[100] Cuevas, J. Introduction to density functional theory, **2010**.

[101] Zhao, Y. & Truhlar, D. G. *Theor. Chem. Acc.* **2008**. *120*, 215.

[102] Chattaraj, P. K. *Chemical reactivity theory: a density functional view.* CRC Press, **2009**.

[103] Stankovic, S., Catak, S., D'hooghe, M., Goossens, H., Abbaspour Tehrani, K., Bogaert, P., Waroquier, M., Van Speybroeck, V. & De Kimpe, N. *J. Org. Chem.* **2011**. *76*, 2157.

[104] Mennucci, B. *WIREs Comput Mol Sci* **2012**. *2*, 386.

[105] Cramer, C. J. & Truhlar, D. G. *Chem. Rev.* **1999**. *99*, 2161.

[106] Mennucci, B., Tomasi, J., Cammi, R., Cheeseman, J., Frisch, M., Devlin, F., Gabriel, S. & Stephens, P. *J. Phys. Chem. A* **2002**. *106*, 6102.

[107] Keith, T. & Frisch, M. *Modeling the hydrogen bond* **1994**. *569*, 22.

[108] Fukui, K. *J. Phys. Chem.* **1970**. *74*, 4161.

[109] Frisch, M., Trucks, G., Schlegel, H. B., Scuseria, G., Robb, M., Cheeseman, J., Scalmani, G., Barone, V., Mennucci, . B., Petersson, G. e. et al. Gaussian 09, **2009**.

[110] Legault, C. *Université de Sherbrooke* **2009**.

[111] Raczyńska, E. D., Hallmann, M. & Duczmal, K. *Comput. Theor. Chem.* **2011**. *964*, 310.

[112] Raczynska, E. D., Kosinska, W., Osmialowski, B. & Gawinecki, R. *Chem. Rev.* **2005**. *105*, 3561.